SUSPENSIONS OF GRANULAR PARTICLES GENERATED BY UPWARD FLOW

Thesis by

Francis Clay McMichael

In Partial Fulfillment of the Requirements

For the Degree of

Doctor of Philosophy

California Institute of Technology

Pasadena, California

1963

ACKNOWLEDGMENTS

The writer gratefully acknowledges the encouragement, assistance and criticism enthusiastically offered by Professor Norman H. Brooks throughout the course of this investigation.

The laboratory investigation was carried out with the aid of research grant WP-174(C2) from the Research and Training Grants Branch, Division of Water Supply and Pollution Control, United States Public Health Service.

During the academic year 1961-62, the writer carried on the research with the aid of a National Defense Education Act Fellowship.

The writer thanks Professors Vito A. Vanoni and Donald R. F. Harleman for their criticism of the turbulent diffusion model for the fluidized suspension.

To Mr. Elton F. Daly, Mr. Robert Greenway, and Mr. Arthur Schmitt the writer extends his gratitude for their assistance in the construction and design of the equipment used in this study.

Special thanks is due Dr. Haskell Shapiro for his aid in devising the method for measuring concentration with an electrical resistance probe.

This work is dedicated to my wife Sharon, who shared all the problems in bringing it to completion.

ABSTRACT

A laboratory study was made of the local properties of suspensions of granular particles generated by an upward flow of water. Four granular materials covering a range of particle sizes having particle Reynolds numbers between 10 and 70 were studied by making detailed measurements within ten suspensions. Measurements were made of the mean properties of over one hundred suspensions. Concentrations in the suspensions generated by upward flow were generally greater than those of typical hindered settling experiments, but less than those of typical fluidization experiments by chemical engineers.

Measurements of the mean concentration for an entire suspension and the ratio of superficial velocity to particle free-fall velocity yielded a separate relationship for each material studied. These relationships are strongly dependent on the standard deviation of particle sizes for the parent materials.

Recognizing that granular materials are never perfectly uniform, measurements of concentration and particle size were made on a local basis. The suspensions were found to sort themselves with the fine particles near the top and the coarse particles at the bottom, and the local concentration was observed to decrease from the bottom to the top of the suspension.

Granular particles with mass densities approximately two and one-half times the density of water and having particle Reynolds numbers in the range from 10 to 70 produce highly turbulent systems when fluidized with water. It was observed that there is local generation of turbulence throughout the suspension with the highest intensity of turbulence being in the region where the local concentration is the largest.

Measurements of the hindered settling velocity of a suspension and the superficial velocity necessary to maintain the suspension show the two quantities to be identical for all practical purposes. The turbulence was observed visually to be less for the settling suspension than for the fluidized suspension.

TABLE OF CONTENTS

TABLE OF CONTENTS (Cont'd)

TABLE OF CONTENTS (Cont'd)

LIST OF FIGURES

LIST OF FIGURES (Cont'd)

LIST OF FIGURES (Cont'd)

LIST OF FIGURES (Cont'd)

LIST OF FIGURES (Cont'd)

LIST OF TABLES

CHAPTER 1

INTRODUCTION

1-1 Definition of Fluidization

A fluid flowing vertically upward through a bed of discrete non-cohesive particles exerts a drag force on each particle. Also acting on each particle is a net downward gravity force equal to the submerged weight of a particle and an intergranular contact force necessary for equilibrium. As the fluid velocity is increased, a point will be reached where the fluid drag force equals the submerged weight of each particle, particle-to-particle contact ceases, and a state of fluidization is produced in which particles are no longer held in position by neighboring particles. This is a state analogous to the so-called "quicksand" found in nature. The particles, which were formerly held together by gravity in a fixed matrix, are now free to move. The movement of each particle depends on the motion of the fluid and the motion and position of neighboring particles.

A group of particles suspended in an upward flow is commonly referred to as a fluidized bed, a term which is a carryover from the study of flow through beds of particles undisturbed from the static position, hereafter called simply fixed beds of particles. Since the term "fluidized bed of particles" can be misleading, the particles in the state of fluidization will subsequently be referred to by the more appropriate descriptive terms, suspension or fluidized suspension.

A phenomenon analogous to fluidization is the hindered settling of a suspension or the settling of a group of particles in a still fluid.

In a more general way, one might think of the hindered settling of a suspension as merely the Galilean transformation of the fluidized suspension.

Morphologically, the suspension consists of two distinct phases: the particles and the fluid. The fluid has the property of being continuous, while the particles are discrete. The fluid may be gaseous or liquid, while the "particles" may be gaseous, liquid, or solid. Table 1-1 is a tabulation of six possible systems of fluid and particles.

Table 1-1

Possible Fluidized Suspensions

The arrows indicate the relative motion between the fluid and the particles.

Example	Fluid	Particles
1	Gas ↑	Solid ↓
2	Liquid ↑	Solid ↓
3	Liquid ↓	Gas ↑
4	Gas ↑	Liquid ↓
5*	Liquid ↑	Liquid ↓
6*	Liquid ↓	Liquid ↑

*The two liquids must be immiscible in these two cases.

The gas-solid system is frequently employed by chemical engineers in chemical reactions. A system of the liquid-solid type is encountered, for example, by sanitary engineers during the backwashing of sand filters. The literature as surveyed by Leva (16) and Zenz and Othmer (17) contains a great many examples of systems of the liquid-solid and

gas-solid types. Of the six examples, only the first two, the gas-solid and liquid-solid systems, are generally recognized as fluidization phenomena.

1-2 Previous Analyses Based on Modification of the Darcy Equation

Many investigators have attempted to analyze fluidization phenomena by methods analogous to those employed in the study of flow in porous media. In fact, the expression "flow in expanded porous media" is commonly used to describe fluidized suspensions. However, unlike a porous medium, such as a bed of sand in a gravity field, the particles in a suspension produced by fluidization are not fixed but are characterized by a state of highly turbulent motion.

Leva (16) presents a comprehensive analysis of the technique by which the upward flow through a suspension is treated as if the particles were fixed. In general, the Darcy equation, which is well established for flow in porous media, is applied by modifying the permeability coefficient. The Darcy equation is:

$$\vec{u} = -\frac{k\gamma_f}{\mu} \text{ grad } h \qquad (1\text{-}1)$$

where $\vec{u}$ = superficial velocity = discharge per unit of total cross-sectional area = $[LT^{-1}]$*

k = permeability coefficient = $[L^2]$

γ_f = specific weight of fluid = $[FL^{-3}]$

μ = dynamic viscosity of fluid = $[FTL^{-2}]$

h = piezometric head of fluid = $[L]$

* Letters in brackets indicate dimensions: L = length, T = time, F = force, M = mass, $F = MLT^{-2}$.

The Darcy equation as written in equation 1-1 has a permeability coefficient, k, which depends on the properties of the medium only. In some fields, such as groundwater hydrology, investigators combine k, μ, and γ_f in the form $K = \frac{k\gamma_f}{\mu}$ where K is called the hydraulic conductivity or permeability. The form of equation 1-1 is more common to the petroleum industry, where one is interested in the flow of fluids of many different viscosities and specific weights in nearly identical media. The permeability coefficient, k, is actually a second rank tensor for an anisotropic medium, such as rock or soil with distinct strata of varying grain size, but it reduces to a scalar for an isotropic medium. Furthermore, several investigators, such as Carman, Kozeny, Fair and Hatch, whose ideas are extensively discussed in Scheidegger (28), Leva (16), and Zenz and Othmer (17), developed semi-empirical relationships between the permeability coefficient, k, and the geometry of the porous medium. The form of this relationship, derived on the basis of a fixed bed of particles is:

$$k \sim \frac{D^2\epsilon^3}{(1-\epsilon)^2} = \frac{D^2(1-C)^3}{C^2} \qquad (1\text{-}2)$$

where D = diameter of the particles forming the porous medium [L]

C = volume concentration of solids, and

ϵ = porosity of the medium $\equiv$ 1-C

To apply Darcy's equation to the fluidized suspension, one also makes use of the condition that the gradient of the piezometric head must equal the submerged weight of the suspended particles per unit cross-sectional area after the bed is fluidized, that is

$$\rho_f g \text{ grad } h = - C(\rho_s - \rho_f)g \tag{1-3}$$

where C = volume concentration of the particles = $[L^3L^{-3}]$

ρ_s = mass density of particles = $[ML^{-3}]$

ρ_f = mass density of fluid = $[ML^{-3}]$

g = gravitational acceleration = $[LT^{-2}]$

Combining the relationships from equations 1-1, 1-2, and 1-3, the following expression is obtained for upward flow through a suspension:

$$\bar{u} \sim \frac{D^2(\rho_s - \rho_f)\,(1-C)^3 g}{\mu C} \tag{1-4}$$

where $\bar{u} = |\vec{u}|$

A great deal of data has been amassed in the form of equation 1-4 for liquid-solid systems (see Leva (16), Chapter 3). However, the factor of proportionality necessary to complete equation 1-4 has by no means been universally established. For spherical particles, with particle Reynolds numbers (based on particle diameter and free fall velocity) less than 10, Leva (16, p. 90) presents the equation:

$$\bar{u} = \frac{0.005g(\rho_s - \rho_f)\,D^2\,(1-C)^3}{\mu C} \tag{1-5}$$

The range of concentrations, C, over which equation 1-5 applies is not clearly stated. Also, at this time, it should be stated that so far it has been tacitly assumed that the suspensions in question are composed of uniform particles and that the concentration of particles is uniform throughout the suspension; these assumptions are based on the

conception of a suspension as a dilated porous medium in which the particles are fixed in space in uniform arrangements.

Dividing equation 1-5 by the Stokes' free-settling velocity of a sphere, w, where

$$w = \frac{(\rho_s - \rho_f) g D^2}{18\mu} \tag{1-6}$$

Leva obtains:

$$\frac{\bar{u}}{w} = 0.09 \frac{(1-C)^3}{C} \tag{1-7}$$

Equation 1-7 is restricted by Leva to concentrations by volume greater than 20 per cent. For lower concentrations, one sees that the functional behavior of equation 1-7 is incorrect in that as $C \to 0$, $\bar{u}/w \to \infty$. In figure 1-1, equation 1-7 is graphically presented along with other functional relations between $\bar{u}/w$ and C which will be discussed in detail in the following sections.

1-3 Dimensional Analysis

Let us consider the important variables in a fluidized suspension as tabulated below:

Fluid Properties

$\bar{u}$ = superficial velocity - $[LT^{-1}]$

ρ_f = fluid mass density - $[ML^{-3}]$

μ = dynamic viscosity - $[FTL^{-2}]$

Particle Properties

w = free-fall velocity - $[LT^{-1}]$

ρ_s = particle mass density - $[ML^{-3}]$

D = particle diameter - [L]

σ_w - geometric standard deviation of free-fall velocities

Suspension Properties

C - concentration of particles by volume $[L^3L^{-3}]$

The eight variables listed above are functionally related by some function:

$$\phi_1 (\bar{u}, \rho_f, \mu, w, \rho_s, D, \sigma_w, C) = 0 \qquad (1\text{-}8)$$

In this case, the eight variables have three fundamental dimensional units, and therefore, by dimensional analysis the functional relationship may be expressed as follows:

$$\phi \left(\frac{\bar{u}}{w}, \frac{wD\rho_f}{\mu}, C, \sigma_w, \frac{\rho_s}{\rho_f}\right) = 0 \qquad (1\text{-}9)$$

The ratio $\bar{u}/w$ can be interpreted as the relative settling velocity of the suspension. The second term in equation 1-9 is a form of Reynolds number, a parameter which is indicative of the condition of the flow about a particle. Both the concentration and geometric standard deviation of the free-fall velocities are dimensionless by themselves. ρ_s/ρ_f is the ratio of the densities of the particles and the fluid and is a measure of the relative momentum of the particles and the fluid.

1-4 Functional Relationship of Richardson and Zaki

A form of dimensional analysis with results similar to equation 1-9 was carried out by Richardson and Zaki (4) considering a uniform material and thus neglecting σ_w; also, they did not include ρ_s as

one of the variables. This is one of the most troublesome pitfalls of the method of dimensional analysis in that it requires judgment in choosing the significant variables. The particle density, ρ_s, may not be neglected since experimental evidence (see Leva (16), Zenz and Othmer (17) indicates that gas-solid systems and liquid-solid systems show very different fluidization properties. Furthermore it would have been preferable if Richardson and Zaki had used concentration rather than porosity in presentation of their results, especially for low concentrations. The point should be made that the choice between porosity and concentration is not merely one of semantics or algebra. If one considers the full range of porosities from a fixed bed to that of a single suspended particle, the range is approximately $0.5 \leq \epsilon \leq 1.0$. However, the concentration, C, ($C = 1-\epsilon$) changes by orders of magnitude over this same range, $0.5 \geq C \geq 0$. If one had certain physically determined data for a range of porosities up to 0.8, one might not feel adverse to extrapolating the data for $\epsilon \rightarrow 1.0$. However, one is probably more hesitant to extrapolate the same data over orders of magnitude, as would be the case when thinking in terms of the concentration.

In order to make the point more clear, let us look at the results of Richardson and Zaki (4). From a series of experiments, using various liquids and particles, Richardson and Zaki found that their data could be fitted with the functional relationship:

$$\frac{\bar{u}}{u_i} = (1-C)^n = (\epsilon)^n \qquad (1\text{-}10)$$

where n is a function of the particle Reynolds number, $\frac{wD\rho_f}{\mu}$. For

the range of their experiments, they found

$$n = (4.35 + 17.5 \frac{D}{D_t}) (\frac{wD\rho_f}{\mu})^{-0.03} \quad \text{for } 0.2 < \frac{wD\rho_f}{\mu} < 1 \qquad (1\text{-}10a)$$

$$n = (4.45 + 18 \frac{D}{D_t}) (\frac{wD\rho_f}{\mu})^{-0.1} \quad \text{for } 1 < \frac{wD\rho_f}{\mu} < 200 \qquad (1\text{-}10b)$$

$$n = 4.45 (\frac{wD\rho_f}{\mu})^{-0.1} \quad \text{for } 200 < \frac{wD\rho_f}{\mu} < 500 \qquad (1\text{-}10c)$$

$$n = 2.39 \quad \text{for } \frac{wD\rho_f}{\mu} > 500 \qquad (1\text{-}10d)$$

where D is the particle diameter and D_t is the fluidization column diameter. The relationship expressed in equation 1-10 resulted from the plotting of a great deal of experimental data where C is the mean concentration based on the total weight of granular material in suspension and the overall dimensions of the suspension. Richardson and Zaki found that their data for uniform materials could be easily fitted with a straight line if they plotted the logarithm of the superficial velocity vs. the logarithm of the mean porosity. The slope of this line yielded the value of the exponent, n, and the intercept of the straight line for $\log \epsilon \rightarrow 0$ gave the value of u_i, the representative free-fall velocity for the suspended particles. However, Richardson and Zaki found that the value of the superficial velocity obtained from the extrapolation $\log \epsilon \rightarrow 0$ did not agree with the free-fall velocity, w, for their materials as calculated by other means. Disagreements between u_i and w of magnitude of 2 to 25 per cent were found for the range of particle Reynolds number between 0.5 and 7000. These differences were attributed to container wall effects on the particles. Richardson and Zaki choose to present equation

1-10 with u_i being called identical to w, the free-fall velocity for the particles. Further comments on the disagreement between u_i and w will be made in chapter 5, but the writer believes that the discrepancy is not primarily due to wall effects but is attributable to the fact that equation 1-10 cannot be extrapolated to very low concentrations without further knowledge of the physical laws governing the behavior of low concentrations of suspended particles.

Because of the uncertainty of the physical laws governing low concentrations of suspended particles, it was decided to present the various theoretical and experimental relationships in a graphical form which does not compress the relationships at low concentrations, that is, the logarithm of the concentration is plotted against the ratio $\overline{u}/w$ on an arithmetic scale (see figure 1-1). The log C scale allows information which would occupy only a small portion of the logarithm (1-C) scale to be plotted over several cycles, thus amplifying the trend of the data at the low values of C. For example, the experimentally determined results of Richardson and Zaki, equation 1-10, are presented in this form, but the curves are plotted only over the range covered by Richardson and Zaki's experimental data, that is, $0.05 \leq C \leq 0.60$. Also equation 1-10 is plotted in figures 1-1 and 1-2 neglecting the D/D_t dependence, i.e. D/D_t is taken as zero.

Additional functional relationships, presented in figures 1-1 and 1-2, will be discussed in the rest of this chapter.

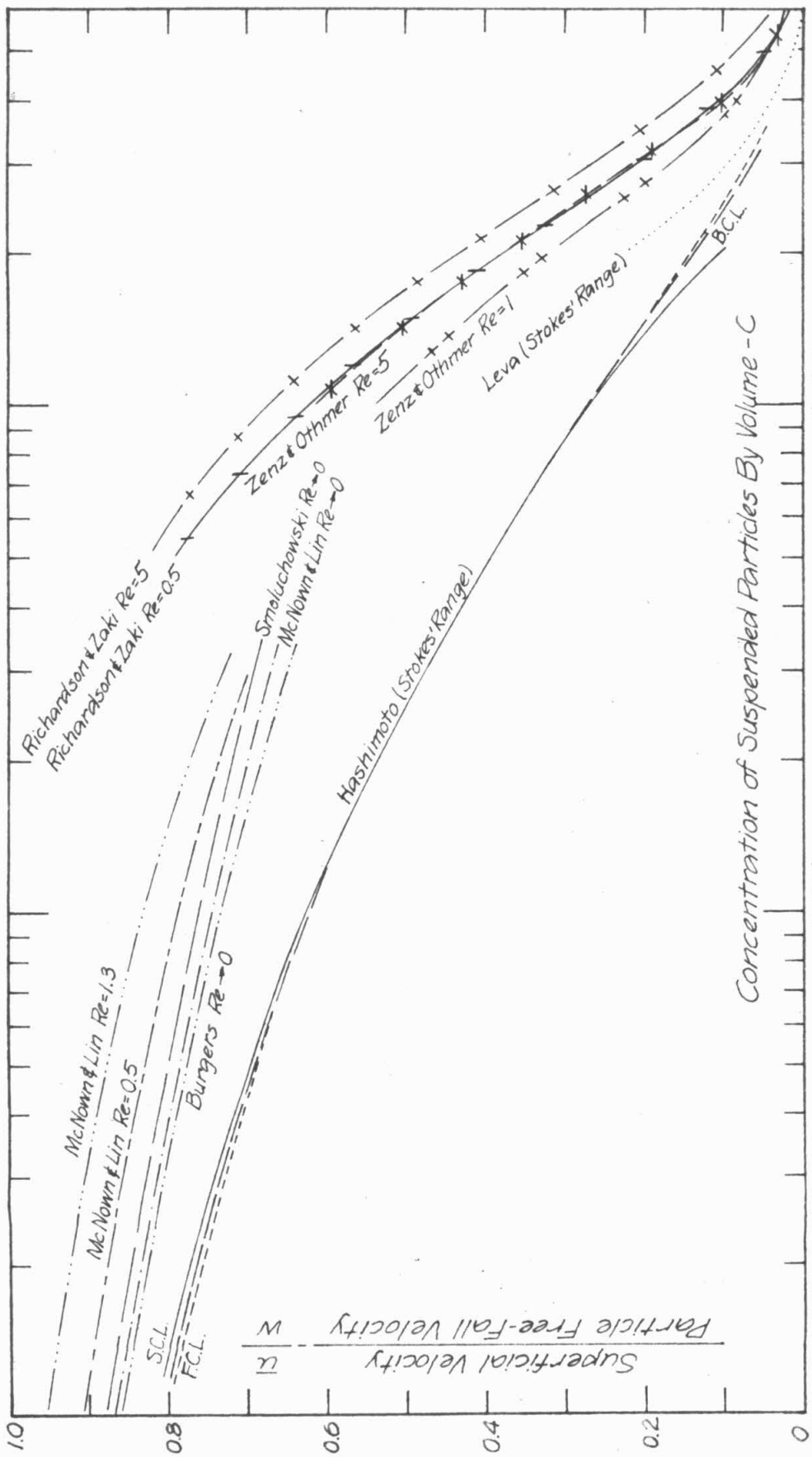

Fig. I-1 Some Experimental and Theoretical Relationships between $\frac{u}{w}$ and C for Low Reynolds Numbers

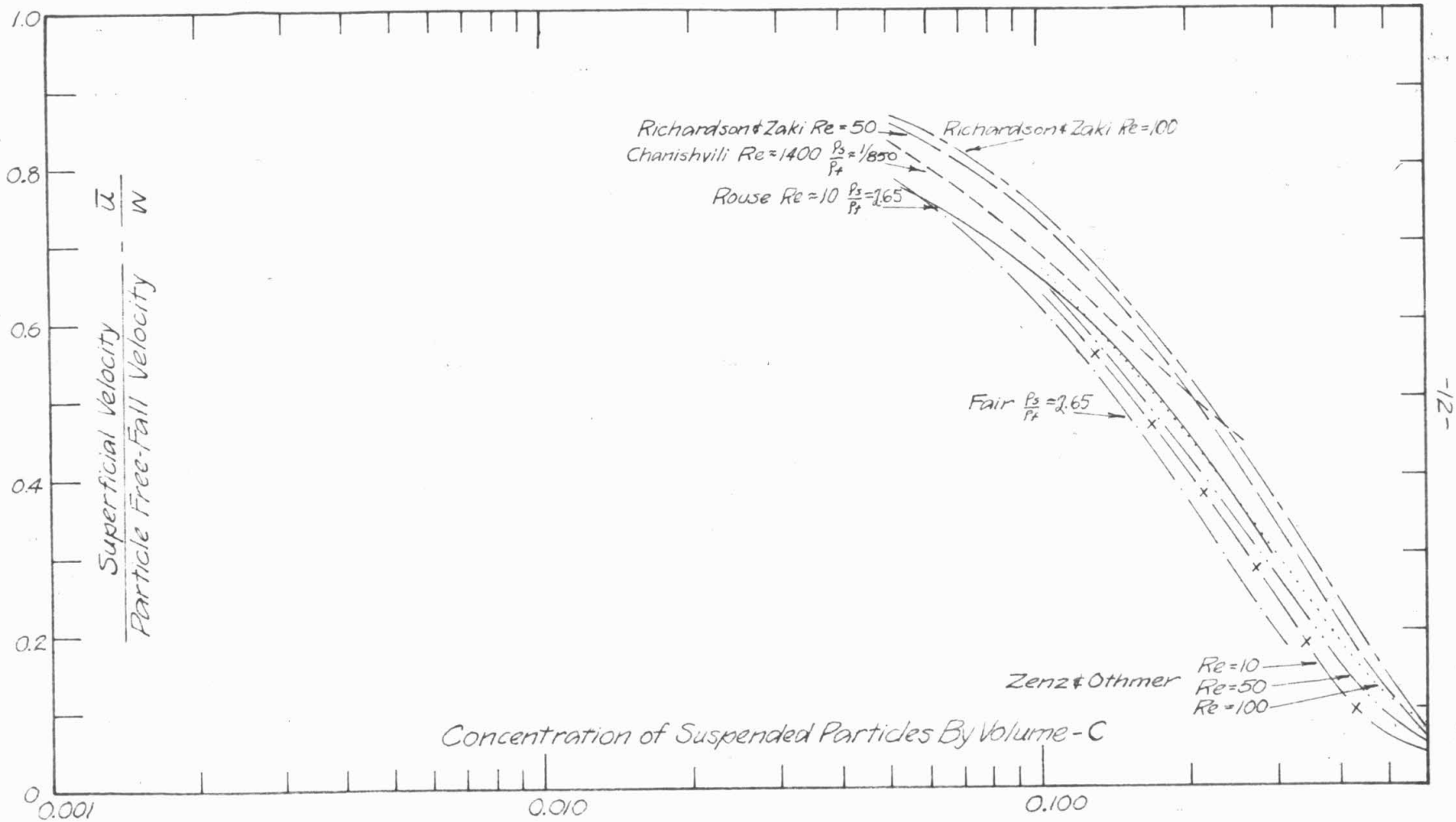

Fig. 1-2 Some Experimental and Theoretical Relationships between $\frac{u}{w}$ and C for Higher Reynolds Numbers

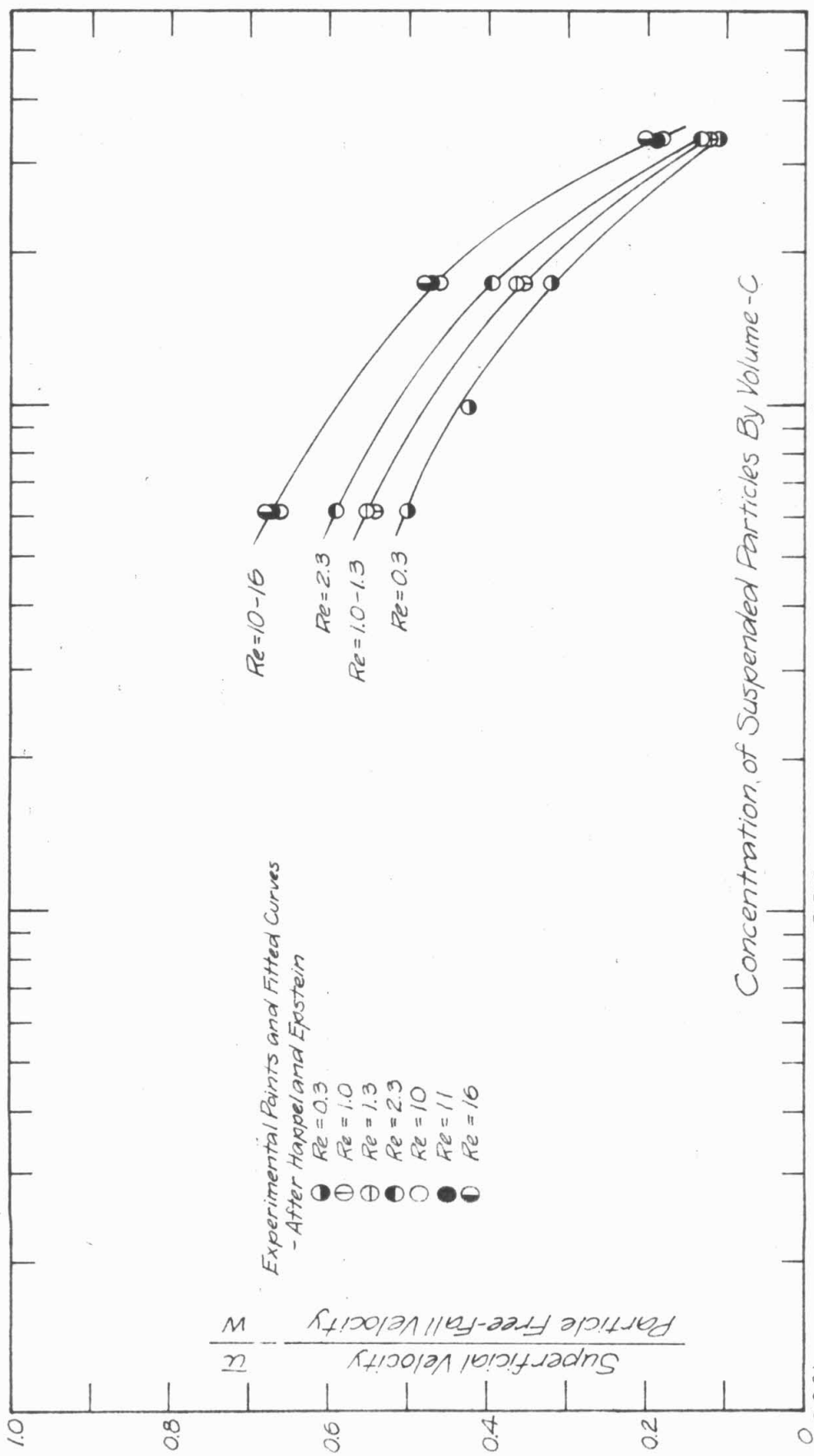

Fig. 1-3 Experimental Data Resulting from Flow through Fixed Assemblages of Spheres - After Happel and Epstein

1-5 Some Relationships Between $\bar{u}/w$ and C for Low Reynolds Numbers

Figure 1-1 contains the graphical form of several theoretical relationships derived for particle Reynolds numbers below 1. This is in the so-called viscous range of flow where one neglects the inertia terms in the Navier-Stokes equations.

McNown and Lin (5) studied the hindered settling of dilute suspensions of sand grains and glass spheres with Reynolds numbers near 1 in water and volume concentrations less than 3 per cent. The analytic expression derived by McNown and Lin which closely fits their data is shown graphically in figure 1-1.

For studies of settling suspensions, the hindered settling velocity is considered analogous to the superficial velocity associated with the fluidized suspension. The hindered settling velocity is defined as the rate of fall of a suspension relative to an observer in a fixed horizontal plane, after the mechanism making the suspension, such as the upward flow of fluid has been stopped.

Additional theoretical relationships between $\bar{u}/w$ and C have been derived by Burgers and Smoluchowski for the same range of Reynolds numbers as the McNown and Lin curves. These relations are also plotted in figure 1-1(after McNown and Lin (5)).

Zenz and Othmer (17) present a functional relationship based on curves quite similar to the drag coefficient vs. Reynolds number curve for a single sphere. From the results of tabulating and evaluating a large amount of experimental data obtained from several investigators, Zenz and Othmer plotted a series of curves paralleling the

Reynolds number vs. drag coefficient curve for a single sphere. The offset of each curve depends on the volume concentration of the suspended particles. These curves of Zenz and Othmer are presented in the form of $\bar{u}/w$ vs. C in figure 1-1 for Reynolds numbers 1 and 5. (For other Reynolds numbers, see figure 1-2). Although the trends are similar, there is a noticeable difference between values on the curves of Richardson and Zaki and Zenz and Othmer, for example, see the curves for Reynolds number equal to 5.

1-6 Comparison of Fixed Assemblages of Particles with Free Suspensions

Hashimoto (2) investigated the viscous flow past a cubic array of fixed, uniform-diameter particles. His work is purely theoretical with no associated experimental data. Hashimoto's results are presented in the form of the ratio $\frac{F}{3\pi\mu D\bar{u}}$ vs. C where F is the drag force on each sphere, $\bar{u}$ is the superficial velocity of the fluid through the array, and C is the volume concentration of the spheres. The term $3\pi\mu D\bar{u}$ is the Stokes' drag force on a sphere for a given superficial velocity, $\bar{u}$. An isolated sphere in free-fall settles with a terminal velocity such that the drag force on the sphere equals the submerged weight of the particle. By analogy, consider the fixed matrix of spheres settling in a fluid. In this state of free-fall, the drag force on each sphere must equal its submerged weight, that is, F on each particle is equal to $\frac{\pi D^3}{6}(\rho_s-\rho_f)g$. By Stokes' law, the drag force is equal to the submerged weight, $\frac{\pi D^3}{6}(\rho_s-\rho_f)g$, when $F = 3\pi\mu Dw$ where w is the free-fall, or terminal, velocity of an isolated sphere. Therefore for the settling matrix of spheres, the ratio $\frac{F}{3\pi\mu D\bar{u}}$ can be interpreted as the ratio of $\frac{w}{\bar{u}}$. In figure 1-1 are presented

the results of Hashimoto interpreted as $\frac{\bar{u}}{w}$ vs. C for the range of concentrations over which he presented numerical values of the ratio $\frac{F}{3\pi\mu D\bar{u}}$ vs. C. These curves are for three cubic arrangements of uniform spheres – the simple-cubic lattice (S.C.L.), the face-centered lattice (F.C.L.), and the body-centered lattice (B.C.L.). Each of these regular arrays of particles is a repetition of a particular unit cell. For example, the simple cubic lattice has a unit cell in which there is a particle placed at each of the eight corners of a cube. The unit cell for the face-centered lattice has a particle in each of the eight corners of a cube and a particle in the center of each of the six faces of the cube, and similarly, the unit cell of the body centered lattice is composed of particles at each corner of a cube plus a particle at the center of the body of the cube. One observes in figure 1-1 that the various lattice arrangements have little effect on the relationship between $\frac{\bar{u}}{w}$ and C.

A very interesting approach to the study of fluidization was employed by Happel and Epstein (18). They studied the upward vertical flow of aqueous glycerol through a pipe of 10 cm inside diameter which was fitted with a series of rods (1.10 mm diameter) extending longitudinally on which 4.9 mm diameter beads could be aligned at desired intervals. They measured the pressure drop for a given flow with an empty tube, then for the tube with rods only, and finally with the entire assemblage in place. They assumed that these pressure drops could be algebraically subtracted in order to determine the effect of the beads alone on the flow. The basis for this assumption was that the flow regime was laminar for their experiments (as determined by dye injection test).

However, their reasoning is open to criticism because laminar flow is not necessarily described by equations which are linear. From the pressure drop measurements, Happel and Epstein computed drag coefficients for the various assemblages which led them to the ratio of the superficial velocity for a given assemblage to the free-fall velocity for an isolated sphere of the same diameter in the same fluid medium under the same frictional drag. The experimental points of Happel and Epstein are presented in figure 1-3. Curves drawn through these points, for the various particle Reynolds numbers, show a trend similar to the experimental results of Richardson and Zaki and Zenz and Othmer for $0.15 \leq C \leq 0.40$; but for a given value of C, the Happel and Epstein data show a smaller value of $\bar{u}/w$. This difference appears to get larger as the concentration gets smaller, which indicates for a given value of $\bar{u}/w$ the fixed assemblage of particles shows a larger expansion (i.e., smaller concentration) than the suspension in which the particles are not fixed but are free to move about randomly. In terms of hindered settling, for a given concentration, the suspension in which the particles are free to move will settle faster than a suspension in which the particles are fixed in a specific cubic arrangement. A similar difference is found between the theoretical relationship of Hashimoto for a fixed assemblage of spheres and the experimentally verified relationship of McNown and Lin for spheres that are free to move in the fluid medium.

Let us compare in Table 1-2 the value of $\bar{u}/w$ obtained from the experimental results of Happel and Epstein (figure 1-3) for fixed assemblages and the experimental results of Richardson and Zaki for

various concentrations of particles that are free to move.

Table 1-2

Comparison of $\bar{u}/w$ for Fixed Assemblages of Particles and Free Suspensions for $\frac{wD\rho_f}{\mu} = 10$

Volume Concentration C	Fixed Assemblage $\bar{u}/w$ Happel and Epstein (figure 1-3)	Free Suspension $\bar{u}/w$ Richardson and Zaki (equation 1-10)
0.06	0.68	0.80
0.10	0.59	0.69
0.20	0.42	0.45
0.30	0.25	0.28

The difference between the two values of $\bar{u}/w$ increases as the concentration decreases, being less than 11 per cent of $\bar{u}/w$ value by the Richardson and Zaki equation for C = 0.30 and increasing to 15 per cent for C = 0.06.

1-7 Some Relationships Between $\frac{\bar{u}}{w}$ and C for Higher Reynolds Numbers

In figure 1-2 are plotted the experimental results of Richardson and Zaki (4) and Zenz and Othmer (17) for particle Reynolds numbers 10 to 100. Also included are curves based on the investigations of Fair (29), Rouse (7), and Chanishvili (22).

For calculating the expansion of a rapid sand filter during backwashing, Gordon Fair (29) suggests the experimentally determined relationship:

$$\frac{\bar{u}}{w} = (1-C)^{9/2} \qquad (1-11)$$

Equation 1-11 is of the same form as equation 1-10 proposed by Richardson and Zaki, except that in the Richardson and Zaki equation the exponent, n, is dependent on the particle Reynolds number, whereas in equation 1-11, the exponent is a constant. Although it is not directly stated, Fair restricts equation 1-11 to systems in which the relative density, $\frac{\rho_s}{\rho_f}$, is about 2.5 and Reynolds numbers are between 10 and 100.

An early, but less well-known, investigation of a liquid-solid suspension was carried out by Rouse (7). By analysis, Rouse predicted that the equation describing the suspension should be of the form:

$$C = \frac{A}{(\frac{\rho_s}{\rho_f} - 1)} (1 - B \frac{\bar{u}}{w})^{3/2} \qquad (1\text{-}12)$$

where A = a coefficient depending on the shape and relative density of the materials and the local flow conditions

B = a coefficient depending on rate of settling for a group of particles relative to the upward flow velocity

Using an artificially graded quartz sand having a geometric mean size, D_g, of 0.235 mm and a geometric standard deviation, σ_g, of 1.64, Rouse determined that equation 1-12 best fitted the experimental data for A = 0.83 and B = 1.0. Rouse is to be complimented for his efforts; for although his techniques were somewhat crude, he seems to be the first investigator to attempt to investigate a suspension in detail. Rouse determined the local concentration by measuring the slope of the piezometric head curve for a suspension. The piezometric head for the various points within the suspension was measured relative to

the clear water above the suspension. From samples withdrawn at various levels within the suspensions, Rouse determined by timing the fall in still water of a hundred or more representative particles the average value of w for each sample. Rouse commented on the "appreciable amount of scatter" of his data but felt that the trend of equation 1-12 was followed. A good part of the scatter is probably due to the difficulty of measuring the slope of the piezometric head curves in order to determine concentration.

There was some question to Rouse as to whether or not the factors A and B are really constants. The factor B is in the most doubt since Rouse expected it to depend upon the state of turbulence in the system. In a previous experimental study, Rouse (6) had shown that using a mechanical shaker to generate turbulence in a still column of water it was possible to create a state of suspension with no upward flow at all. This type of suspension had a very ordered structure with the concentration of the suspended material decreasing from the bottom to the top of the suspension. Further, Rouse (7) commented on the turbulent nature of the fluidized suspension as follows: "....a definite pattern of eddies was noticeable through the transparent walls of the cylinders, apparently due neither to imperfect stilling of the approaching flow, nor to the wake behind each individual grain, but rather to characteristic momentary fluctuations in the density of the water sediment mixture."

It should be noted that Rouse includes the effect of relative density, $\frac{\rho_s}{\rho_f}$, directly in equation 1-12. In figure 1-2, equation 1-12 is plotted for $\frac{\rho_s}{\rho_f} = 2.65$ and A = 0.83 and B = 1.0. These values of the

coefficients, as previously stated, were determined experimentally for a sand with a mean particle Reynolds number of about 10. However, because the sand used by Rouse was composed of a distribution of sand sizes, the range of particle Reynolds numbers covered by the experiments was between 1 and 25.

Chanishvili (22) measured the concentration of air bubbles in a downward flow of water in a pipe. He produced air entrainment at the top of his pipe, the quantity of which depended on the magnitude of the water discharge and the height of the fall of the water jet. The concentration of the air bubbles was obtained from measurements of the piezometric head along the column. Chanishvili assumed that the air bubbles in his experiments were of nearly uniform size and that w, the free-fall (rise) velocity of a single bubble, was constant. Using a value of w = 27 cm per sec for water discharges from 1 to 2.85 liters per sec, and an air discharge from zero to 640 cm^3 per sec, Chanishvili found the following equation to fit his data best:

$$\aleph = 6.17C^2 - 3.72C + 1 \qquad (1\text{-}13)$$

where $\aleph = \frac{w_*}{w}$ = relative settling velocity

w = free-fall (rise) velocity of a bubble $[LT^{-1}]$

$w_* = \frac{Q_f}{A} + \frac{Q_s}{A}\left(\frac{1-C}{C}\right) = [LT^{-1}]$

Q_f = water discharge = $[L^3T^{-1}]$

Q_s = air discharge = $[L^3T^{-1}]$

A = cross-sectional area of pipe = $[L^2]$

C = volume concentration of air $[L^3L^{-3}]$

If one lets the air discharge, Q_s, be zero, then w_* becomes merely the

superficial fluid velocity, Q_f/A, and the ratio w_*/w becomes the familiar ratio of superficial velocity divided by the particle free-fall (rise) velocity.

Equation 1-13 is plotted in figure 1-2 with $\aleph$ interpreted as $\overline{u}/w$. The numerical coefficients in equation 1-13 were determined from a system in which the relative density, ρ_s/ρ_f, was about 1/850 and the particle Reynolds number about 1400.

1-8 Behavior of Two or More Spheres in a Viscous Flow

Kynch (1) analytically considered the slow motion of two or more spheres in a viscous fluid. This is the condition of flow in which the inertia terms of the Navier-Stokes equations are neglected. Perhaps some understanding of the type of local conditions within a suspension which generates disturbances can be drawn from a qualitative discussion of Kynch's results. If one considers two equal spheres in a state of free fall, where the center-to-center distance is less than about 10 diameters, the results predicted are different from those for higher concentrations of spheres. Namely, the fall velocity of two equal spheres, five diameters apart, is predicted by Kynch to be about 10 per cent greater than the free-fall velocity of a single sphere. If the two spheres are one diameter apart from center to center and arranged so that one sphere is directly above the other, then Kynch predicts the velocity of the group to be about one and one-half times the free-fall velocity of a single sphere. Two equal spheres for which the line joining their centers is not vertical or horizontal will not fall vertically in an infinite medium but will possess a horizontal component of velocity so that the spheres will tend to settle downward along the line passing through the centers of the two particles.

If one considers two spheres of unequal diameter, similar effects are predicted as for equal spheres with the additional effect that the smaller of two spheres with the same Stokes velocity (i.e., free-settling velocity) will move faster than the larger. Kynch (1) makes some comments on sedimentation phenomena, that is, the settling of dense suspensions of particles. He believes that "a finite assembly of identical particles falling freely under gravity cannot do so in the form of a regular lattice array. Differences between the motion of particles near the edge and those near the center of the assembly produce perturbations which spread inwards from the boundary and spoil the regularity."

The theoretical expression of McNown and Lin (5) shows a behavior similar to that predicted by Kynch. As the concentration approaches zero (i.e. $C < 0.0001$) McNown and Lin predict that the settling velocity of a group of particles will be greater than the free-settling velocity of a single particle.

This type of unusual behavior at low concentrations (predicted by Kynch and by McNown and Lin) seems to be a strong reason for considering the concentration of a suspension rather than the porosity of a suspension.

1-9 Purpose of this Study

The purpose of this study was to examine in detail the properties of a suspension of granular particles generated by an upward flow. The results of previous investigators discussed in this chapter are based upon the measurement of such average properties as mean concentration

and average particle diameter. Recognizing that granular materials are not composed of uniformly sized particles, it was decided to employ procedures whereby the distribution of concentration and particle sizes could be observed on a local basis within a suspension. Whether or not the experimental relationships determined from the measurement of the mean concentration for a whole suspension hold true locally within a suspension has not been previously examined.

There were three main objectives of the experiments: (1) To determine experimentally what are some of the relationships among the basic variables, such as local and mean concentration, relative depth, distribution of particle sizes, particle Reynolds number, and superficial velocity for a suspension generated by upward flow of water. (2) To compare the relationships for the entire suspension derived by other investigators with similar ones for local values observed at various levels within a suspension. (3) To attempt to describe the physical mechanism responsible for the nature of the suspension produced by an upward flow.

With these objectives in mind, four granular materials, the physical properties of which are described in chapter 3, were fluidized and studied in detail. Equipment was developed and experiments carried out to measure the concentration-depth profile, the distribution of particle sizes at various levels, and the relation between the local properties of the suspended particles and the properties of the parent material which composed the entire population of suspended particles.

The apparatus used, the methods employed in the collection and analysis of data, and the results of the study are presented in the following chapters.

CHAPTER 2

APPARATUS AND EXPERIMENTAL PROCEDURE

2-1 The Fluidization Column

The experiments were performed in a vertical tank with lucite walls about 174 cm high with a nearly square cross-section 30.6 x 30.8 cm average dimensions. The column and the related flow system are shown schematically in figure 2-1 and by photographs in figures 2-2 and 2-3. Filtered Pasadena tap water flowed upward through the column, to a pair of overflow weirs at the top, and returned to a reservoir tank from which it was recirculated by a pump. The quantity of discharge was regulated by valves and measured by means of a Fischer-Porter Flowrator (KHWR Lab. No. Q27) for low flows, or a 3 in. venturi meter (KHWR Lab. No. Q3) for higher flows. The experiments were generally carried out with mean velocities of 2 to 5 cm per sec in the vertical lucite column. Both the Flowrator and the venturi meter were calibrated in place using a weighing tank. The errors in the discharge measurements are considered to be less than 1 per cent.

2-2 The Stilling Chamber at the Base of the Column

As shown in figure 2-1, the water enters the lower section of the column through a vertical 2-in. pipe which is about 25 cm long, perforated, and capped at its upper end. Sixty-four 1/4 in. (6.33 mm) diameter holes were symmetrically drilled in the pipe wall, making a total hole area approximately equal to the cross-sectional area of the pipe. From the lower chamber, which is approximately 30 cm square,

SCHEMATIC OF FLOW CIRCUIT

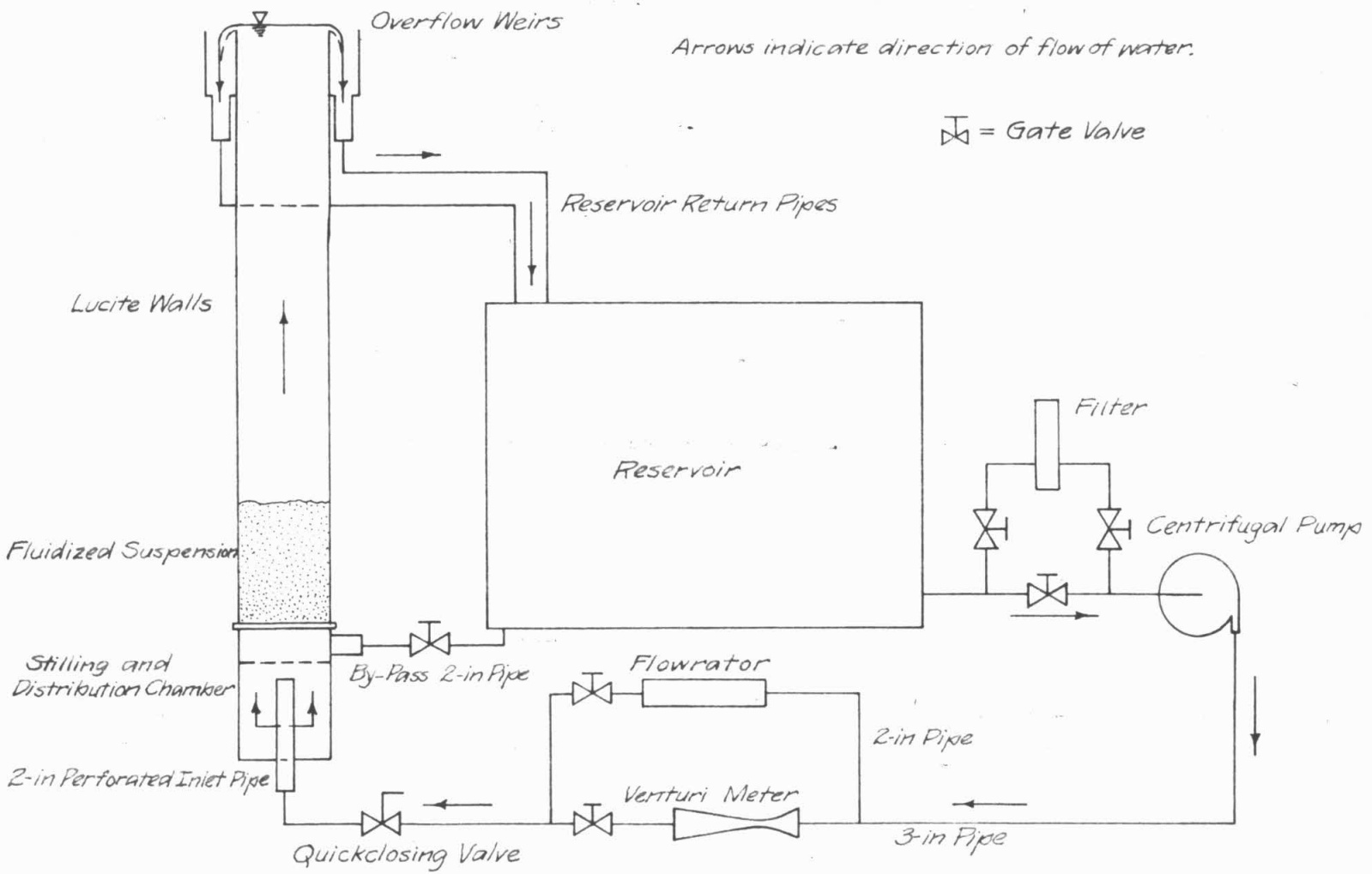

Fig. 2-1 Schematic Diagram of Fluidization Column and Flow Circuit

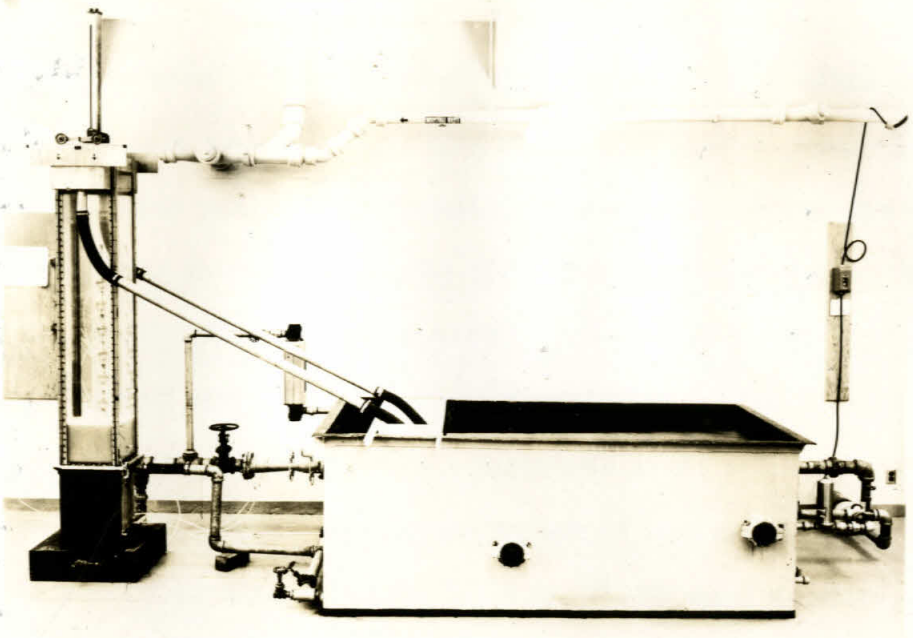

Fig. 2-2 Photograph showing a general view of the Fluidization Column, Reservoir, and Flow Circuit.

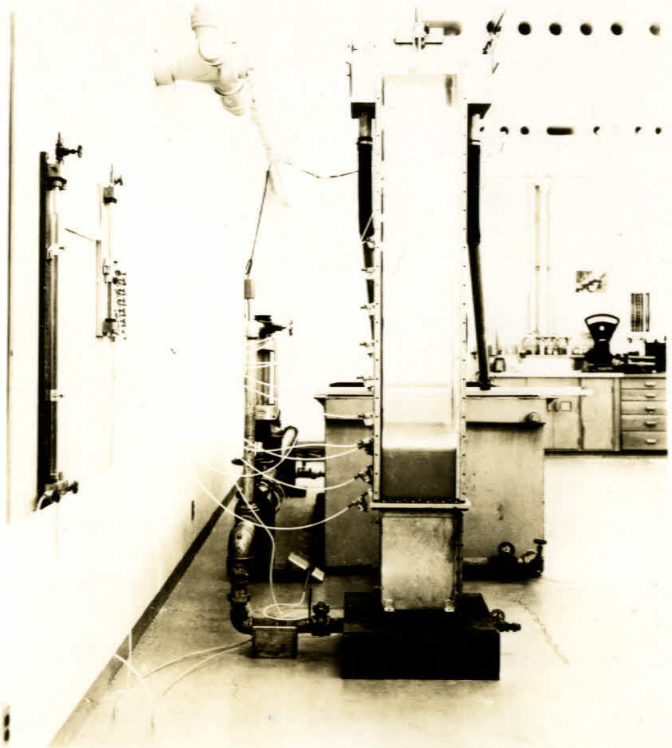

Fig. 2-3 Photograph of Fluidization Column showing a typical fluidized suspension.

the water passes upward through a perforated metal plate which again has a total hole area equal to that of the perforated pipe. Making the discharge pass through the small holes tends to reduce the scale of the turbulence in the flow to the size of the holes and distributes the flow uniformly over the cross-section of the column. The section above the perforated plate is about 5 cm deep. From this section, the discharge passes upward through a stainless steel 100 mesh (0.149 mm) screen and a stainless steel plate which is perforated with 1/32 in. (0.795 mm) diameter holes on 5/64 in. (1.98 mm) centers, having thus about 15 per cent open area. The stainless steel screen and plate further reduce the scale of the turbulence in the water and make the flow distribution uniform, and, in addition, serve as a support for the settled bed of granular material in the lucite section.

2-3 The Lucite Section

The lucite section is made of four walls of 1/2 in. (12.7 mm) thick lucite sheets. On one wall are located eleven static pressure taps at elevations of 4.4, 7.9, 20.1, 31.4, 42.8, 58.6, 73.0, 88.8, 103.6, 118.0, and 131.5 centimeters above the top of the stainless steel perforated plate. In the early stages of the experiments, static pressure measurements were taken at these taps by means of an air-water differential manometer. Granular material entering the manometer lines through the static pressure openings, at first caused trouble, but later, this problem was alleviated by placing small automobile fuel-line filters in the manometer lines close to the lucite wall. In order to measure static pressure at closer intervals within the column, it

was necessary to fabricate a static pressure probe which is described in the next section.

2-4 Static Pressure Probe

The static pressure probe shown in figure 2-4 was made from a 3/8 in. (9.525 mm) diameter stainless-steel heavy-wall tube with a solid stainless-steel hemispherically shaped tip. A 0.3 mm circumferential slot is located 5 diameters or 1-7/8 in. (37.6 mm) from the tip of the hemispherical end. Through this slot the static pressure within the suspension was measured. All static pressure measurements were made relative to a static pressure wall tap located 131.5 cm above the bottom of the lucite section. For all the experimental runs, this tap remained in clear water. Static pressures were measured with an air-water differential manometer which was read to ±0.0005 ft of water.

2-5 Electrical Resistance Probe

The local concentration, that is, the volume of solids per unit volume of suspension, was measured by means of an electrical resistance probe (see figure 2-4). The probe consists of two stainless steel balls of 0.25 in. (6.35 mm) diameter, plated with platinum metal and located 20.2 mm apart. For support, the balls are connected to the ends of two iron drill rods 15.5 cm long, which are insulated with coats of General Electric Glyptal and clear Tenaco. The whole probe assembly was attached to a movable carriage at the top of the column, and electrically connected as a leg of an AC Wheatstone Bridge. In addition, the electrodes were coated with platinum black to minimize polarization effects.

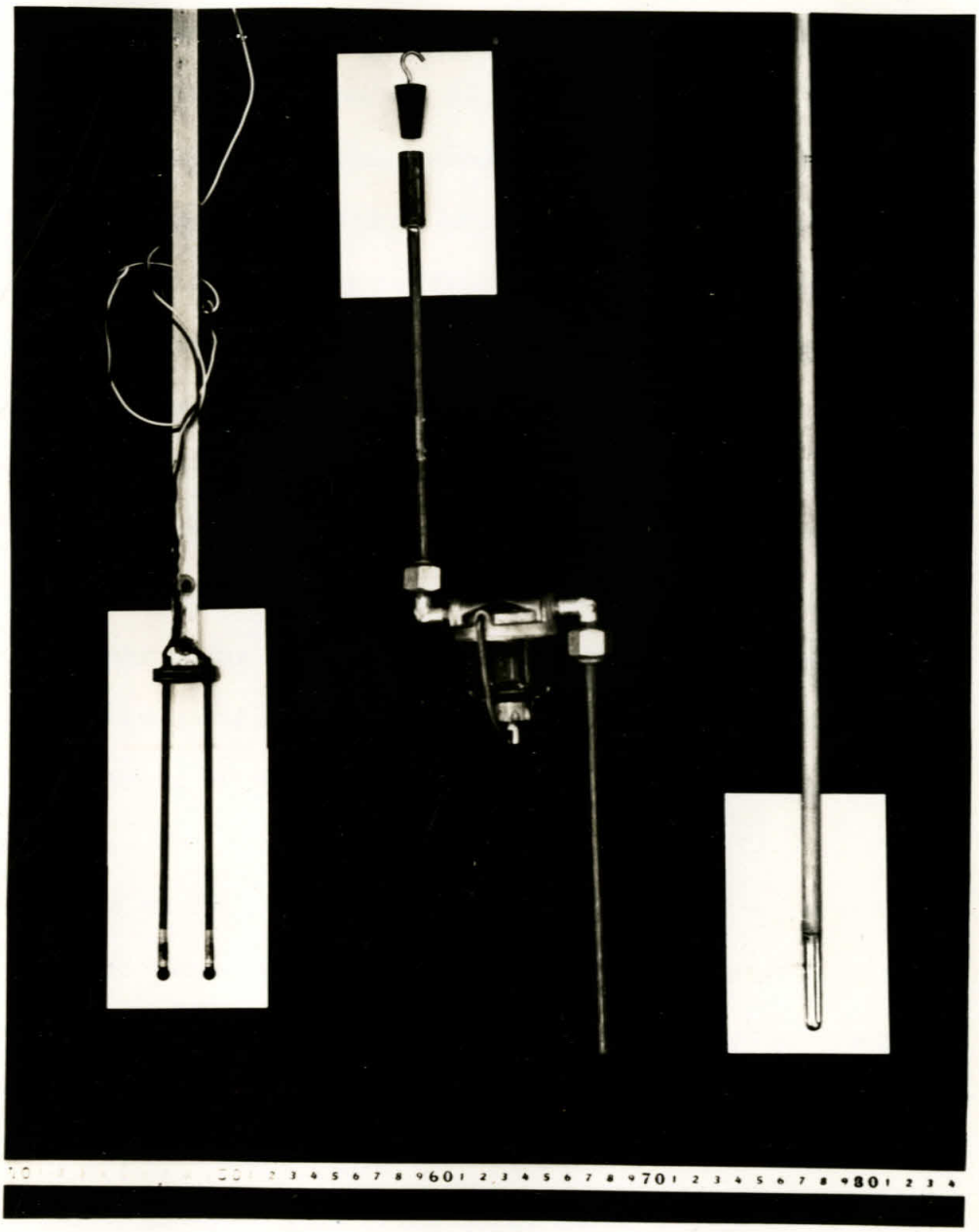

Fig. 2-4 Photograph of Electrical Resistance Probe, Siphon Sampler, and Static Pressure Probe. Note that scale is marked in centimeters.

2-6 The AC Wheatstone Bridge Circuit

The bridge circuit is shown schematically in figure 2-5. A Hewlett Packard Low Frequency Function Generator, Model 202A, sending out a 1000 cps sine wave was used to operate the bridge. The two fixed resistances, General Radio Decade Resistance Boxes, were set in the ratio 10:1, that is, 10,000 ohms and 1000 ohms, so that the variable leg of the bridge would require 10 times the resistance across the probe in order to balance the bridge. An Eico Decade Resistance Box having readings from 1 to 99,999 ohms by 1 ohm increments was used as the variable leg of the bridge. The variable capacitance is a Heathkit Decade Condenser. As an indicator of bridge balance, a Dumont Cathode-Ray Oscillograph, Model 304A, was used. When the bridge is unbalanced, an elliptical shaped pattern appears on the oscilloscope screen. The angle of the major axis of the ellipse with the horizontal indicates the resistive unbalance, and the amount of the opening of the ellipse, that is, the ratio of the minor and major axes, indicates the capacitive unbalance.

The resistance of the tap water varied with the ion content of the water and water temperature. No control of the conductivity was attempted. At intervals in each experiment, the probe was withdrawn from the suspension, and the resistance of the clear water above the suspension was measured. This procedure enabled one to prepare a graph of resistance of the clear water vs. time for each experiment. The resistance of the clear water, as measured with the resistance probe, might change from 650 ohms to 700 ohms in

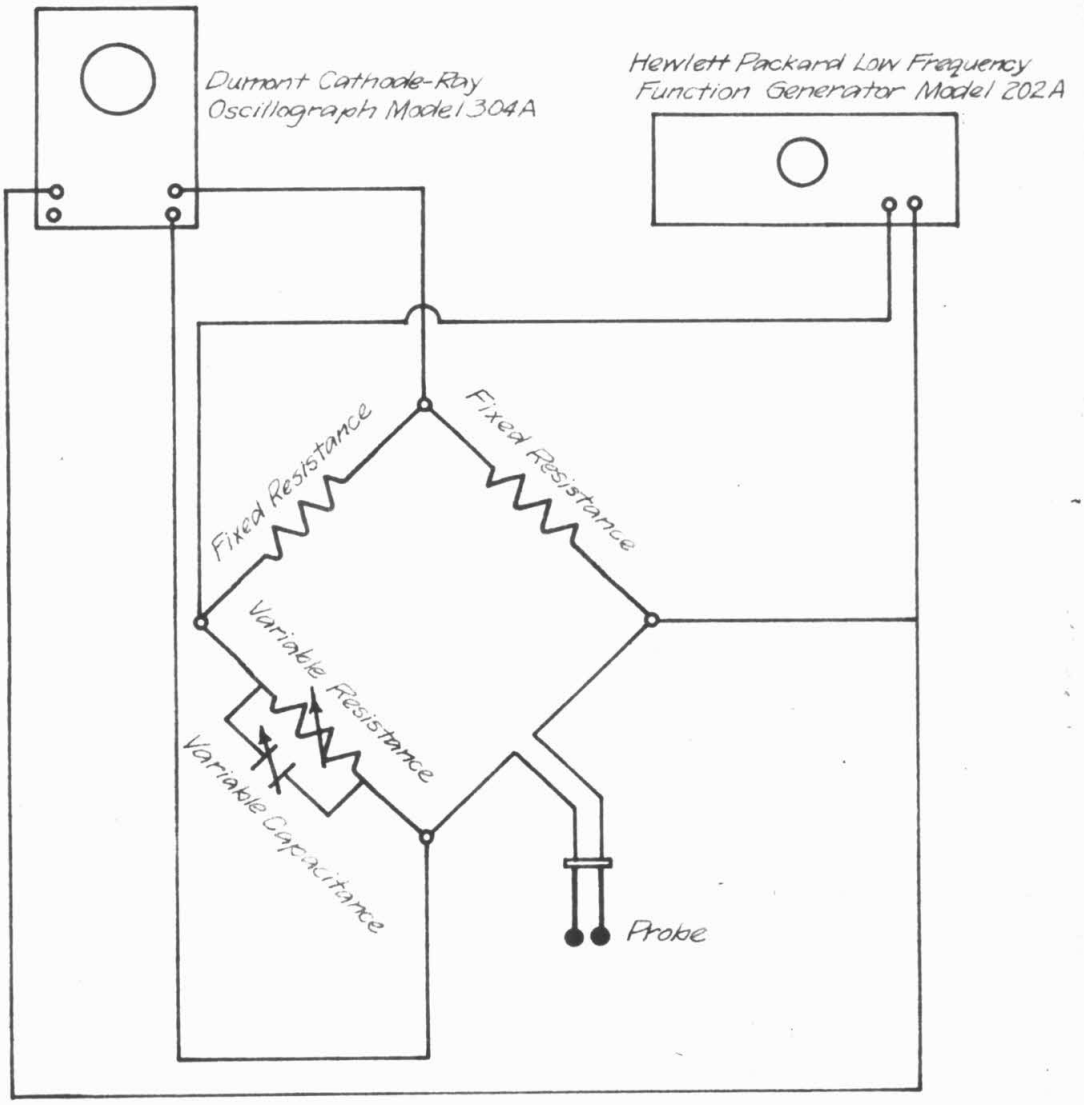

Fig. 2-5 Schematic of AC Wheatstone Bridge Circuit

one hour. This was due, most likely, to the wearing away of the platinum black from the electrodes. Before each run, the electrodes were given a fresh coat of platinum black by means of a 6 volt dry cell battery and a solution of platinum potassium chloride and lead acetate in distilled water. The resistance of the clear water was very easy to measure and could always be determined, for example to ±0.05 ohms over the range of the clear water values. Very large changes in the resistance of the tap water often occurred if the whole reservoir was emptied and replaced with new tap water. The tap water resistance might be 350 ohms one week and as high as 650 ohms a week later. Resistance measurements within the suspension were more difficult to determine, because one had to balance an elliptical oscilloscope pattern which was continually flip-flopping. At high concentrations of suspended particles, the resistance seemed to vary the greatest amount. Variations of ± 5 ohms in a reading of 950 ohms were not uncommon.

2-7 Concentration Measurements with a Resistance Probe

The use of an electrical device for measuring local concentration within suspensions of particles has been successfully employed by Lamb and Killen (13), Velock and Gorin (14), and Morse and Ballou (12).

Maxwell (30) solved a potential problem for the resistivity of a conducting medium filled with conducting spheres. Maxwell's expression for the resistivity of such a medium is:

$$P = \frac{2p_1 + p_2 + C(p_1-p_2)}{2p_1 + p_2 - 2C(p_1-p_2)} p_2 \qquad (2\text{-}1)$$

where P = resistivity of the compound medium

p_1 = resistivity of the spheres

p_2 = resistivity of the medium

C = volume concentration of spheres

Equation 2-1 is derived for low concentrations, that is, the distance between spheres must be large compared to the sphere diameter. Lamb and Killen (13) found equation 2-1 to be reliable for measuring air concentrations as high as 90 per cent by volume in high velocity water flows.

Since a suspension of sand grains or glass beads in water does not represent the ideal suspension of uniform spheres, it becomes necessary to check the reliability of the application of Maxwell's formula for the measurement of the concentration of non-conducting particles suspended in tap water. For a suspension of non-conducting spheres in a conducting medium, equation 2-1 reduces to:

$$C_r = \frac{R-R_f}{R+\frac{1}{2}R_f} = \frac{R/R_f-1}{R/R_f+\frac{1}{2}} \qquad (2\text{-}2)$$

where R_f = resistivity of the medium (fluid)

R = resistivity of the suspension

C_r = volume concentration of the spheres

Since only the value of R/R_f is needed in equation 2-2, one may substitute resistance measured with a probe for resistivity. The probe geometry of two spherical electrodes was chosen because the spherical

shape offers the same drag resistance to fluid flow from any direction. Since the probe was designed to be placed in a flow in which the fluid and the suspended particles would be moving locally in many directions, the spherical electrode seemed preferable to the flat plate which is more commonly chosen for resistance measurements due to its excellent collimation of the electrical field.

2-8 Method of Calibration of Resistance Probe

A fluidized suspension of solid particles, that is, sand grains or glass beads, was made in the fluidization column. Electrical resistance measurements were then taken at various levels along the vertical axis of the column. Periodic measurements in the clear water above the suspension were made in order to record any changes in the resistance of the clear water. The time was recorded for each reading of resistance. From equation 2-2, the value of C_r was computed using the value of the resistance within the suspension and the calculated value of the resistance of the clear water from a graph of the clear water resistance vs. time.

Various longitudinal static pressure profiles within several suspensions were made in order to determine whether or not the static pressure for a given level within a suspension was uniform over the cross-section of the column. Within the relative error for making the measurements with an air-water differential manometer, the static pressure was constant for a given level within a suspension. Similarly, electrical resistance profiles were made over the depth at various positions within a suspension over the cross-section of the

column. Again, the profiles seemed to be the same everywhere with the exception that when the probe came within about two electrode spacings (4 cm) of the side of the column, wall effects appeared to change the resistance. Similarly, the effect of the wall with the probe in clear water was noticed also by bringing the probe close to the wall.

The experimental measurements for the study herein reported were subsequently confined to profiles taken along the central axis of the fluidization column. It was assumed that any wall effects could be neglected and that all the results would be interpreted as if the suspension had properties which varied only in the vertical direction.

A plot of C_r vs. elevation in the suspension, y, was made and the area under this curve, that is,

$$\int_a^b C_r(y)dy \qquad (2-3)$$

was evaluated either by use of a planimeter or by Simpson's rule. With the assumption of uniform static pressure and uniform concentration for any level within a suspension, equation 2-3 may be interpreted as a measure of the total amount of material between levels of integration.

From a static force balance for the suspension, one can show quite easily that the difference in static pressure between any two elevations depends on the total weight of solid material in suspension between these two levels. Thus it is possible to compare the results of a static pressure profile and the integral of the electrical resistance formula for measurements along the central axis of the column

in order to determine the calibration for the resistance probe.

The algebraic procedure will now be explained. From a static force balance, one obtains:

$$\rho_f g \frac{dh}{dy} = -C(\rho_s - \rho_f)g \tag{2-4}$$

where h = piezometric or static head of fluid [L]

C = volume concentration of solids in suspension [L^3-L^{-3}]

ρ_s = mass density of solid particles [ML^{-3}]

ρ_f = mass density of fluid [ML^{-3}]

g = acceleration of gravity [LT^{-2}]

Assuming $C = KC_r$ where K is a constant, and C_r is given by equation 2-2,

$$K = \frac{h_a - h_b}{(\frac{\rho_s}{\rho_f} - 1)\int_a^b C_r(y)dy} \tag{2-5}$$

K can be evaluated from equation 2-5. Various levels at which the static pressure was measured were chosen as the limits a and b. In this manner, for any given suspension, it was possible to evaluate K over a range of concentrations. For each suspension, a graph of K vs. C_r was prepared, using the mean value of C_r for the interval of integration used to evaluate K. Measurements of resistance (i.e., C_r) were usually taken about 1.5 cm apart and measurements of the static head were made about 2.5 cm apart. The usual interval of integration for C_r was 5 cm. For integration by Simpson's rule steps of 1.25 cm, and five values of C_r read from the C_r vs. depth profile,

were used. To obtain the values of concentration, C, the values of C_r were multiplied by appropriate values of K read from the graph of K vs. C_r for the suspension.

In Appendix II are found the calibration curves, K vs. C_r, for the experimental runs herein reported. Generally, one notes that K has a large value, about 1.3 to 1.4, for small values of C_r, about 0.02 to 0.04. At higher values of C_r, that is, about 0.12 to 0.28, K has a value of 1.05 to 0.98. The scatter of the K vs. C_r measurements is explainable when one considers the accuracy of making the pressure measurements. At low values of the concentration, one must take the difference of two static head measurements in which the relative error can be quite large. For example, in Run G18 (figure 4-6), near the top of the suspension, one might observe a difference in the static head over the interval of integration of (0.0100 ± 0.0005 ft) minus (0.0020 ± 0.0005 ft) H_2O, which equals 0.0080 ± 0.0010 ft or a relative error of 12.5 per cent. Near the bottom of the suspension, one might observe for the same interval of integration a difference of static head equal to 0.0550 ± 0.0010 ft (i.e., (0.3101 ± 0.0005 ft) minus (0.2460 ± 0.0005 ft) H_2O) or a relative error of only 1.8 per cent in static head. However, although the scatter of the K vs. C_r is explainable, no reason for the trend of the K values can be given.

2-9 Relative Error in C_r Values

Let us now consider the relative error in equation 2-2 arising from the error in local values of the resistance, R, within the

suspension. In terms of relative error, equation 2-2 becomes:

$$\frac{\Delta C_r}{C_r} = \frac{\Delta R/R_f}{\frac{R}{R_f} - 1} - \frac{\Delta R/R_f}{\frac{R}{R_f} + \frac{1}{2}} \qquad (2\text{-}7)$$

Using data from Run G 18 as illustrative of relative error in C_r, let us consider values of the resistance from the same two intervals discussed in section 2-8 for relative error in the static head. Table 2-1 contains a summary of these data. The value of $\Delta C_r/C_r$ given for both positions is the sum of the values of both terms on the right hand side of equation 2-7.

Table 2-1

Relative Error in Electrical Resistance Equation

for Data Taken from Run G18

Position	$R \pm \Delta R$ (ohms)	R_f (ohms)	C_r	ΔC_r	$(\frac{\Delta C_r}{C_r})$	K (from fig. II-1)	$KC_r = C$
1	666 ± 1	648	.0182	.0010	.0551	1.41	.0257
2	930 ± 5	685	.1925	.0034	.0179	1.00	.192

One sees that the relative error in C_r for the low concentration is about 6 per cent and for the higher concentration is only about 2 per cent for the data in Table 2-1. The trend for the relative error in C_r to be higher at low concentrations than at high concentrations is the same trend as for relative error of the static head.

To summarize, one observes that the static head measurements and the electrical concentration measurements show large relative

errors for low values of the concentration. To reduce these errors one should develop instrumentation to determine more accurately the mean value of the static pressure and also the magnitude and period of any fluctuation of the static pressure from its mean value. Further work should be done on the electrical resistance probe in order to enable one to measure the magnitude of the fluctuations in the resistance (i.e., concentration) from its mean value. The method used to determine the mean value for the electrical resistance measurements reported herein was manually balancing the bridge circuit using a flip-flopping oscilloscope pattern as an indicator of balance. This method gives no direct measurement of the deviation of the instantaneous resistance values from the mean. As for the static head measurements, the inertia of the air-water manometer system was so large that no fluctuation of the water level in the manometers was noticed.

2-10 Siphon Sampler

A siphon sampler shown in figure 2-4 was made to allow small samples of the suspended particles to be taken from various levels within a suspension. Because of the lack of information, such as local velocity in the suspension, the siphon sampler was relied upon only to determine the characteristics of the suspended particles from a given sampling location and not as a means of determining the local concentration of particles. These samples, which were later analyzed to determine the local distributions of particle free-fall velocity, were

of the order of 2 to 10 gms from a typical total suspension of some 14 to 18 kg of solid particles. The siphon sampler consists mainly of an automobile fuel-line filter jar connected with two vertical copper tubes with inside diameters of about 4 mm. The total volume capacity of the filter bowl and tubes is about 50 cm^3. A rubber stopper was placed in the open end of the upper tube. If the whole sampler was placed under water and the stopper removed, the difference in pressure across the open copper tubes would cause the water to flow into the sampler and displace the air. If the sampler was filled completely with air, that is, an air volume of about 50 cm^3, it would take approximately 3.5 seconds for the water to displace the air. Thus the discharge was about 14 cm^3/sec. The bottom of the lower copper tube is belled to about 7 mm diameter, so that the inlet velocity at the bellmouth is about 38 cm/sec. The total volume of sample removed from the suspension at any level could be varied by partially filling the siphon sampler with water, thus changing the effective volume, i.e., the amount of air to be displaced, of the sampler. The upper opening through which the air escaped from the sampler was screened to prevent material from entering the sampler through this opening. This was a precaution introduced because for certain samples taken from the bottom of a suspension, the entire siphon sampler was submerged in the suspension.

2-11 Analysis of Granular Materials by Sieving and Measurements of Free-Fall Velocities for Individual Particles

A granular material such as glass beads or sand was selected

for study, and a sieve analysis was made using an appropriate set of $(2)^{1/4}$ Tyler sieves by the standard sieve analysis procedure in a Tyler Rotap Shaker for 10 minutes shaking time. From such an analysis one can determine the distribution of sizes of the granular material by weight as retained on the various sieves. Using a Jones sample splitter, the granular material was divided until a sample of about 50 to 100 particles was obtained. Each of these particles was dropped in a glass-walled column, 4 in. (10.2 cm) diameter, filled with distilled water and the fall time for a measured distance of 124 cm was measured using a hand-held stopwatch read to the nearest 1/20 second. This procedure enabled one to calculate the distribution of free fall velocities by number for the parent material. The parent material refers to all of the material placed in the fluidization column for each particular experiment. The total weight of the parent material placed in the column was determined to the nearest 0.01 pound (4.54 gm).

2-12 Measurement of Mean Concentration

The granular material in the fluidization was put into suspension by the upward flowing water, and the amount of expansion was changed by changing the water discharge. For each suspension, a series of still photographs were taken; the discharge was recorded, and the depth of the suspension was determined by the height of the upper interface above the support plate, measured by a fixed scale on one wall of the column. These measurements enabled one to calculate the mean concentrations of the suspensions for various water discharges

by the relationship:

$$\overline{C} = \frac{W}{\gamma_s A d} \tag{2-8}$$

where $\overline{C}$ = mean concentration $[L^3 L^{-3}]$

W = total weight of granular material in the fluidization column [F]

γ_s = unit weight of the granular material $[FL^{-3}]$

A = cross-sectional area of fluidization column $[L^2]$

d = depth of suspension [L]

2-13 Local Siphoned Samples

For certain selected suspensions, a static pressure profile and an electrical resistance profile were made along the vertical central axis of the fluidization column. From these profiles one is able to determine the concentration vs. depth relationship for each suspension. From various levels in the suspensions, samples of the suspended particles were siphoned off, using the siphon sampler. These siphoned samples were dried and weighed and split down to a sample of about 50 particles, using a Jones sample splitter. Each of these particles was dropped in a column of distilled water and its free-fall velocity determined. Thus, one was able to determine the particle free-fall velocity distributions for the various sampling levels in each suspension, and then associate the individual particle velocity distributions with local concentration as determined from the static pressure and electrical resistance profiles.

2-14 Hindered Settling Velocity Measurements

Measurements were made of the hindered settling velocity of a suspension by quickly stopping the upward flow of water by shutting

the quick-closing valve and measuring the rate of fall of the upper surface of the suspension. Using a 35-mm single-frame still camera, a series of photographs of the falling surface of the suspension were taken. An electric timer was included in each photograph so that the time that the suspension surface passed various levels on the fixed scale on the wall of the column could be recorded. A plot of elevation of the upper surface vs. time was made in order to determine the rate of fall of the suspension, i.e., the hindered settling velocity. Measurements of the hindered settling velocity were also made by visually watching the upper surface and determining the fall time for a measured distance with a hand-held stopwatch. Further discussion of the hindered settling experiments will be made in chapters 4 and 5.

2-15 Temperature Measurements

Since there was no temperature control of the water, the temperature of the water flowing in the column was checked frequently during the experiments. However, it varied little, and for all runs stayed within the range 20 to 24° C.

CHAPTER 3

CHARACTERISTICS OF THE SOLID MATERIALS

The fluidization properties of four granular materials were studied in detail. The characteristics of these materials are summarized in Table 3-1.

3-1 Sieve Analyses

Figures 3-1 and 3-2 show graphically the distribution of the sieve sizes by weight plotted on logarithmic probability paper, on which logarithmic-normal distributions are represented by straight lines. Probability graph paper was introduced by Hazen (21) and extensively used by Otto (23) for the analysis of granular materials. A distribution which is log-normal or nearly log-normal may be identified with a certain geometric mean size, D_g, and a geometric standard deviation, σ_g. For a distribution which is log-normal or nearly log-normal, let D_g be the value of the sieve diameter which represents the mean of the sample population. It follows from the properties of a log-normal distribution that $D_g = \sqrt{D_{84.1}\, D_{15.9}}$ where $D_{84.1}$ is the size for which 84.1 per cent of the material is finer and $D_{15.9}$ is the size for which 15.9 per cent of the material by weight is finer. Similarly, the geometric standard deviation, σ_g, is given by $\sigma_g = \sqrt{D_{84.1}/D_{15.9}}$.

3-2 Specific Gravity

The specific gravity of the granular materials was determined by the standard method of weighing a representative sample (about 0.5 gm) dry in air and then submerged in distilled water in a 25 ml pycnometer. The experimentally determined values of the specific gravity

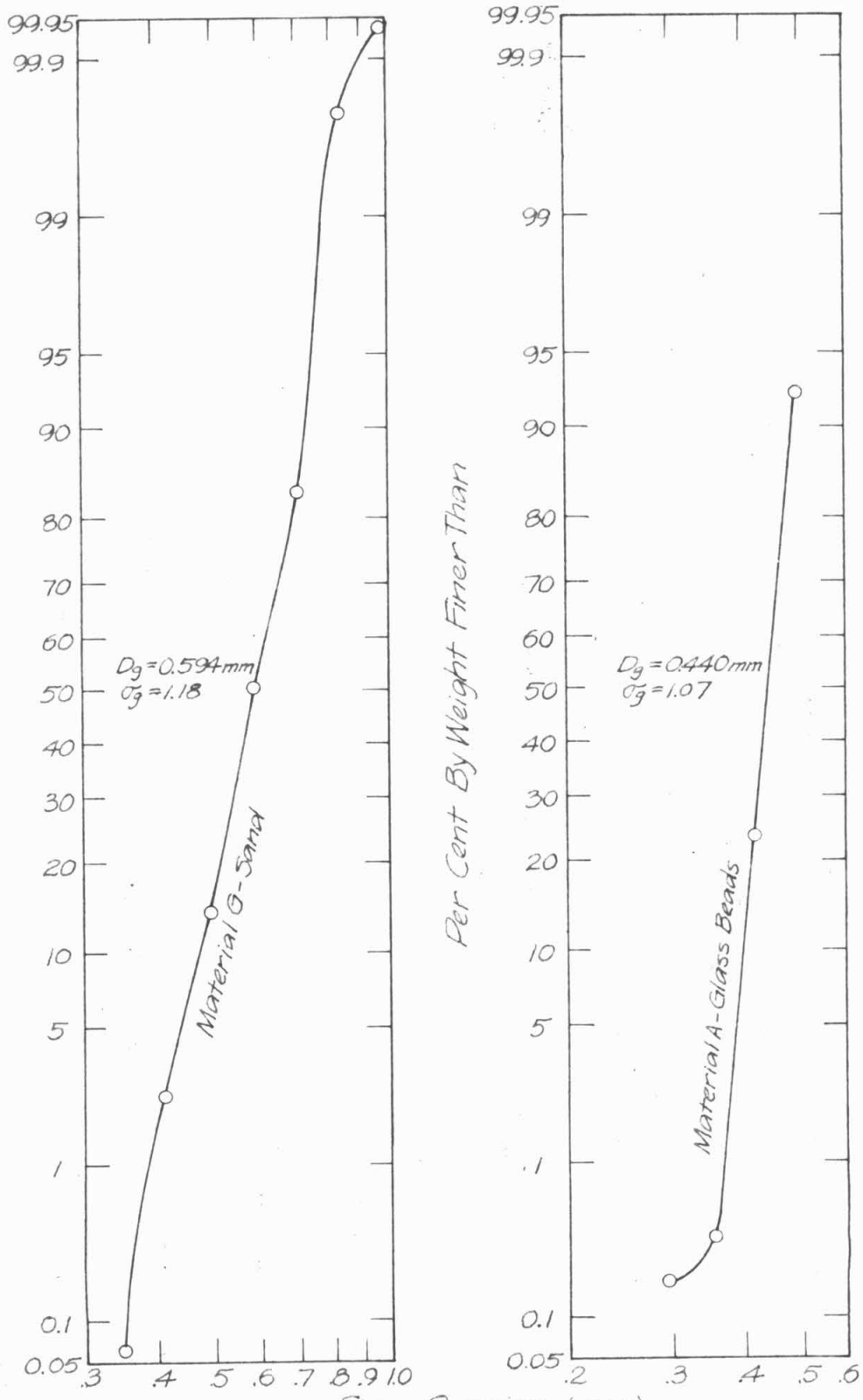

Fig. 3-1 Sieve Analyses of Granular Materials A and G

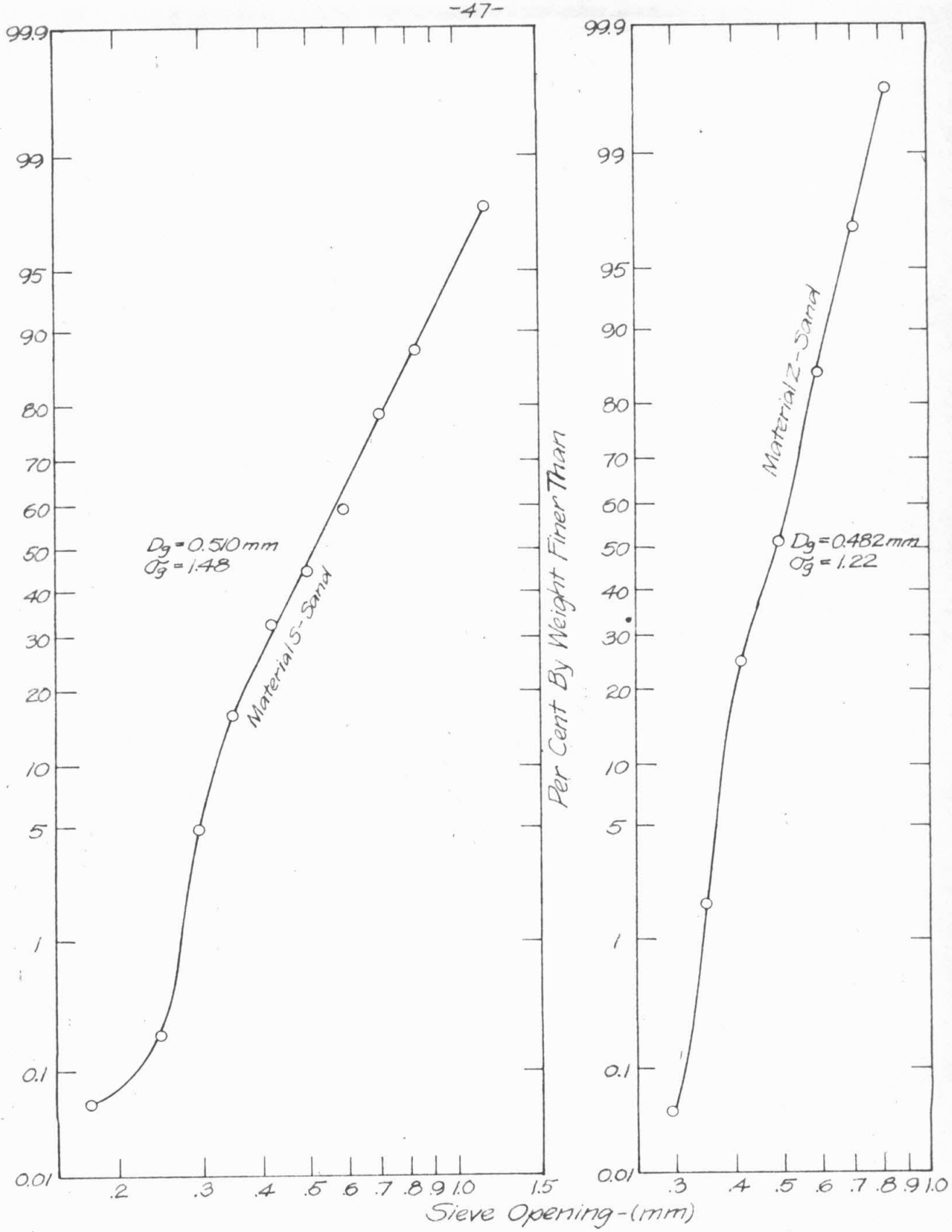

Fig. 3-2 Sieve Analyses of Granular Materials Z and S

are given in Table 3-1.

3-3 Free-Fall Velocity Distributions

Figures 3-3 to 3-6 are graphs of the distributions of the free-fall velocities for the four granular materials by number of particles, uncorrected for particle weight. These data were obtained by dropping a representative sample of the solid particles individually in a column filled with distilled water and measuring the fall time over a fixed distance. Each plotted point represents the observed free-fall velocity of a single particle. All points were plotted except in the central portion of the curves where, when necessary to avoid overcrowding, every other point was plotted. In the figures 3-3 to 3-6, the plotting position on the probability scale is that suggested by Thomas (24),

$$P = \frac{m}{N+1}$$

where m = rank of a particular free-fall velocity, w_m

$m = 1, 2, 3, \ldots\ldots, N$

$w_{m+1} < w_m$

P = per cent of particles with free-fall velocities greater than, or equal to, the corresponding velocity on the ordinate

In order to compare the various materials, it is better to know the distribution of the free-fall velocities by weight than by number of particles. With certain restrictions placed on the magnitude of the spread of the free-fall velocities, one can show (see Appendix I-1) that if the free-fall velocities of spheres are log-normally distributed by number, they will also be log-normally distributed by weight.

Table 3-1

Summary of Characteristics of Granular Materials

Name of Material	A Glass Beads	Z Quartz Sand	G Gold Jacket Sand	S Sand
Main Constituent	Glass	Quartz	Quartz with Iron Oxide Coating	
Geometric Mean Size, D_g (mm)	0.440	0.482	0.594	0.510
Geometric Standard Deviation, σ_g	1.07	1.22	1.18	1.48
Specific Gravity	2.49	2.65	2.66	2.67

Results of Sieve Analyses

Tyler Mesh No.	Sieve Opening (mm)	Per Cent Retained by Weight Material A	Material Z	Material G	Material S
14	1.168				2.33
16	0.991		0	0.06	Not Used
20	0.883		0.36	0.19	9.75
24	0.701		2.63	16.34	9.64
28	0.589	0	12.73	33.11	18.68
32	0.495	7.35	33.47	36.26	15.10
35	0.417	69.17	26.19	11.57	11.15
42	0.351	23.12	22.88	2.41	17.21
48	0.295	0.18	1.70		11.21
60	0.246		0.04		4.66
80	0.175				0.16
Pan		0.18	Trace	0.06	0.05
Sieve Analysis No.		223	228	231	226

Note: For comparison of free-fall velocities see Table 3-2.

The geometric standard deviations of both distributions are the same, but the difference of the geometric means is given in Appendix I-1 by:

$$\log\mu = \log w_g + \frac{3b}{\beta} (\log \sigma_w)^2 \qquad (3\text{-}1)$$

where μ = geometric mean of free-fall velocities by weight

w_g = geometric mean of free-fall velocities by number

σ_w = geometric standard deviation of both distributions

$b = 2.303$

$\beta = \frac{1+m}{2-m}$

$m = -\frac{d(\log C_D)}{d(\log Re)}$ = the negative slope of the curve for drag coefficient, C_D, vs. Reynolds number, Re

Computed values of μ by equation 3-1 for the granular materials used in this study are given in Table 3-2.

A more accurate (but more time-consuming) method of converting the distributions by number to distributions by weight was tried. In this procedure, the Reynolds number-drag coefficient curve was used to compute the sedimentation diameter, D_s, that is, the diameter of the equivalent density sphere having the observed free-fall velocity, w, in the same fluid. Each particle was assigned the relative weight $D_s^3/\Sigma D_s^3$ where ΣD_s^3 is the sum of the cubes of the computed diameters for the entire sample. If the particles are spherical or nearly spherical in shape and have the same density, the ratio $D_s^3/\Sigma D_s^3$ is the relative weight of each particle in the sample. Graphs of free-fall velocity vs. cumulative relative weight based on $D_s^3/\Sigma D_s^3$ were plotted

on logarithmic probability paper and each graph was evaluated for a mean free-fall velocity and a geometric standard deviation. Table 3-2 contains a comparison of the two methods, that is, by $D_s^3/\Sigma D_s^3$ and by equation 3-1, for converting the free-fall velocity distributions by number of particles to distributions by weight.

Table 3-2

Comparison of Methods for Converting Number Distributions to Weight Distributions

	By Number		By Weight			
			By $D_s^3/\Sigma D_s^3$		By Equation 3-1	
Material	w_g ($\frac{cm}{sec}$)	σ_w	μ_1 ($\frac{cm}{sec}$)	σ_w	μ_2 ($\frac{cm}{sec}$)	σ_w
A - Glass Beads	6.67	1.06	6.70	1.06	6.73	1.06
Z - Sand	7.10	1.19	7.70	1.21	7.72	1.19
G - Sand	8.49	1.16	8.95	1.16	9.06	1.16
S - Sand	5.95	1.41	7.59	1.32	8.16	1.41

The comparison of the two methods shows results consistent with the assumptions necessary to derive equation 3-1. When the geometric standard deviation of the distribution is less than 1.2, the means by weight, μ_1, and μ_2, for both methods compare very favorably, i.e., the difference in the two weighted means is 1 per cent or less. For material S, the widely distributed material, the comparison is not as favorable, that is, a difference in the weighted means of about 7.5 per cent is observed. Similarly, a comparison of the geometric standard deviations shows that the assumption of no change in this quantity is good to less

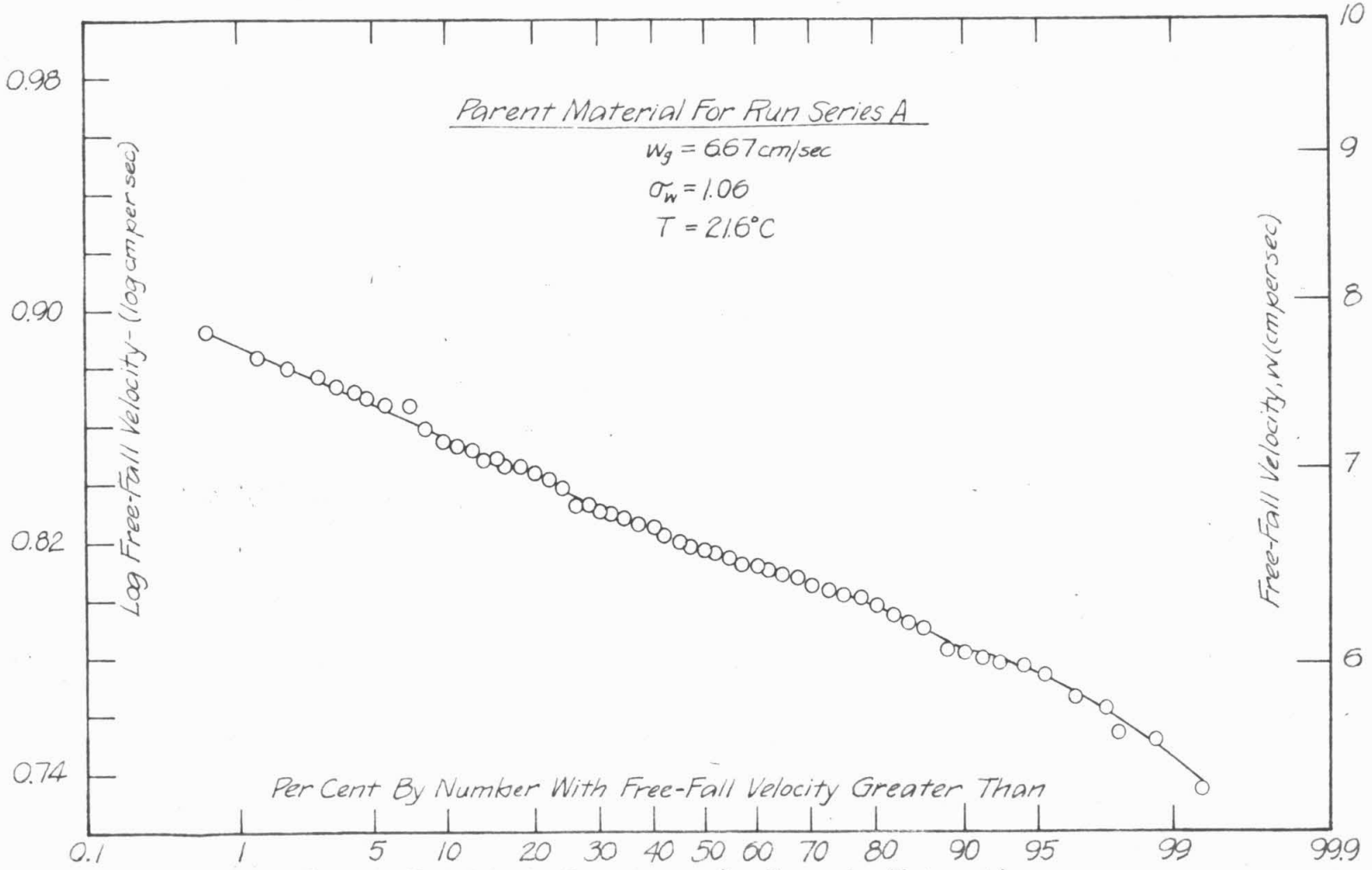

Fig. 3-3 Fall Velocity Distribution for Granular Material A

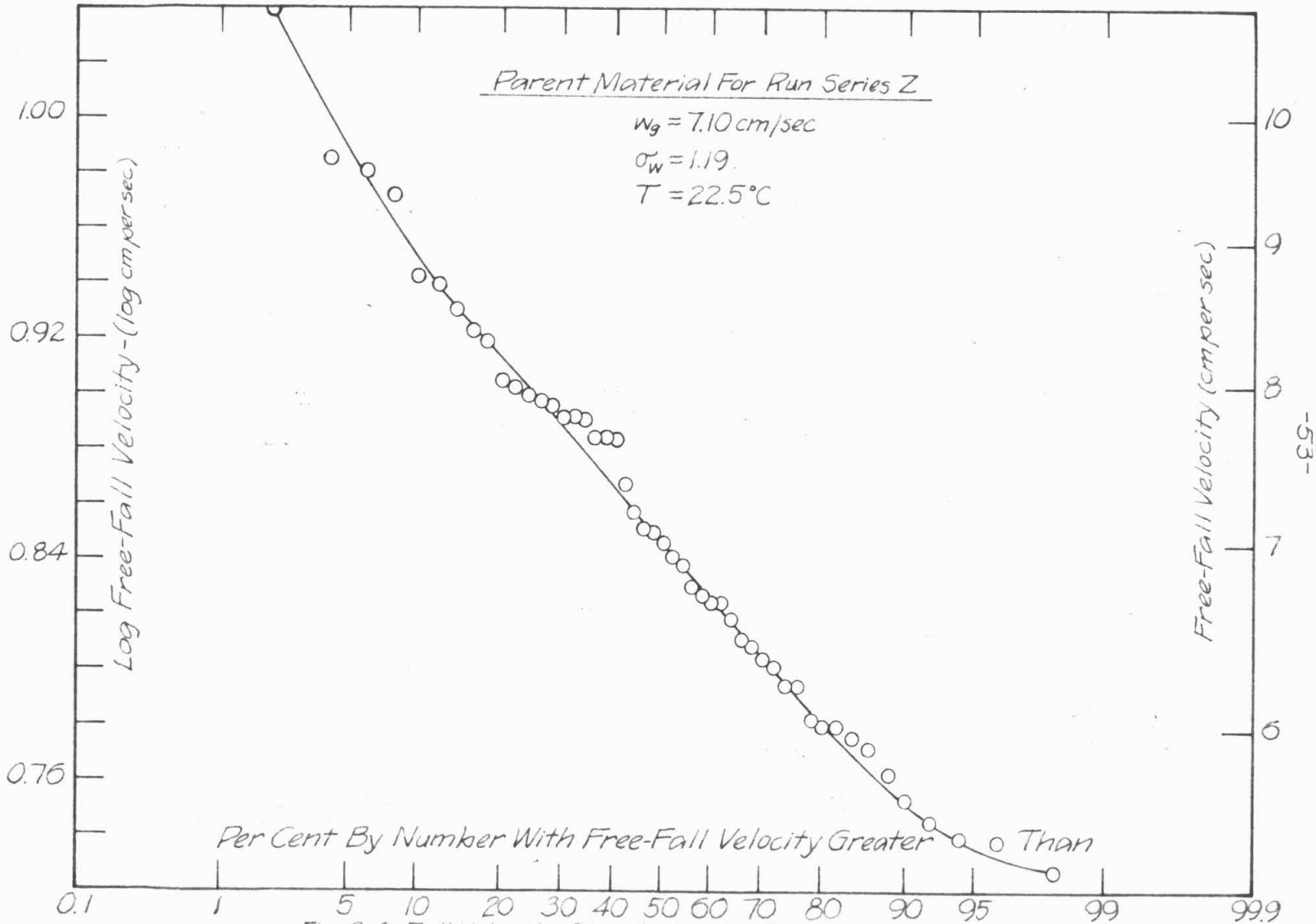

Fig. 3-4 Fall Velocity Distribution for Granular Material Z

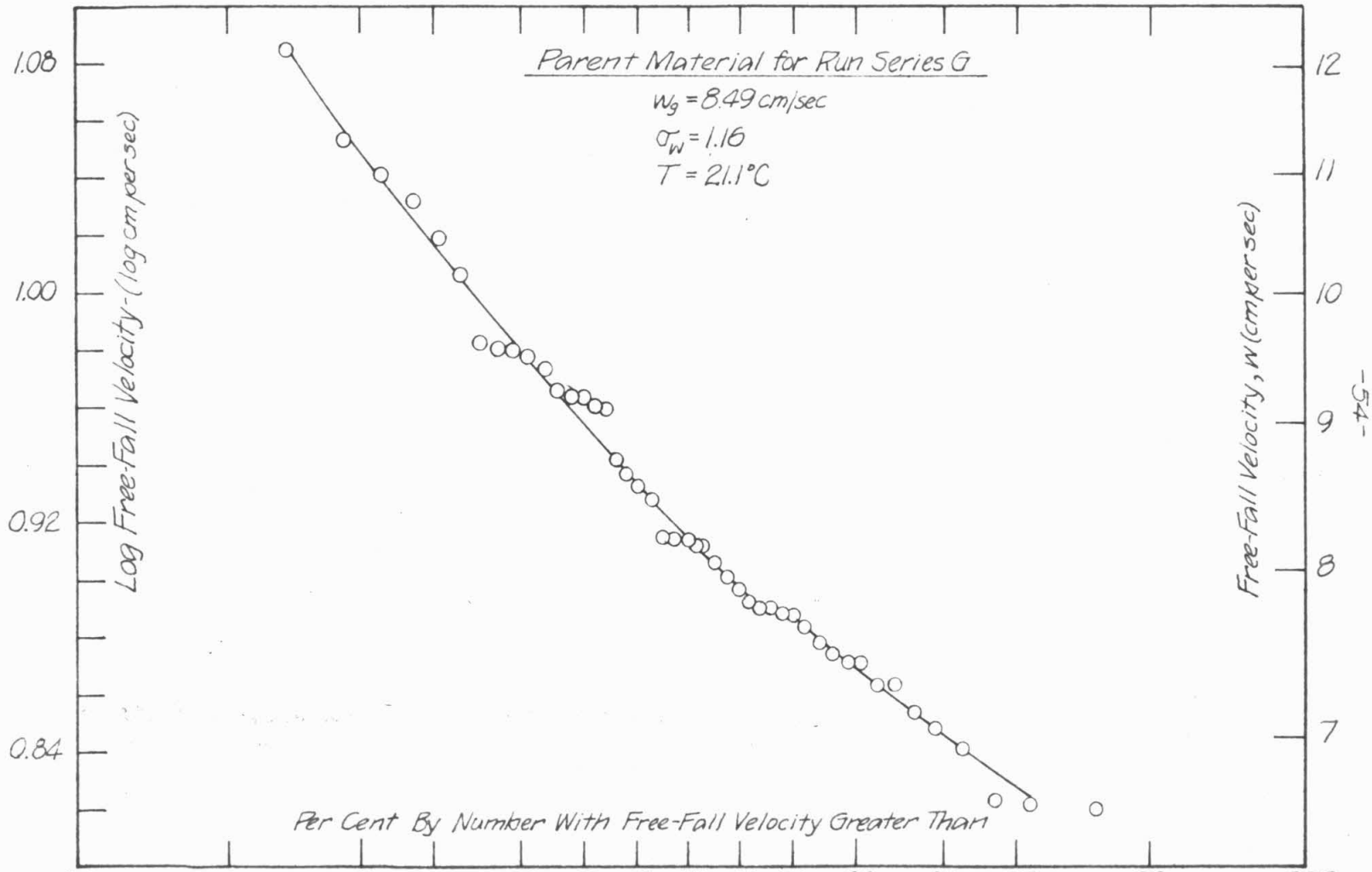

Fig. 3-5 Fall Velocity Distribution for Granular Material G

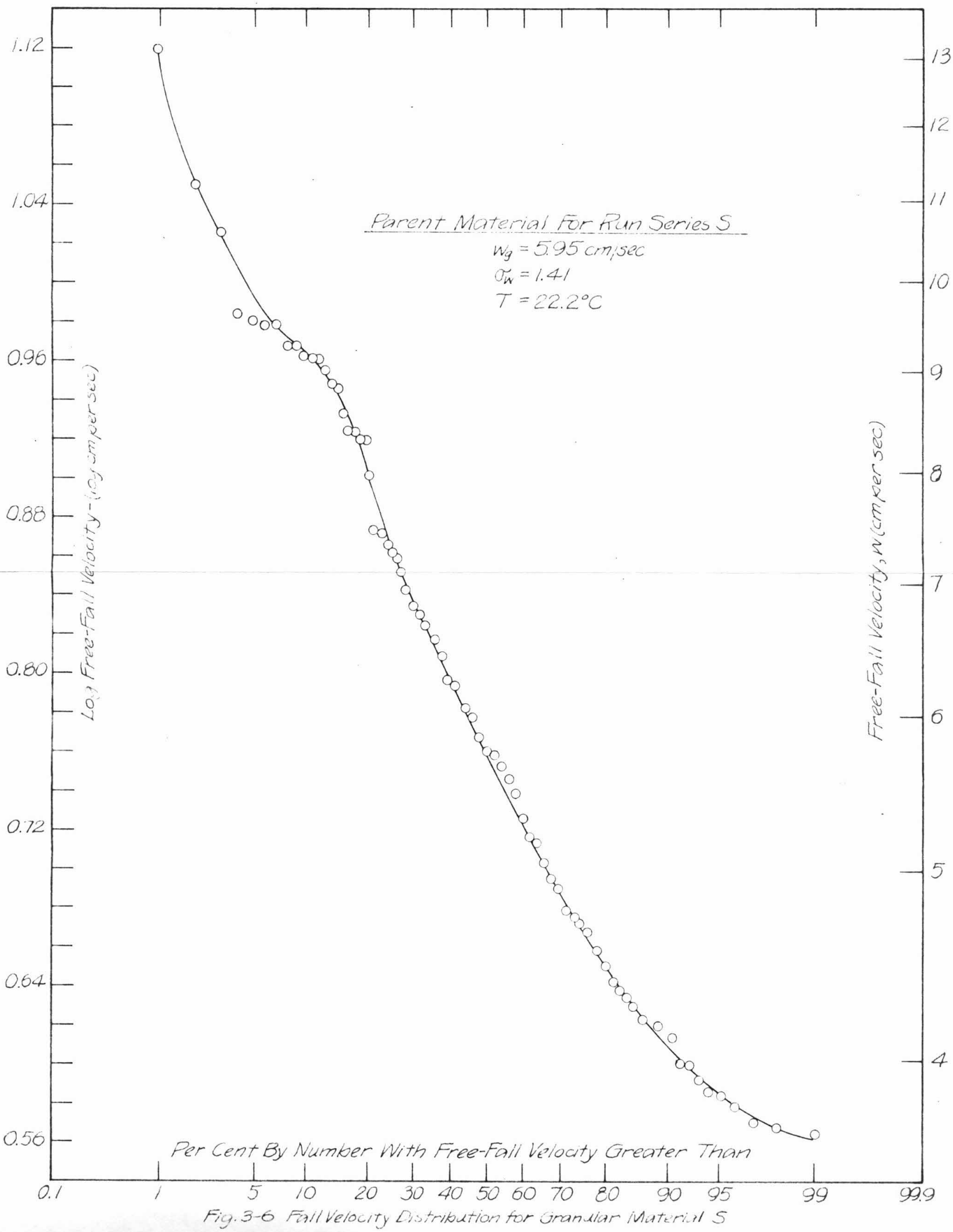

Fig. 3-6 Fall Velocity Distribution for Granular Material S

than 1 per cent for the materials A, Z, and G, but good only to within 8 per cent for material S. On the basis of this evaluation, it was decided to use equation 3-1 to convert the measured distributions of free-fall velocities by number to distributions by weight for those samples for which σ_w, the geometric standard deviation of the free-fall velocities, is less than 1.2. For all samples in which σ_w was measured to be greater than 1.2, the method of $D_s^3/\Sigma D_s^3$ was used to convert to a weight distribution.

3-4 Relationship between Sedimentation Diameter and Sieve Diameter

The sedimentation diameter, D_s, for a particle is defined as "the diameter of a sphere of the same specific gravity and the same terminal uniform settling velocity as the given particle in the same sedimentation fluid" by the Inter-Agency Committee on Water Resources (26). To determine the distribution of sedimentation diameters for each of the four materials studied, graphs of the sedimentation diameter were plotted on log probability paper where the position on the probability scale was based on the relative weight $D_s^3/\Sigma D_s^3$ for each particle. For each material, the distributions could be closely approximated by a log-normal distribution. Table 3-3 gives a summary of the data for comparison of sedimentation diameters and sieve diameters.

The data in Table 3-3 are in close agreement with the relation between sieve diameter and sedimentation diameter given in the Inter-Agency Report (26). This report (26) defines a parameter called a shape factor, S.F., which is used to describe particle shape. The

Table 3-3

Comparison of Sedimentation Diameters and Sieve Diameters

Material	Shape Factor	By Sieve Analysis: Geom. Mean Sieve Diam. D_g (mm)	By Sieve Analysis: Geom. Std. Dev. of Sieve Diam. σ_g	By Settling Analysis: Geom. Mean Sed. Diam. D_s (mm)	By Settling Analysis: Geom. Std. Dev. of Sed. Diam. σ_s
A - Glass Beads	1.0	0.440	1.07	0.450	1.07
Z - Sand	0.7	0.482	1.22	0.515	1.19
G - Sand	0.9	0.594	1.18	0.589	1.15
S - Sand	0.7	0.510	1.48	0.510	1.30

shape factor is defined as S.F. = $c/\sqrt{ab}$ where a, b, and c are, respectively, the longest, intermediate, and shortest of three mutually perpendicular axes of the particle. From visual observations only, with no direct measurements taken, the shape factors in Table 3-3 were estimated. Material S, a sand, is composed of the widest variety of shapes and sizes of particles, and it is the most poorly described by a log-normal distribution of sizes of the four materials studied. For this reason, the apparent agreement between the sieve diameter and sedimentation diameter for material S seems to be fortuitous.

One also notices in Table 3-3 that the geometric standard deviation of the sedimentation diameters appears to be less than the geometric standard deviation of the sieve diameters by an amount which increases as the geometric standard deviation increases. No explanation is available for this trend.

Microphotographs of samples of the granular materials studied are found in chapter 4.

CHAPTER 4

RESULTS OF EXPERIMENTS

The results of the fluidization experiments on four granular materials will now be presented. These experiments were done in order to make a detailed study of the properties of a suspension. As discussed in chapter 1, several investigators have examined the relationships between fluid discharge and mean concentration for suspensions of so-called "uniform" particles. The results reported herein attempt to take into account the nonuniformity of the granular materials studied in an effort to determine, by the measurement of such properties as local concentration and the local distributions of particle free-fall velocity, whether or not the relationships presented in chapter 1 hold true locally within a suspension. A better understanding of the physics of the suspension will permit future investigators, who put forth a theoretical analysis of a suspension, to decide more realistically which properties of a suspension are of primary importance for the basis of their analysis.

4-1 Mean Concentration and Superficial Velocity

Following the custom of previous investigators, the results of the measurement of mean concentration and superficial velocity are presented in graphical form in figure 4-1. On the logarithmic scale in figure 4-1 is plotted the mean concentration of particles, $\overline{C}$, which is the fraction of the total suspension volume occupied by the particles based on the measurement of the total dry weight of granular material in the fluidization column, the unit weight of the material, and the overall dimensions of the suspension. $\overline{C}$ is defined by equation 2-8

in chapter 2. The arithmetic scale for the superficial velocity, $\overline{u}$, is normalized using the mean free-fall velocity of the particles by weight, $\overline{\mu}$. The value of $\overline{\mu}$ used in figure 4-1 was determined by the method of relative weight, $D^3/\Sigma D^3$, described in chapter 3. The data in figure 4-1 cover the interval of mean concentration, $0.05 \leq \overline{C} \leq 0.60$; and a curve has been fitted by eye for each of the four materials over this range showing that $\overline{u}/\overline{\mu}$ increases as $\overline{C}$ decreases. It is important to understand that all the values of $\overline{u}$ for <u>each</u> material were normalized with the same value of $\overline{\mu}$, that is, only four values of $\overline{\mu}$ were used to normalize the data shown in figure 4-1. In Appendix II is a summary of the data covering all the suspensions measured in this study.

Table 4-1 is a summary of particle Reynolds numbers for the granular materials. The particle Reynolds numbers are based on the mean sedimentation diameter, D_s, and the particle mean free-fall velocity by weight, $\overline{\mu}$. Each of the four granular materials has a mean Reynolds number which is definitely outside the range of Stokes' law, and yet each is still in the region where the drag coefficient changes with Reynolds number.

4-2 Local Concentration and Superficial Velocity

For selected experimental runs, the local concentration-depth relationship for the suspension was determined by the method described in chapter 2. From various levels in each of these suspensions local samples of the suspended particles were siphoned off and analyzed. Figure 4-2 is a summary of data obtained from local measurements.

Table 4-1

Particle Reynolds Numbers for the Granular Materials

Material	Geom. Mean Sed. Diam. D_s (mm)	Geom. Std. Dev. of Sed. Diam. σ_s	Geom. Mean Free-Fall Vel. by Weight $\bar{\mu}(\frac{cm}{sec})$	Geom. Std. Dev. of Free-Fall Vel. σ_w	Temp. of Distilled Water T(°C)	Reynolds Number $\frac{D_s\bar{\mu}}{\nu}$
A - Glass Beads	.450	1.07	6.69	1.06	21.6	31
Z - Sand	.515	1.19	7.70	1.21	22.5	42
G - Sand	.589	1.15	8.95	1.16	21.1	54
S - Sand	.510	1.30	7.59	1.32	22.2	40

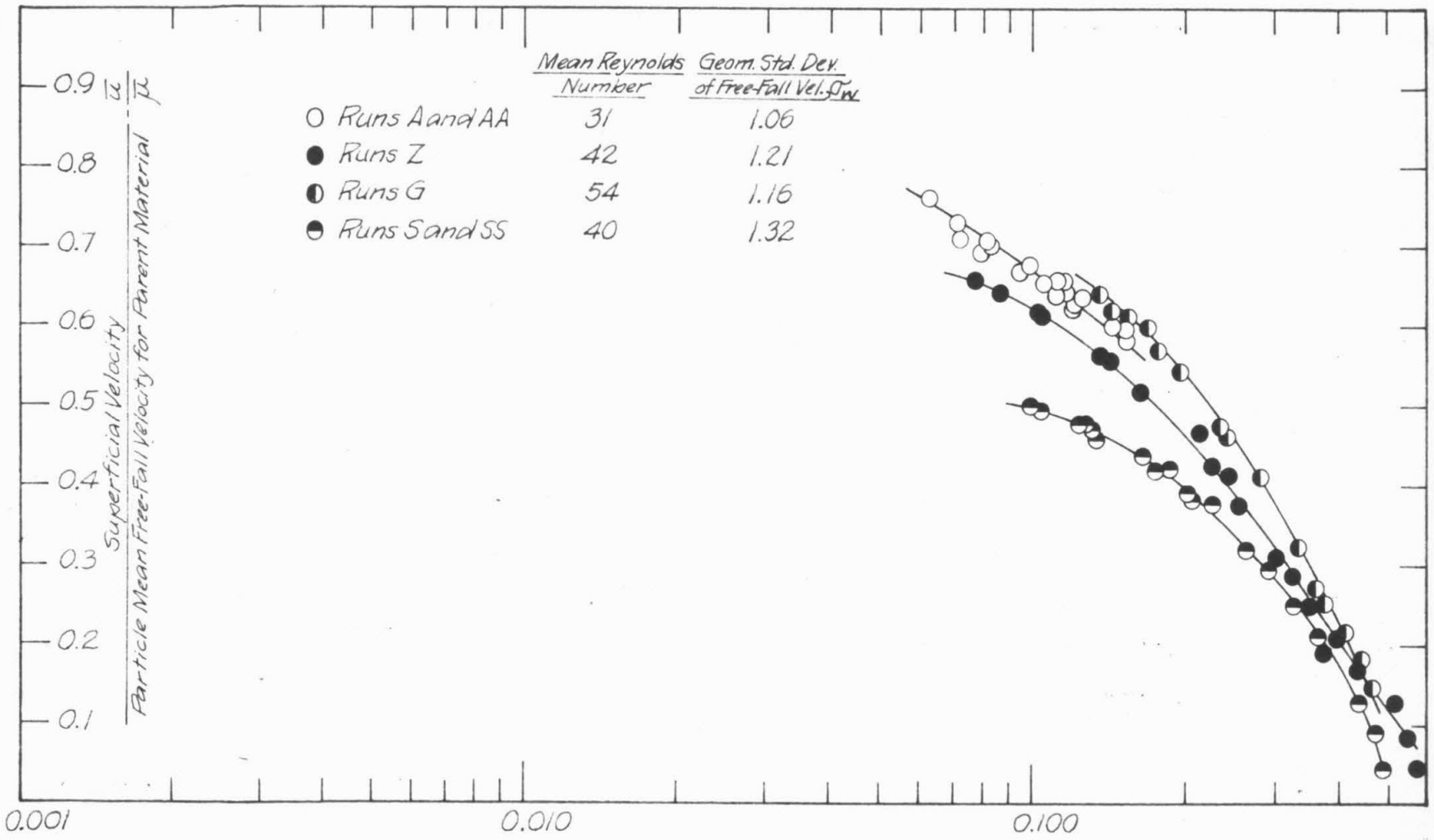

Fig. 4-1 Summary of Mean Concentration Data for Fluidized Suspensions

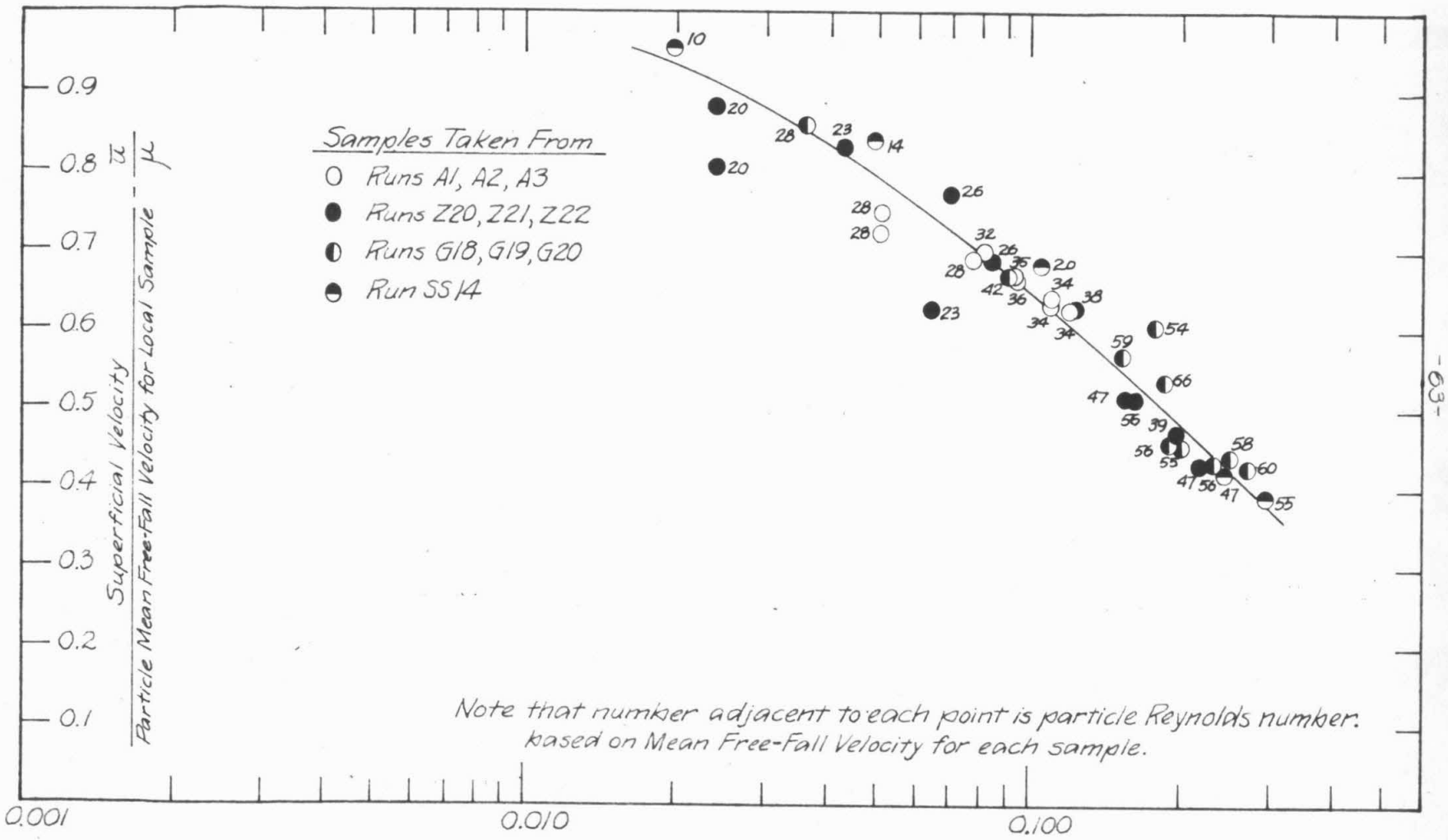

Fig. 4-2 Summary of Local Concentration Data for Fluidized Suspensions

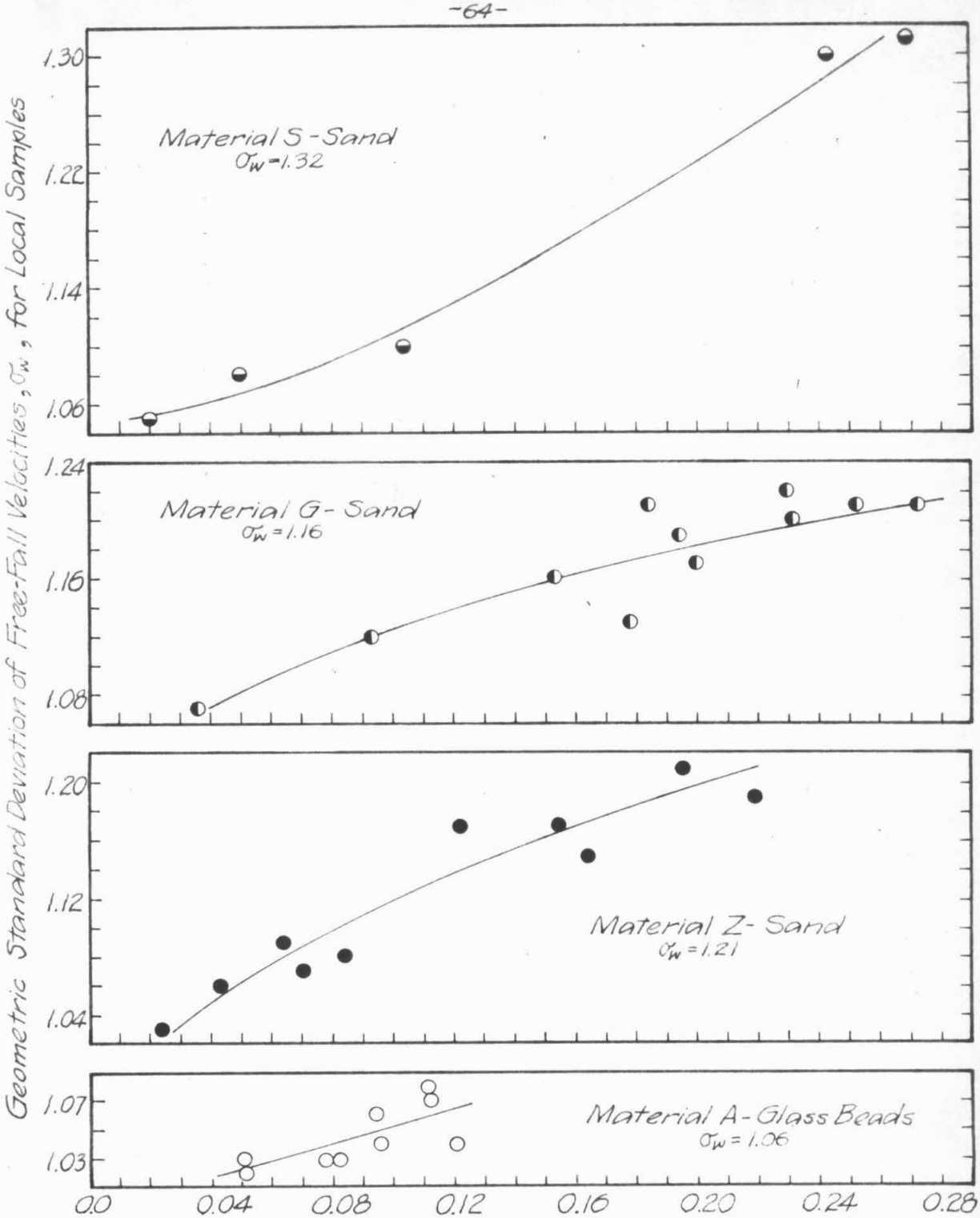

Fig. 4-3 Variation of σ_w with Local Concentration

Table 4-2

Summary of Fluidization Data for Suspensions Sampled Locally

Run No.	Sample No.	Superficial Velocity	Temp. in Upward Flow	Total Depth of Suspension	Mean Concentration	Sample Elevation	Local Concentration	No. of Particles in Sample	Temp. of Distilled Water	By Number: Geom. Mean Free-Fall Velocity	By Number: Geom. Std. Deviation of Free-Fall Velocity	By Weight: Geom. Mean Free-Fall Velocity	By Weight: Geom. Std. Deviation of Free-Fall Velocity	Local Free-Fall Reynolds Number
		$\bar{u}$(cm/sec.)	T(°C)	d(cm)	$\bar{C}$	y(cm)	C		T(°C)	w_g(cm/sec)	σ_w	μ(cm/sec)	σ_w	
A1	A1-1	4.67	21.6	70	.084	68.4	.051	44	21.6	6.21	1.03	6.22	1.03	28
	A1-2					34.5	.082	44	21.6	6.69	1.04	6.70	1.04	32
	A1-3					21.3	.094	43	21.6	6.90	1.07	6.99	1.07	35
A2	A2-1	4.48	22.1	60	.096	57.1	.051	38	22.2	6.18	1.04	6.20	1.04	28
	A2-2					29.5	.096	49	22.2	6.76	1.05	6.80	1.05	34
	A2-3					17.0	.111	38	22.2	7.02	1.09	7.16	1.09	36
A3	A3-1	4.27	22.5	48	.106	47.1	.078	48	22.2	6.15	1.04	6.18	1.04	28
	A3-2					21.2	.112	47	22.2	6.71	1.08	6.83	1.08	34
	A3-2S					21.2	.112	52	21.6	6.68	1.07	6.76	1.07	33
	A3-3					12.6	.121	51	22.2	6.59	1.06	6.76	1.06	34
	A3-3S					12.6	.121	54	21.6	6.65	1.05	6.69	1.05	32
Z20	Z20-1	4.70	22.5	58.5	.109	55.3	.024	50	22.5	5.32	1.03	5.33	1.03	20
	Z20-2					46.8	.043	48	22.8	5.60	1.06	5.65	1.06	22
	Z20-3					34.8	.070	45	22.8	6.05	1.05	6.09	1.05	26
	Z20-4					25.8	.122	45	22.5	7.44	1.17	7.49	1.17	38
	Z20-5					16.8	.164	60	22.5	8.63	1.15	9.14	1.15	56
Z21	Z21-1	4.30	22.8	43	.149	42.8	.024	49	22.5	5.35	1.03	5.36	1.03	20
	Z21-2					31.8	.084	54	22.2	6.11	1.08	6.21	1.08	26
	Z21-3					21.8	.154	49	22.5	7.76	1.17	8.34	1.17	47
Z22	Z22-1	3.60	23.2	29.5	.216	29.3	.064	49	22.5	5.67	1.07	5.74	1.07	23
	Z22-2					20.3	.195	59	22.2	6.92	1.21	7.67	1.21	39
	Z22-3					9.3	.219	63	22.5	7.67	1.19	8.34	1.19	47
G18	G18-1	5.43	21.8	47	.151	44.8	.036	34	21.6	6.26	1.07	6.34	1.07	28
	G18-2					34.8	.093	49	20.6	7.76	1.12	8.05	1.12	42
	G18-3					25.3	.153	45	20.6	9.04	1.16	9.64	1.16	59
	G18-4					15.8	.178	51	20.6	8.62	1.13	9.00	1.13	54
	G18-5					9.3	.184	48	20.6	9.12	1.21	10.13	1.21	66
G19	G19-1	4.18	22.2	29	.243	24.3	.200	51	21.6	8.49	1.17	9.13	1.17	55
	G19-2					14.8	.231	50	21.6	8.87	1.20	9.74	1.20	60
	G19-3					4.3	.272	49	22.2	8.79	1.21	9.74	1.21	60
G20	G20-1	4.21	22.5	29	.243	25.3	.194	48	21.6	8.53	1.17	9.17	1.17	56
	G20-2					14.3	.229	49	20.1	8.40	1.22	9.38	1.22	56
	G20-3					4.3	.252	52	20.6	8.55	1.21	9.50	1.21	58
SS14	SS14-1	3.57	22.5	39.5	.129	37.3	.020	57	22.8	3.72	1.05	3.74	1.05	10
	SS14-2					27.3	.049	47	22.5	4.18	1.08	4.24	1.08	14
	SS14-3					17.8	.104	45	22.5	5.10	1.10	5.23	1.10	20
	SS14-4					7.8	.244	55	20.6	6.97	1.29	8.48*	1.30	47
	SS14-5					2.8	.259	49	20.6	7.38	1.36	9.16*	1.31	55

* Computed by $D_s^3/\Sigma D_s^3$ method described in chapter 3.

The local concentration, C, as determined from electrical resistance and static head measurements, is plotted on the logarithmic scale. On the arithmetic scale, the superficial velocity, $\overline{u}$, necessary to produce the suspension is normalized using the particle mean free-fall velocity by weight, μ, for each sample determined by a suitable method described in chapter 3. Each point in figure 4-2 represents a local sample from within a suspension, and ten different suspensions are represented. One notices that the local concentration data in figure 4-2 show the same trend as the mean concentration data in figure 4-1, but the local concentration data show more scatter.

4-3 Variations of Concentration and Static Pressure with Depth

One of the best indicators of the nonuniform behavior of the suspended particles is the concentration-depth profile for a suspension. Figures 4-4 - 4-7 are normalized graphs of the local concentration and piezometric head vs. depth for profiles taken along the vertical axis of the fluidization column. The elevation, y, measured from the bottom of the suspension, is normalized by d, the total depth of the suspension, so that the ratio y/d represents relative depth in the suspension. The local concentration, C, measured by means of the electrical resistance probe as explained in chapter 2, is normalized by $\overline{C}$, the mean concentration defined by equation 2-8. h is the piezometric head of water within the suspension measured relative to the clear water above the suspension at the wall static pressure tap at y = 131.5 cm (see chapter 2, sec. 2-3), and is normalized by h_*, the theoretical piezometric head at the bottom of the suspension. The normalized concentration,

$C/\overline{C}$, and the normalized piezometric head, h/h_*, are derived from equation 2-4 as follows:

$$\rho_f g \frac{dh}{dy} = - C(\rho_s - \rho_f)g \tag{2-4}$$

using $$\overline{C} = \frac{W}{\gamma_s A d} \tag{2-8}$$

and $$h_* = \frac{W}{A\gamma_s} \left(\frac{\gamma_s}{\gamma_f} - 1\right)$$

Therefore,

$$\frac{C}{\overline{C}} = - \frac{d(h/h_*)}{d(y/d)} \tag{4-1}$$

or

$$\int_a^b \frac{C}{\overline{C}} \, d\left(\frac{y}{d}\right) = \left(\frac{h}{h_*}\right)_a - \left(\frac{h}{h_*}\right)_b \tag{4-2}$$

Using the facts that $(\frac{h}{h_*}) = 1$ at $(\frac{y}{d}) = 0$ and $(\frac{h}{h_*}) = 0$ at $(\frac{y}{d}) = 1$, equation 4-2 shows that the area under the normalized concentration, $C/\overline{C}$, curve equals unity, the area contained in the rectangle bounded by the straight lines, $C/\overline{C} = 0$, $C/\overline{C} = 1$, $y/d = 0$, $y/d = 1$.

An inspection of figures 4-4, 4-5, and 4-6 shows that the area under the normalized concentration curves for several of the runs (A3, Z22, G18, G19, G20) is a few per cent less than unity. This discrepancy is due primarily to the sensitivity of normalizing the local concentration, C, with the mean concentration, $\overline{C}$. A small change in $\overline{C}$, shifting the $C/\overline{C}$ curve to the right or left, can change the area under this curve by a large amount. Because the upper surfaces of the suspensions were

wavy, and the total depths of the suspensions were rather small, a few per cent relative error in the mean concentration is not unlikely.

In general, some comments can be made about the normalized concentration and piezometric head profiles. The concentration is found to be smallest at the top of the suspension and to increase as the depth down in the suspension increases. Although the concentration-depth profiles appear to be monotonic, they do not seem to follow any common distribution. There appears to be a tendency with each material for the concentration-depth profiles to be more uniform for the higher values of $\overline{C}$, the mean concentration. Also the profiles are more uniform if the parent material is more uniform. For all the experimental runs, less than 50 per cent of the solid material is suspended above the mid-depth of the suspension; and it appears that as the mean concentration, $\overline{C}$, decreases, the per cent of the total solid material by weight, h/h_*, suspended above mid-depth, $y/d = 0.5$, also decreases.

4-4 Distribution of Particle Free-Fall Velocities in a Suspension

In order to understand the structure of a suspension, it is helpful to understand how the particles distribute themselves locally. In figures 4-10 to 4-20 are noted the elevations from which local samples of the suspended particles were taken and the local concentration of the suspension at each sampling elevation. Each sample was obtained using the siphon sampler (see figure 2-4) and processed in a manner described in chapter 3. Figures 4-10 to 4-20 are graphs of the particle free-fall velocity distributions by number for each of

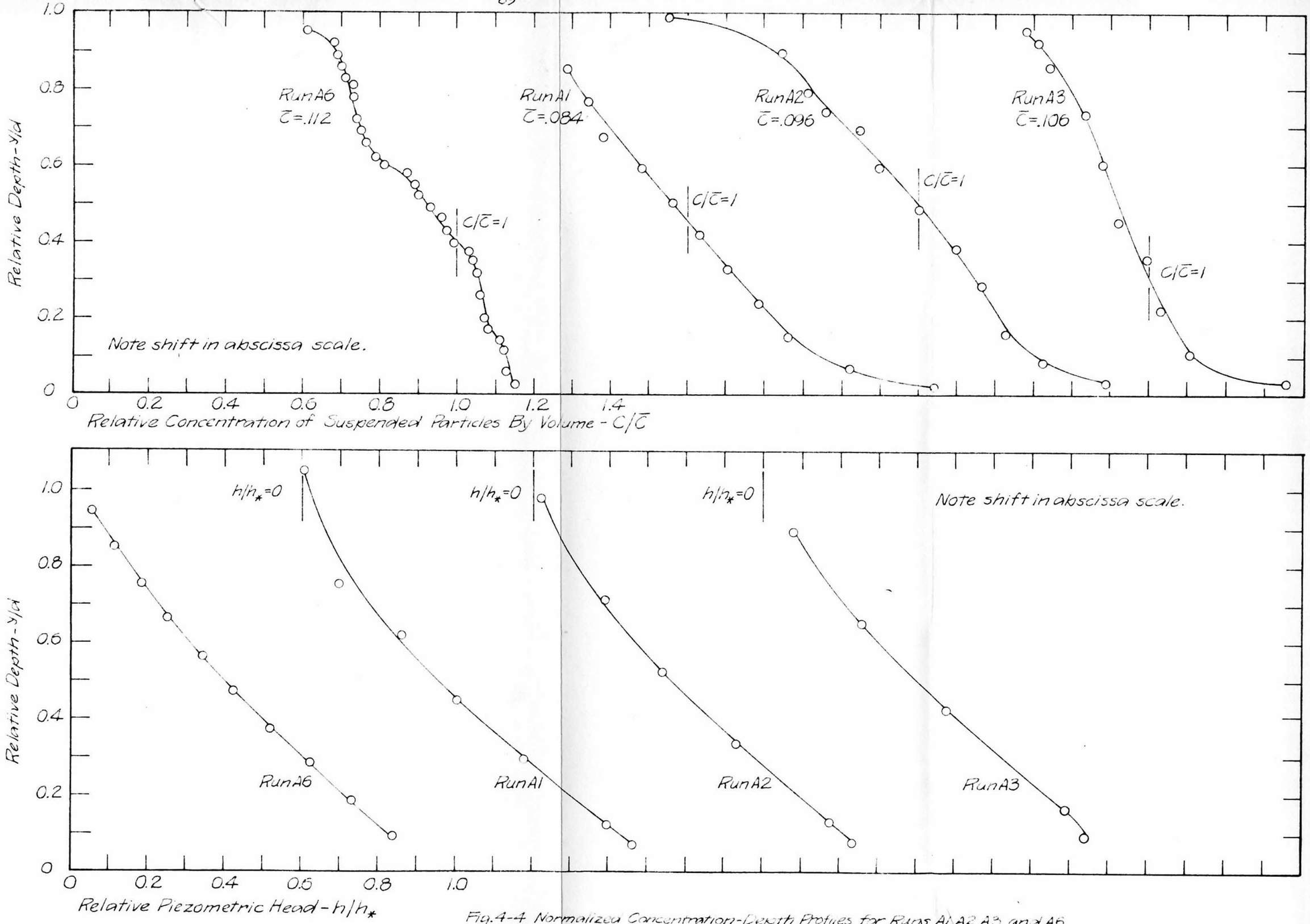

Fig. 4-4 Normalized Concentration-Depth Profiles for Runs A1, A2, A3, and A6

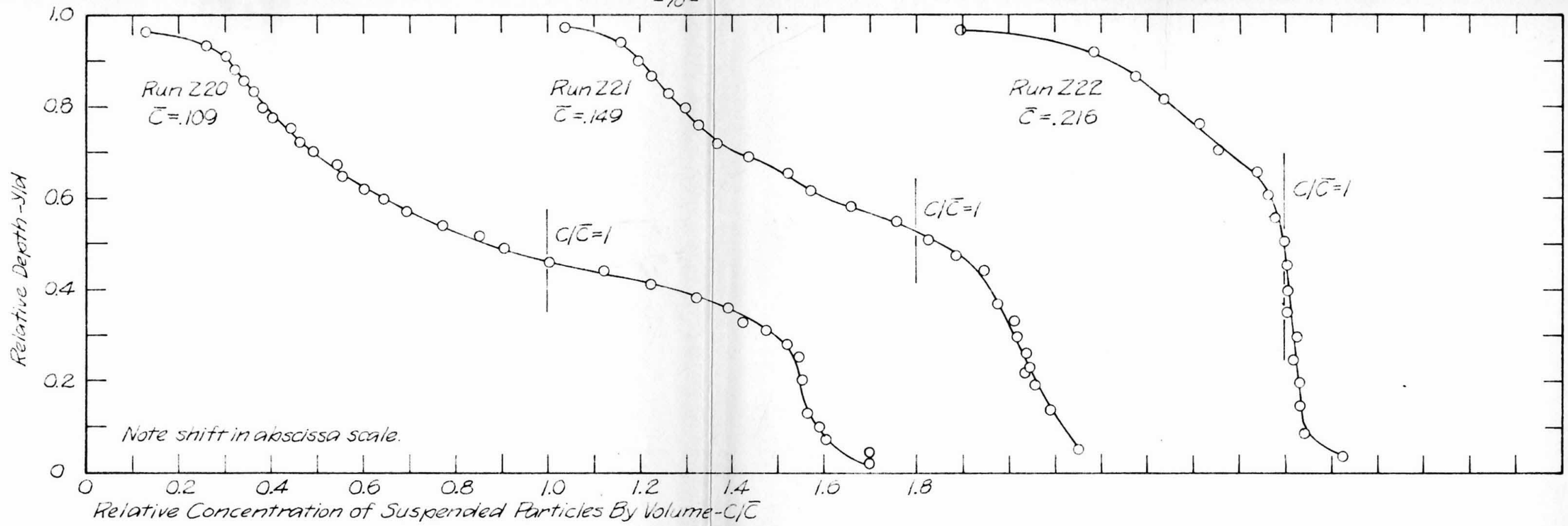

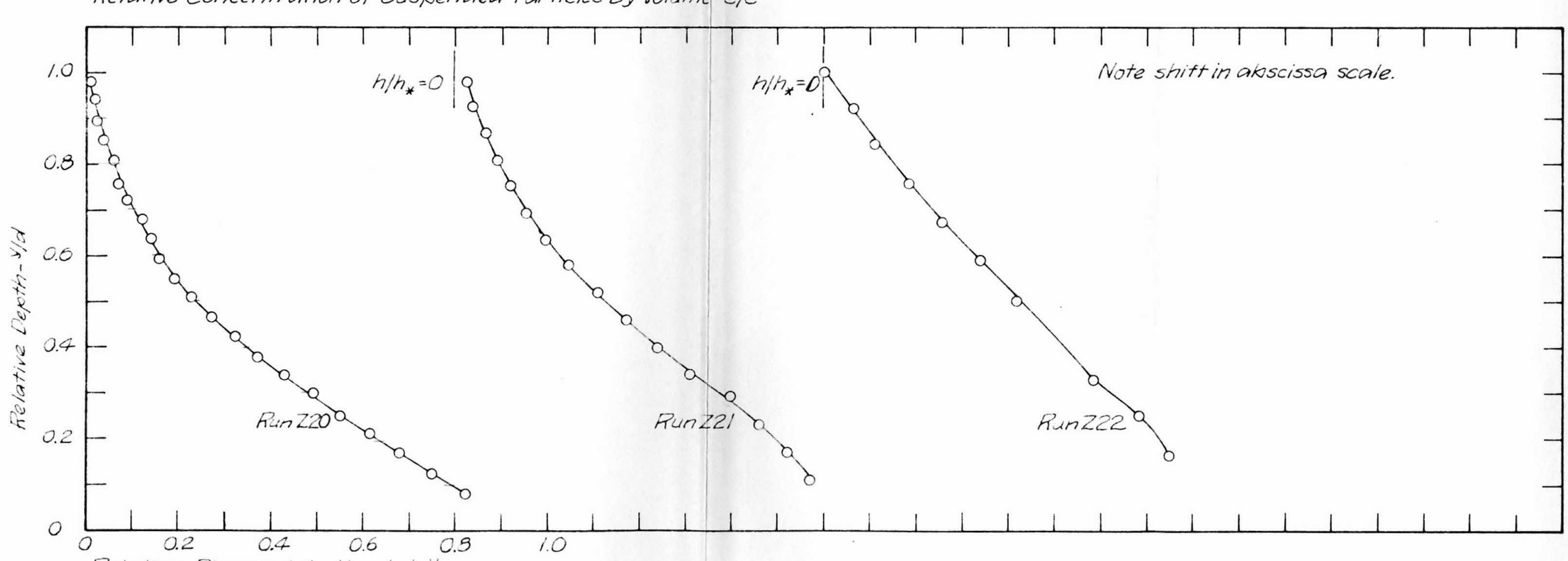

Fig. 4-5 Normalized Concentration-Depth Profiles for Runs Z20, Z21, and Z22

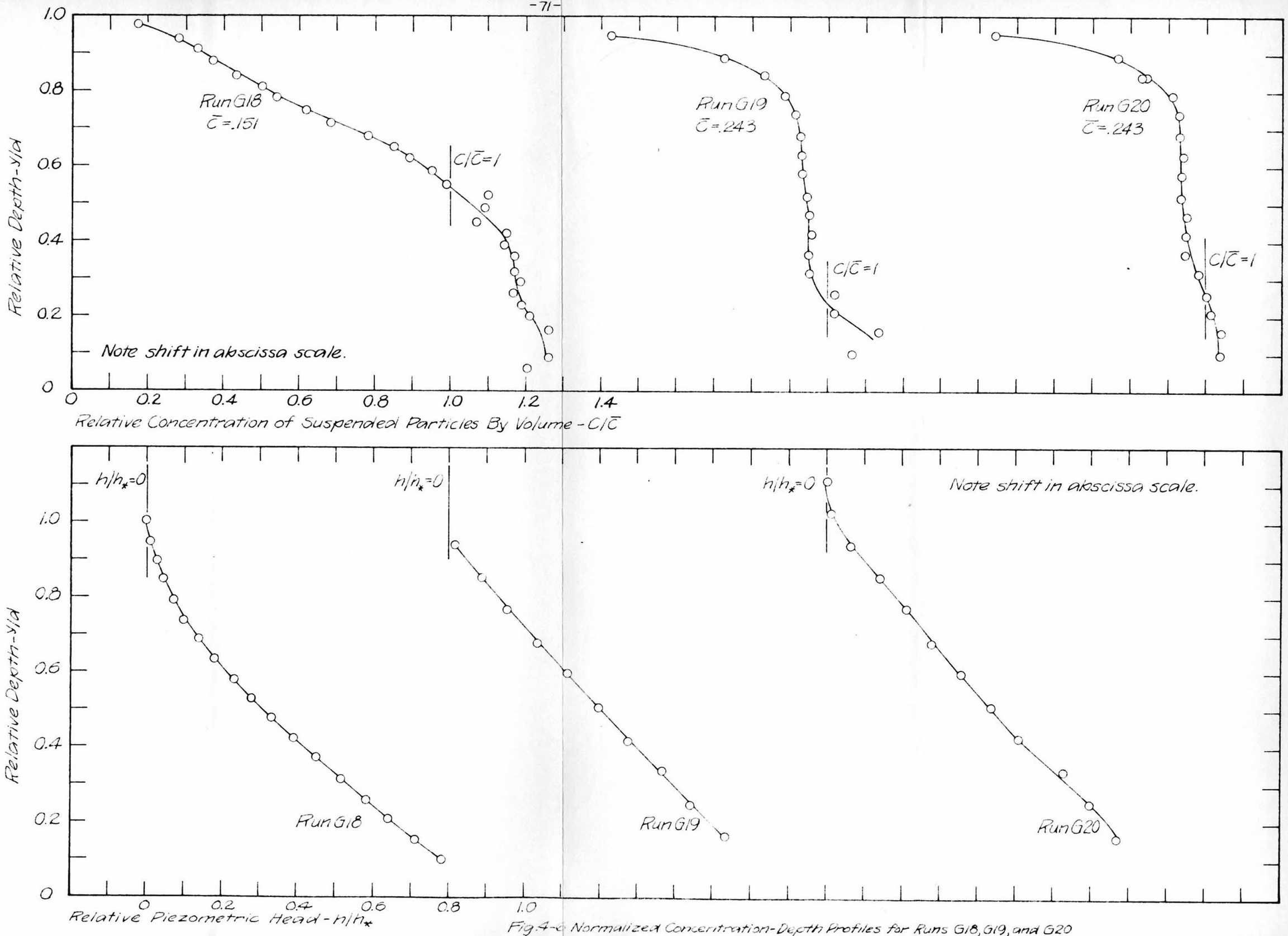

Fig. 4-6 Normalized Concentration-Depth Profiles for Runs G18, G19, and G20

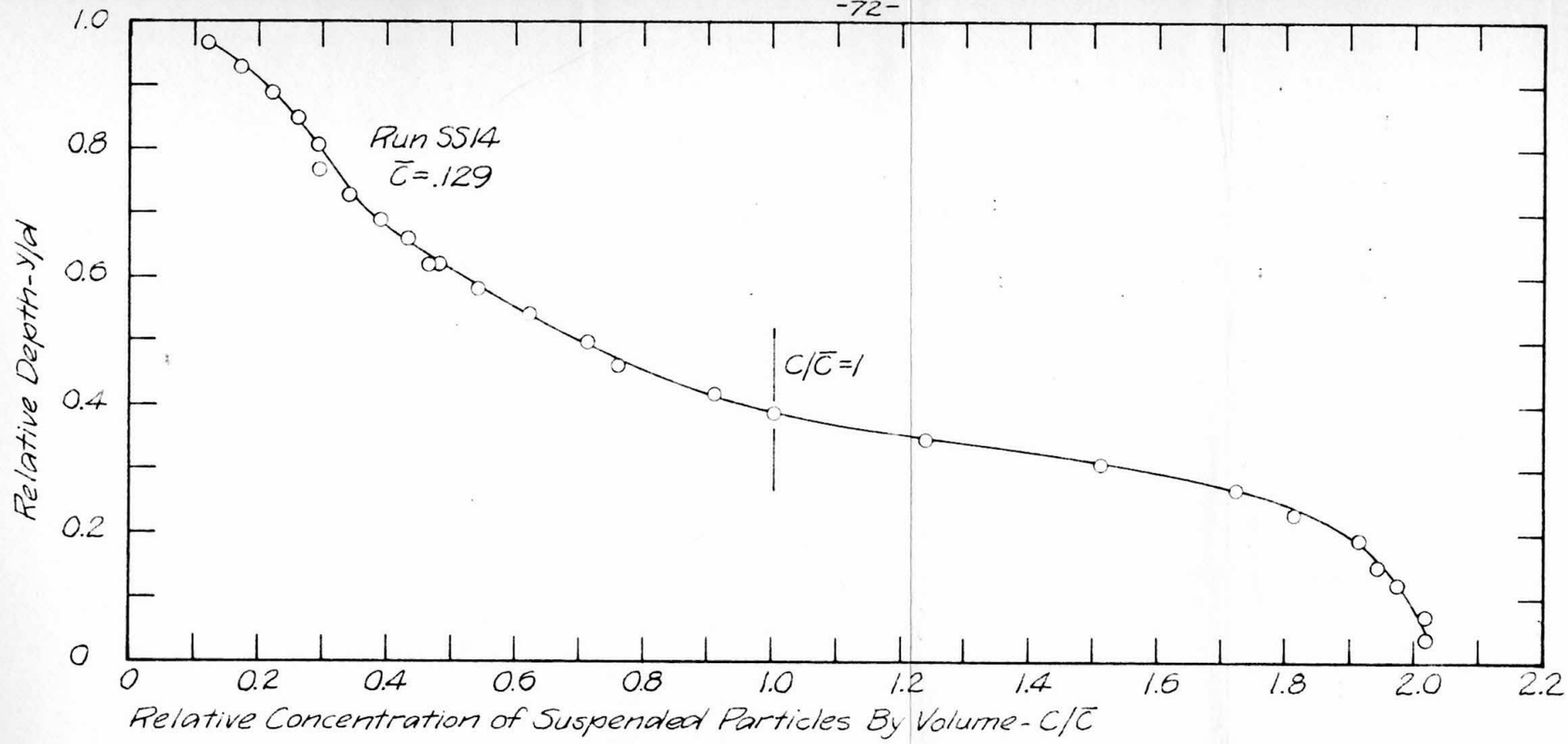

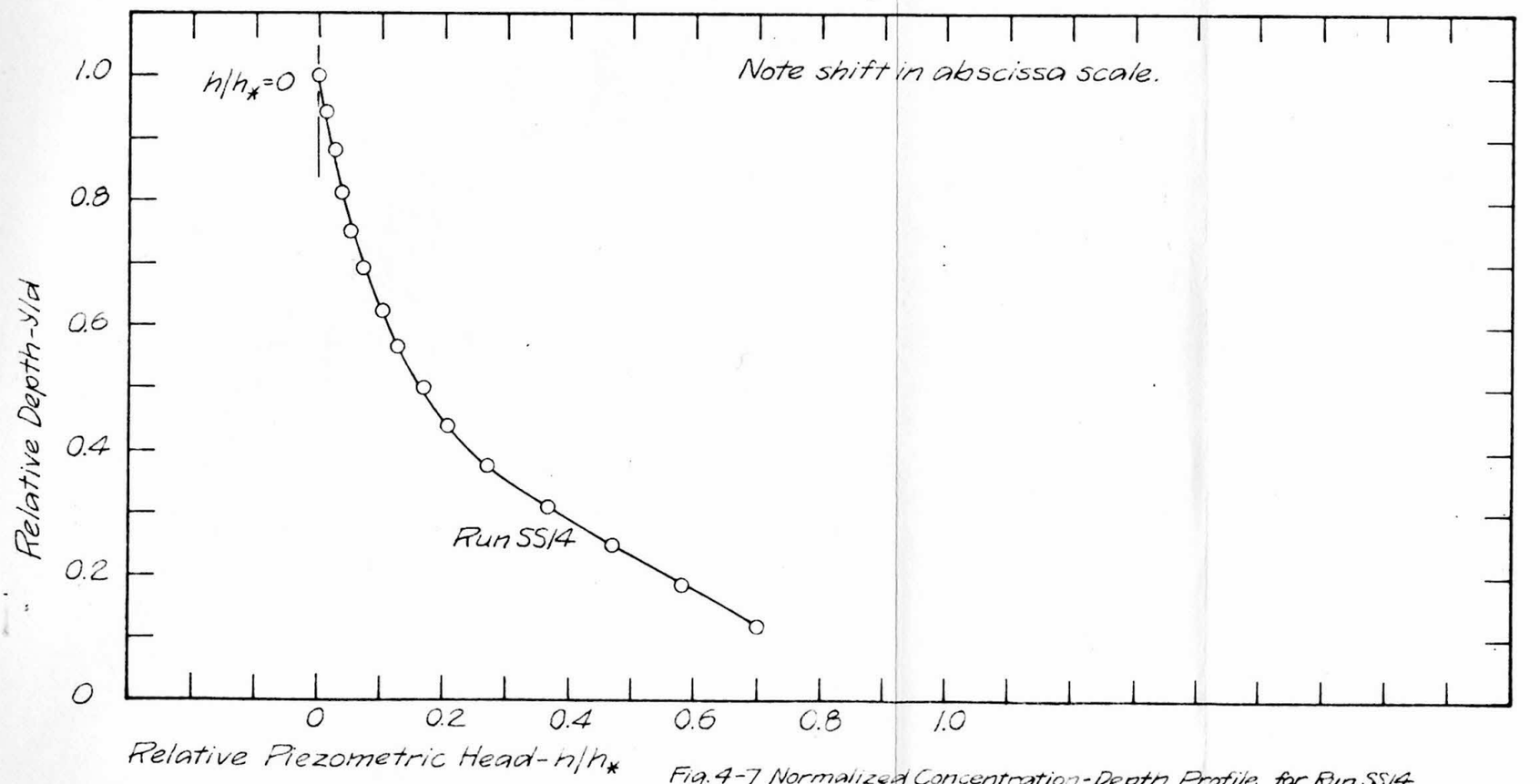

Fig. 4-7 Normalized Concentration-Depth Profile for Run SS14

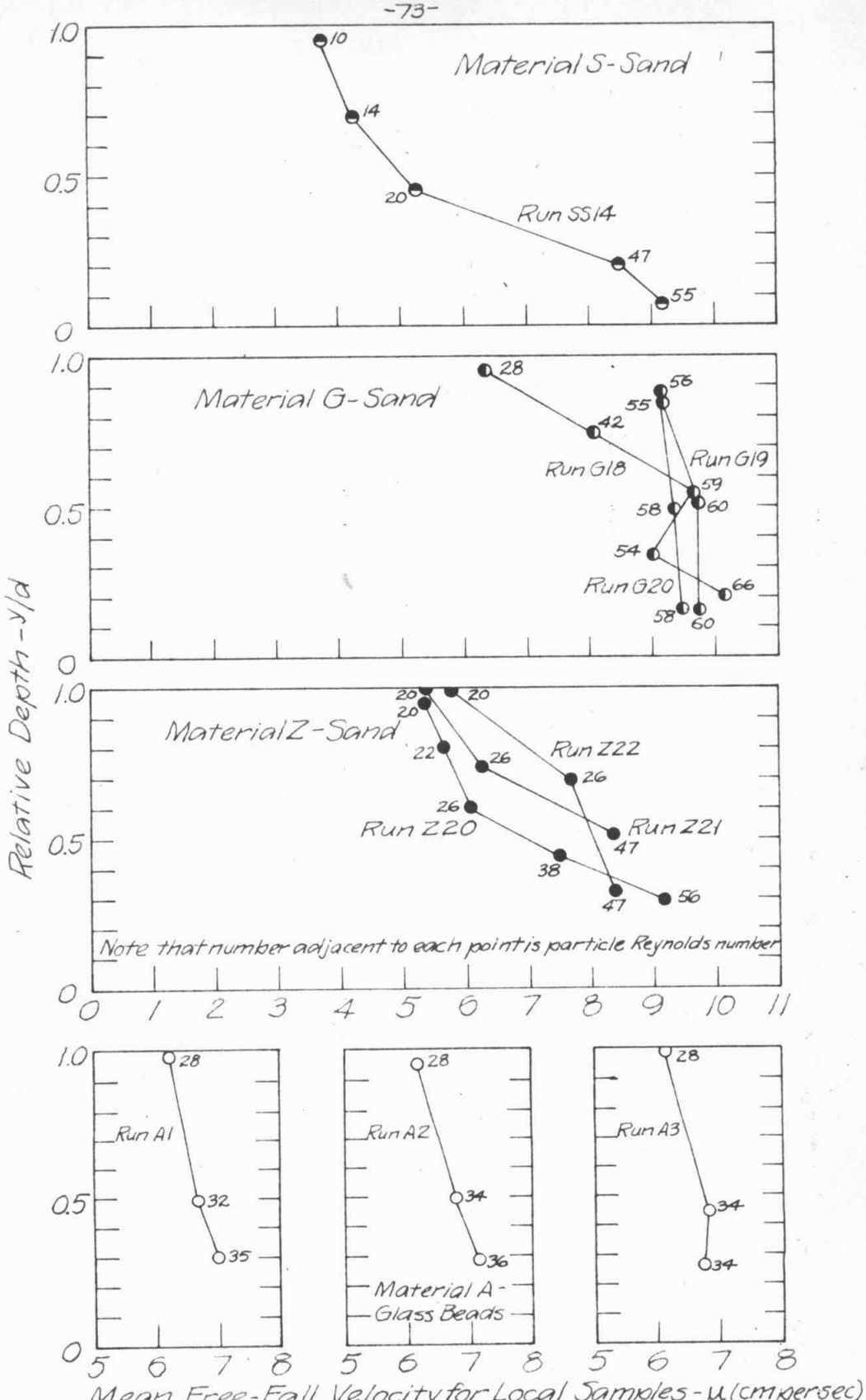

Fig. 4-8 Variation of Mean Fall Velocity with Depth for Fluidized Suspensions

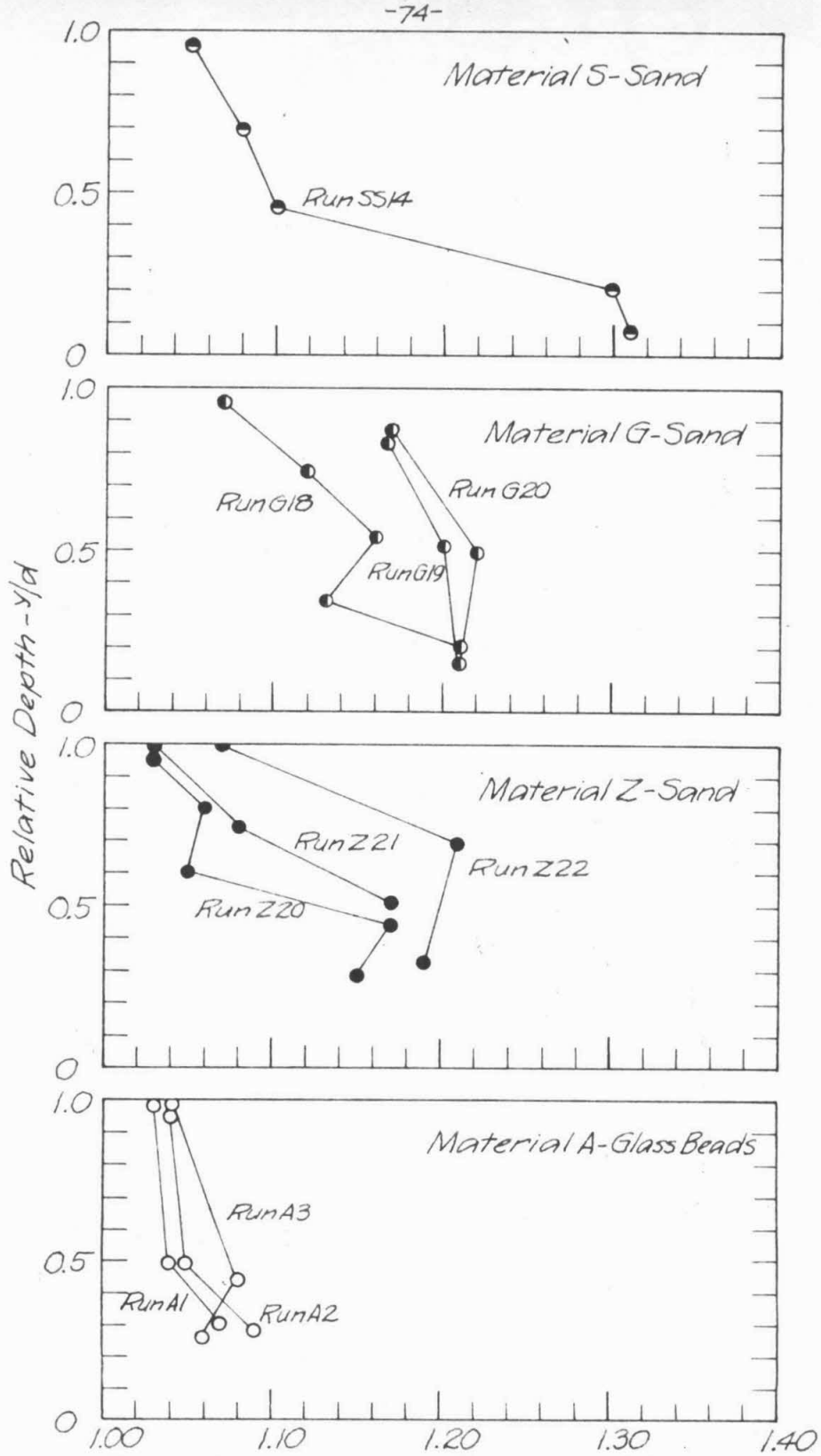

Fig. 4-9 Variation of σ_w with Depth for Fluidized Suspensions

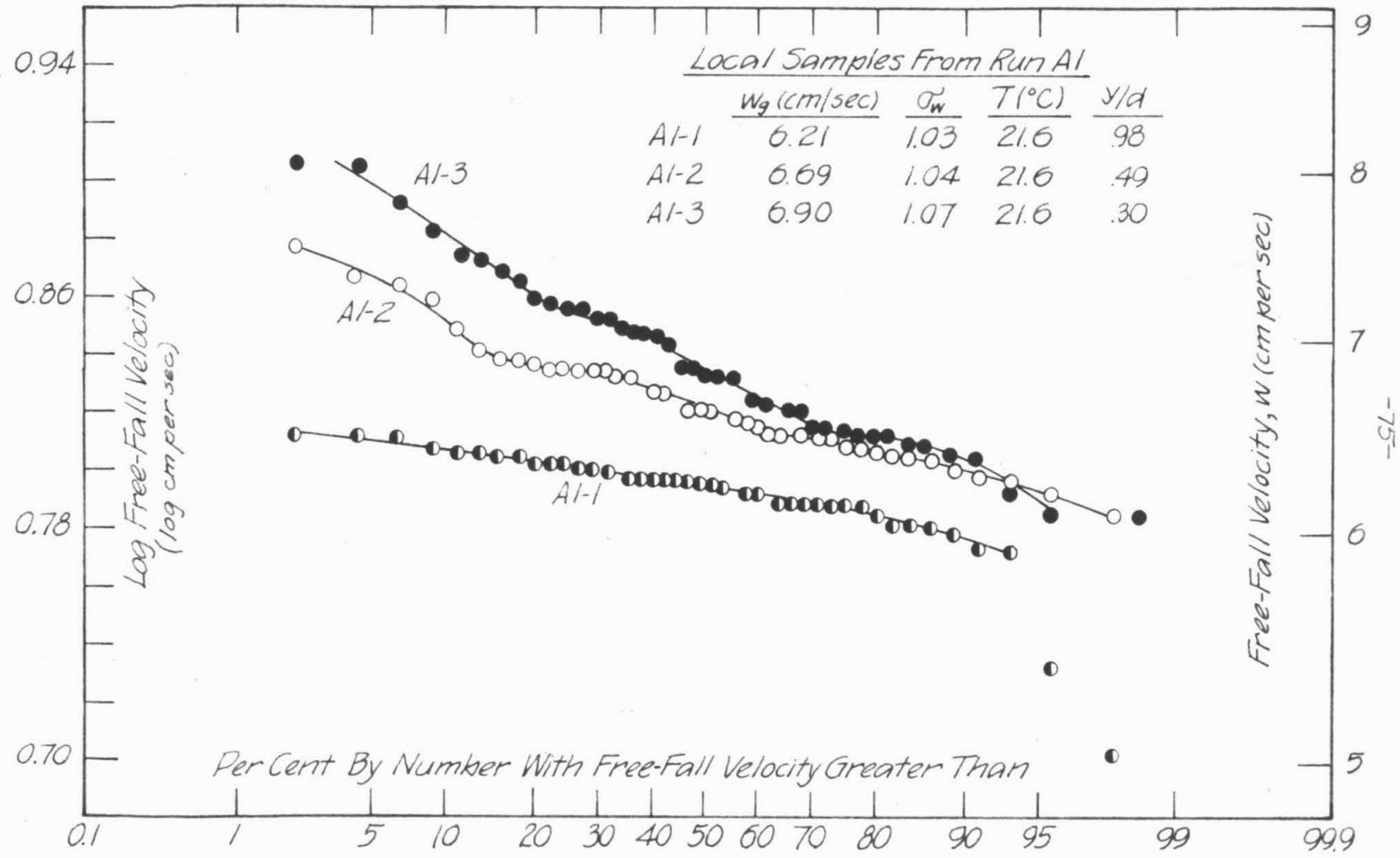

Fig. 4-10 Fall Velocity Distributions of Local Samples from Run A1

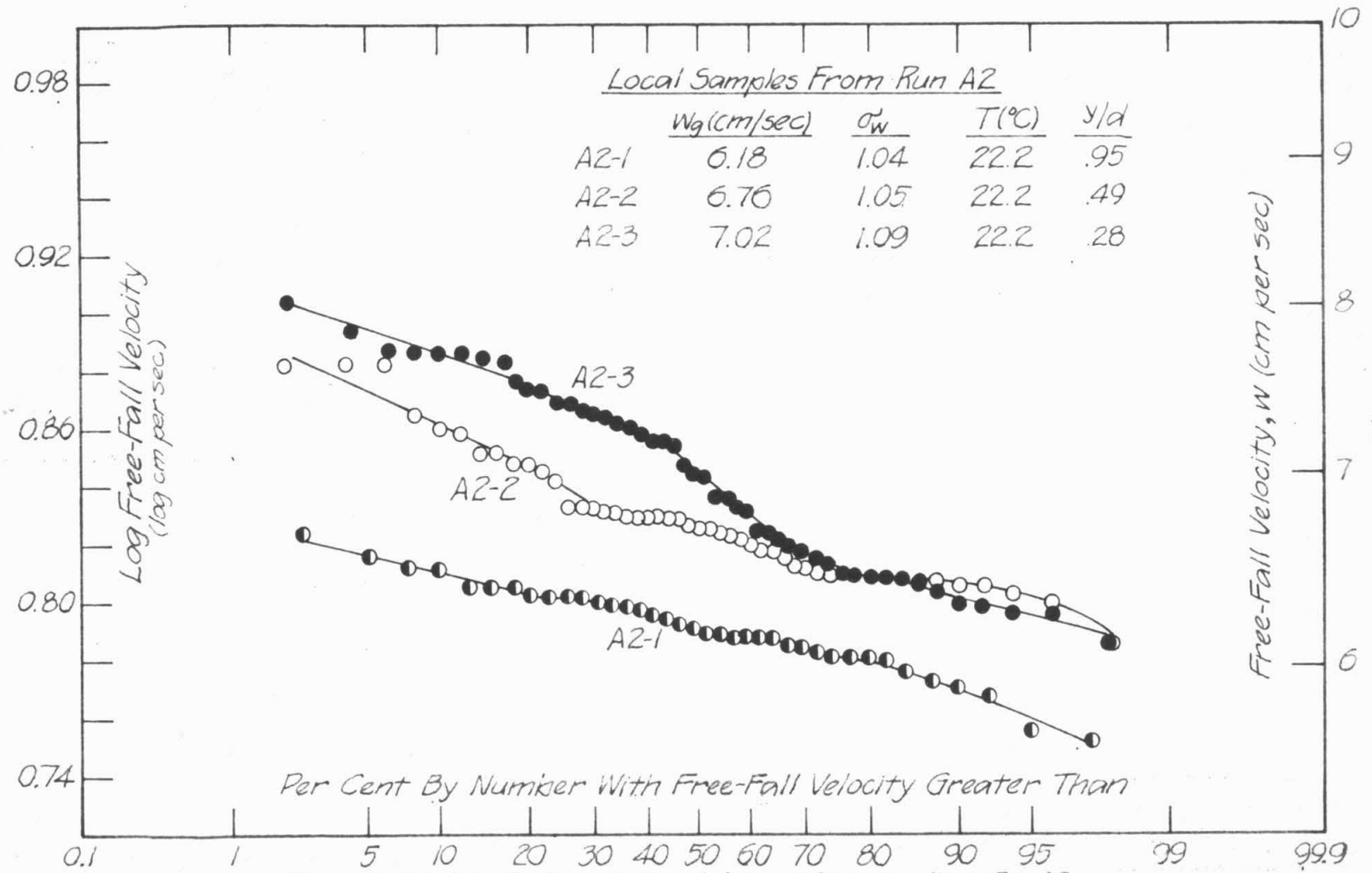

Fig. 4-11 Fall Velocity Distributions of Local Samples from Run A2

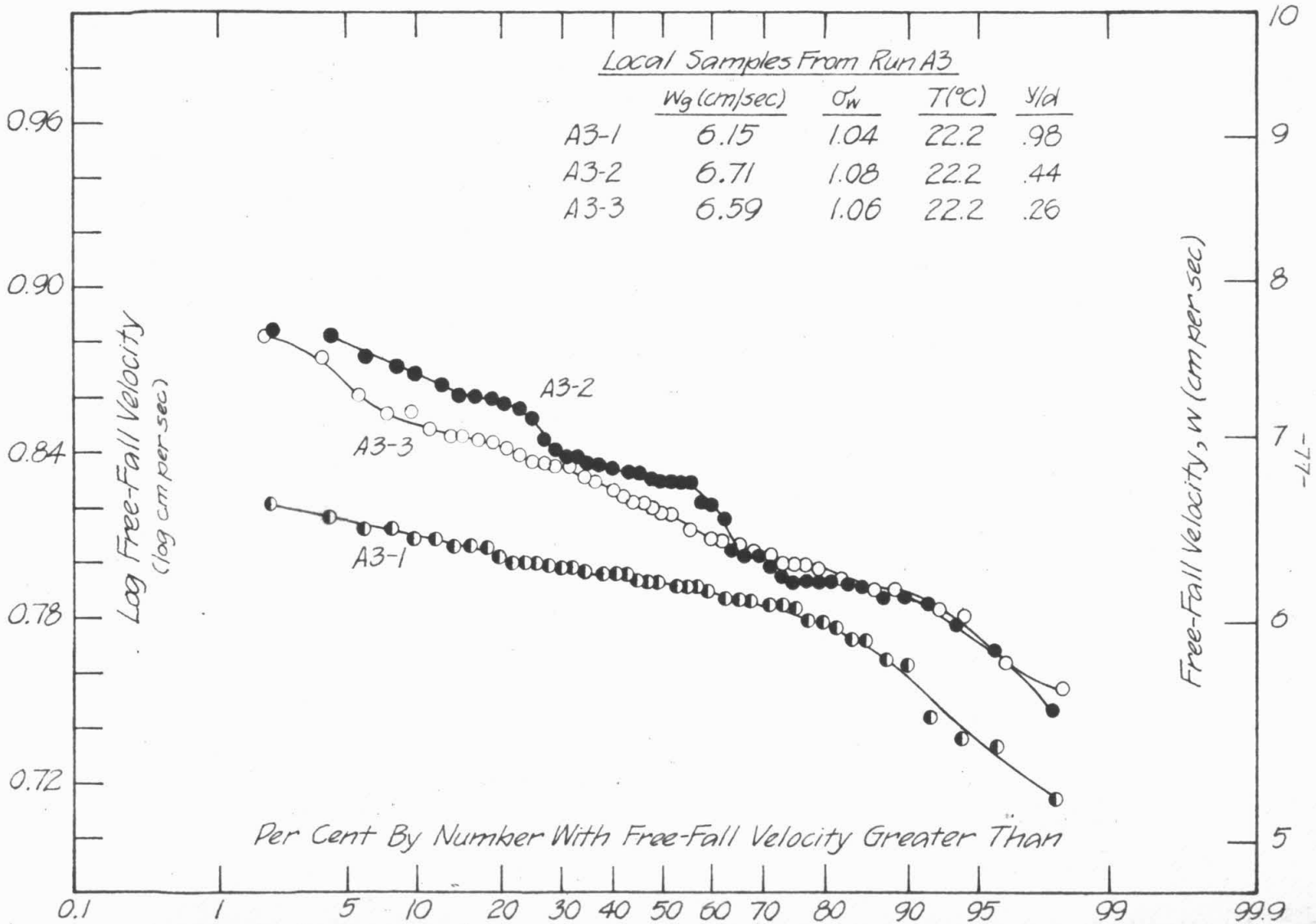

Fig. 4-12 Fall Velocity Distributions of Local Samples from Run A3

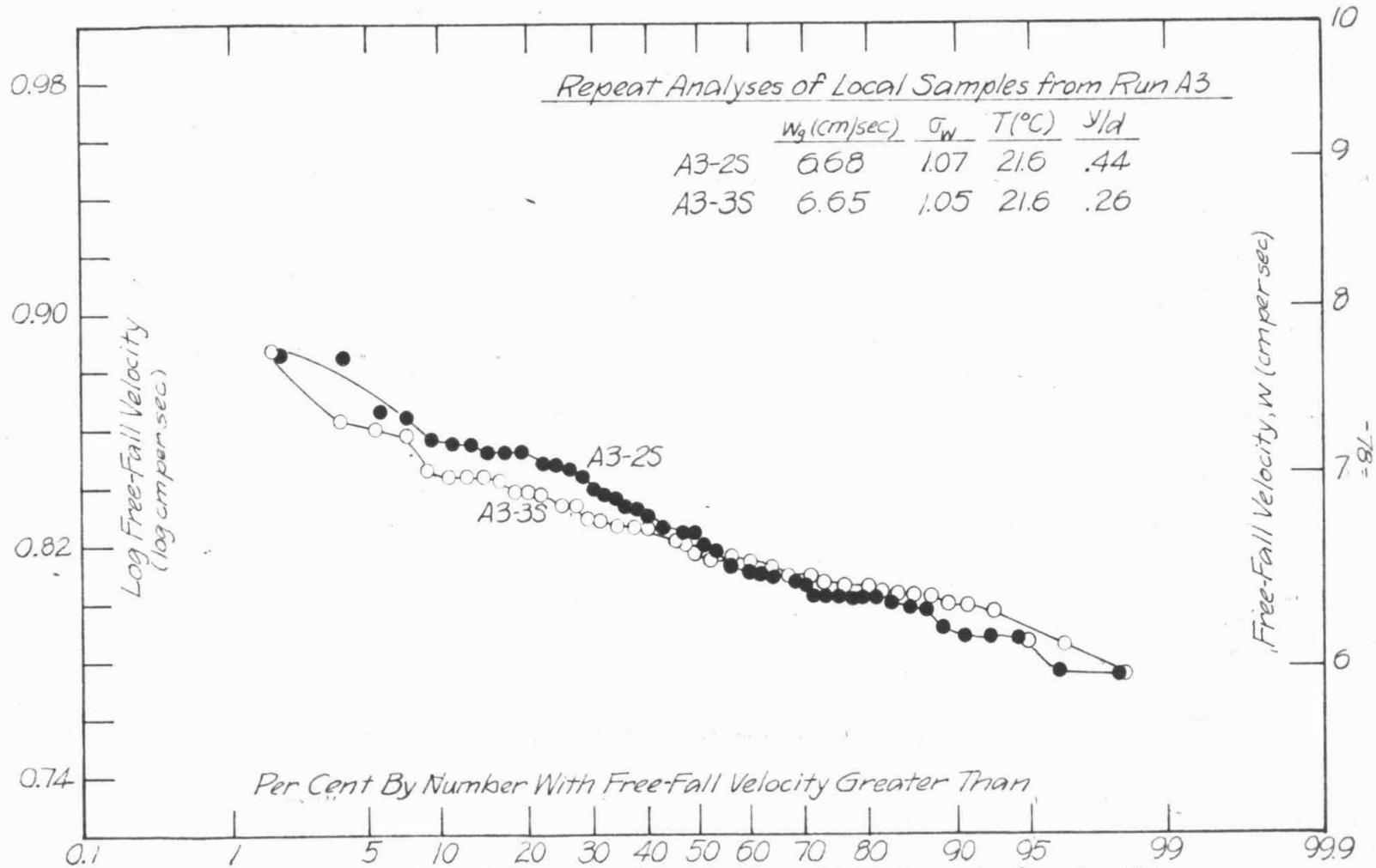

Fig. 4-13 Fall Velocity Distributions of Local Samples from Run A3

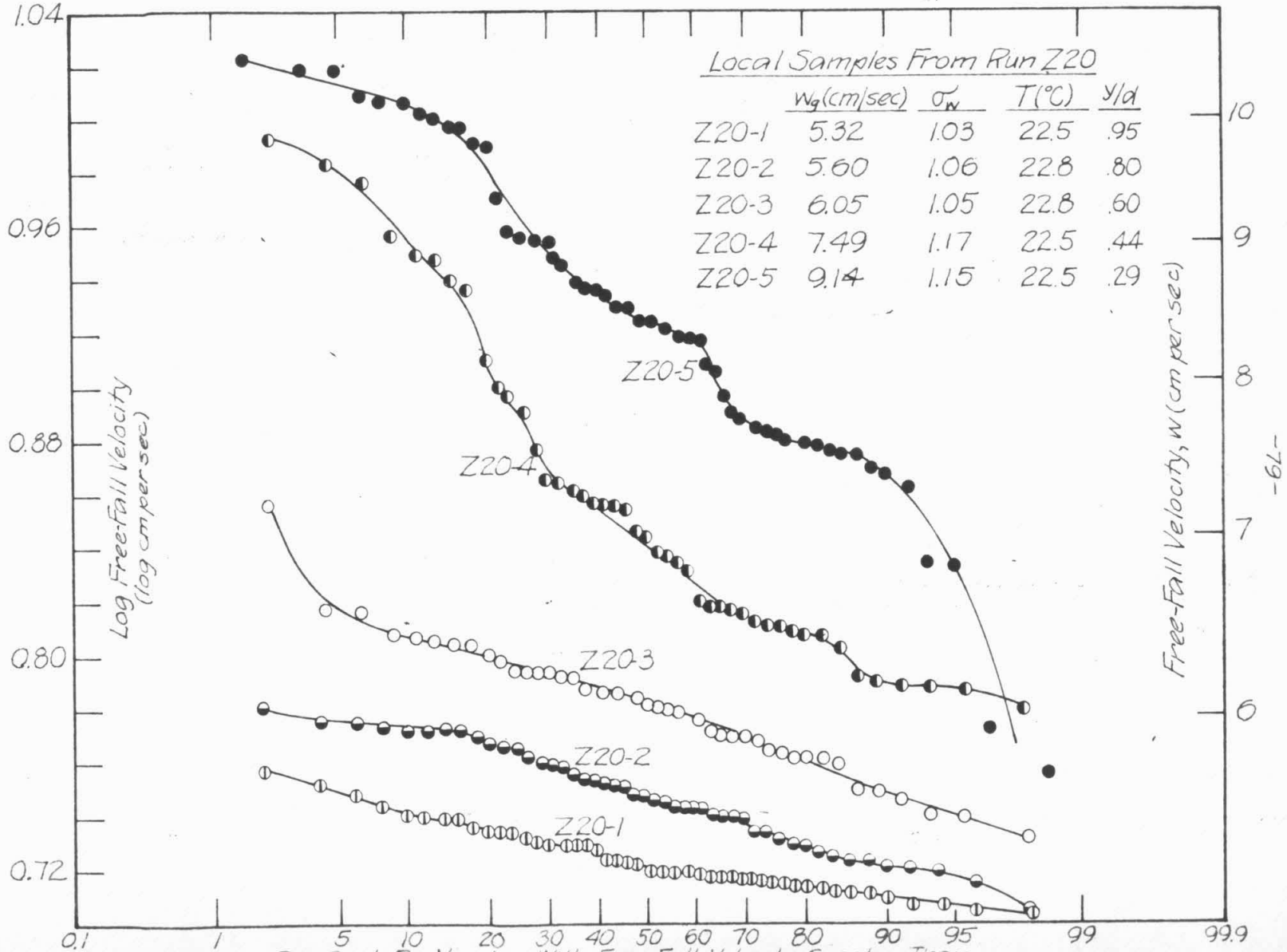

Fig. 4-14 Fall Velocity Distributions of Local Samples from Run Z20

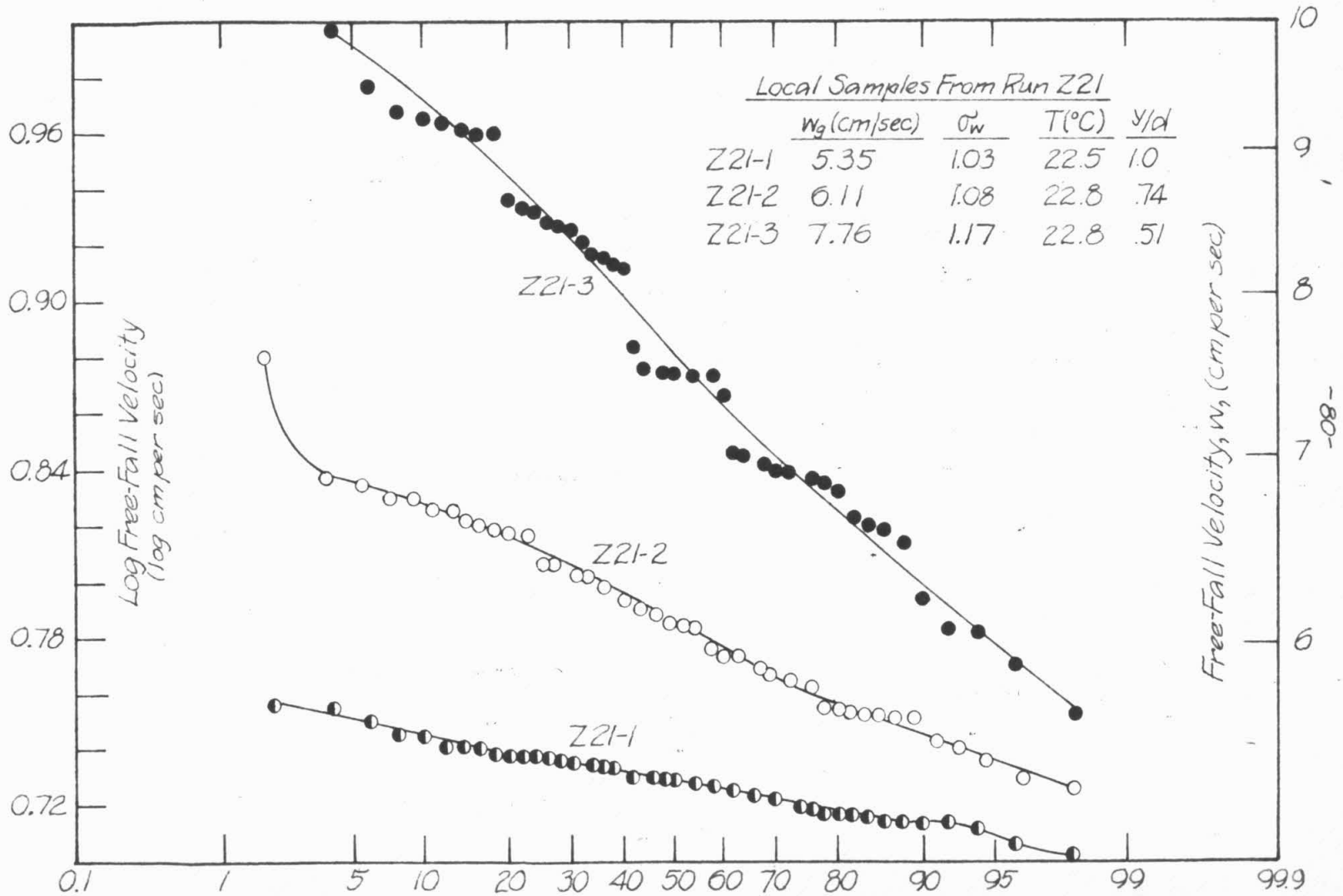

Fig. 4-15 Fall Velocity Distributions of Local Samples from Run Z21

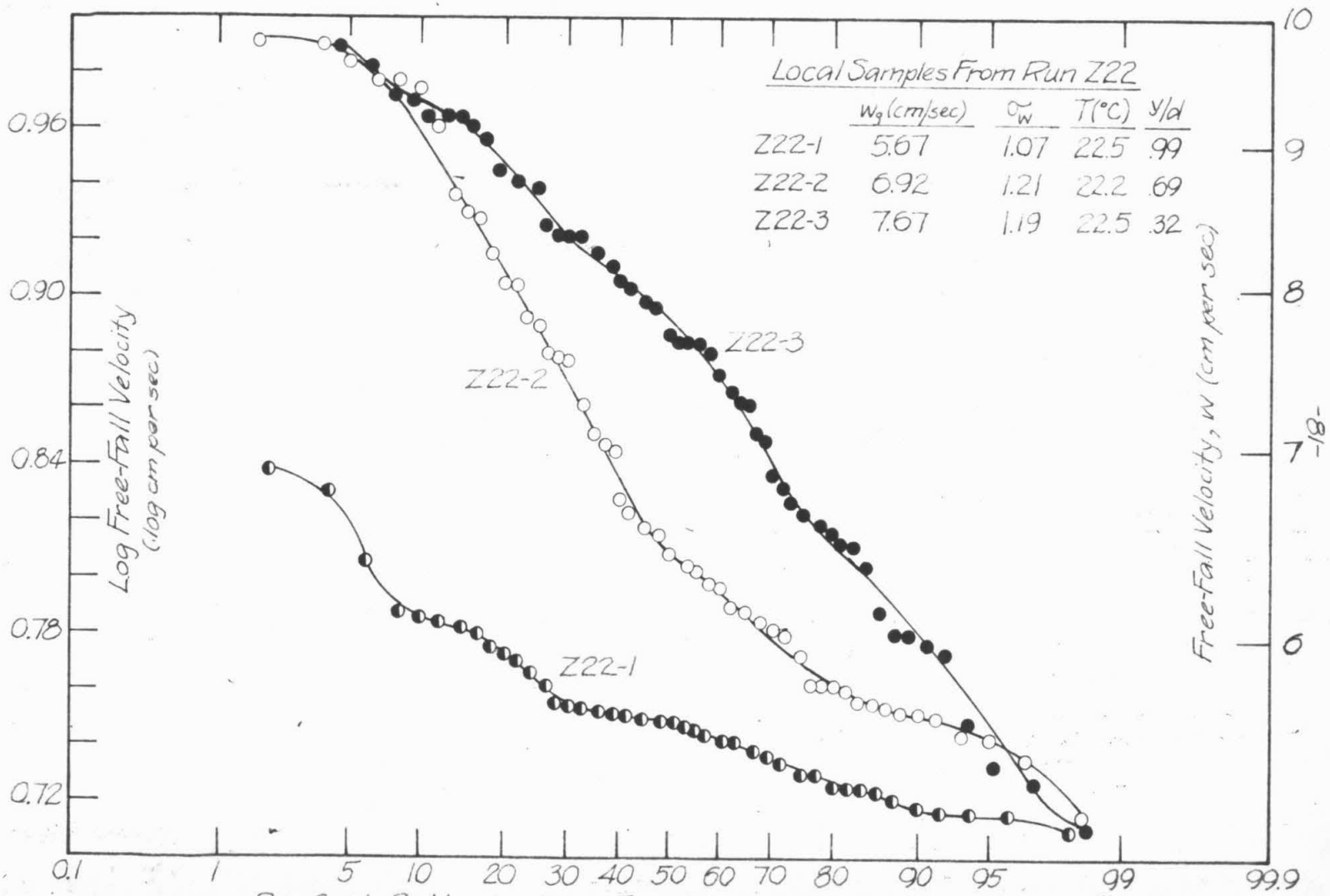

Fig. 4-16 Fall Velocity Distributions of Local Samples from Run Z22

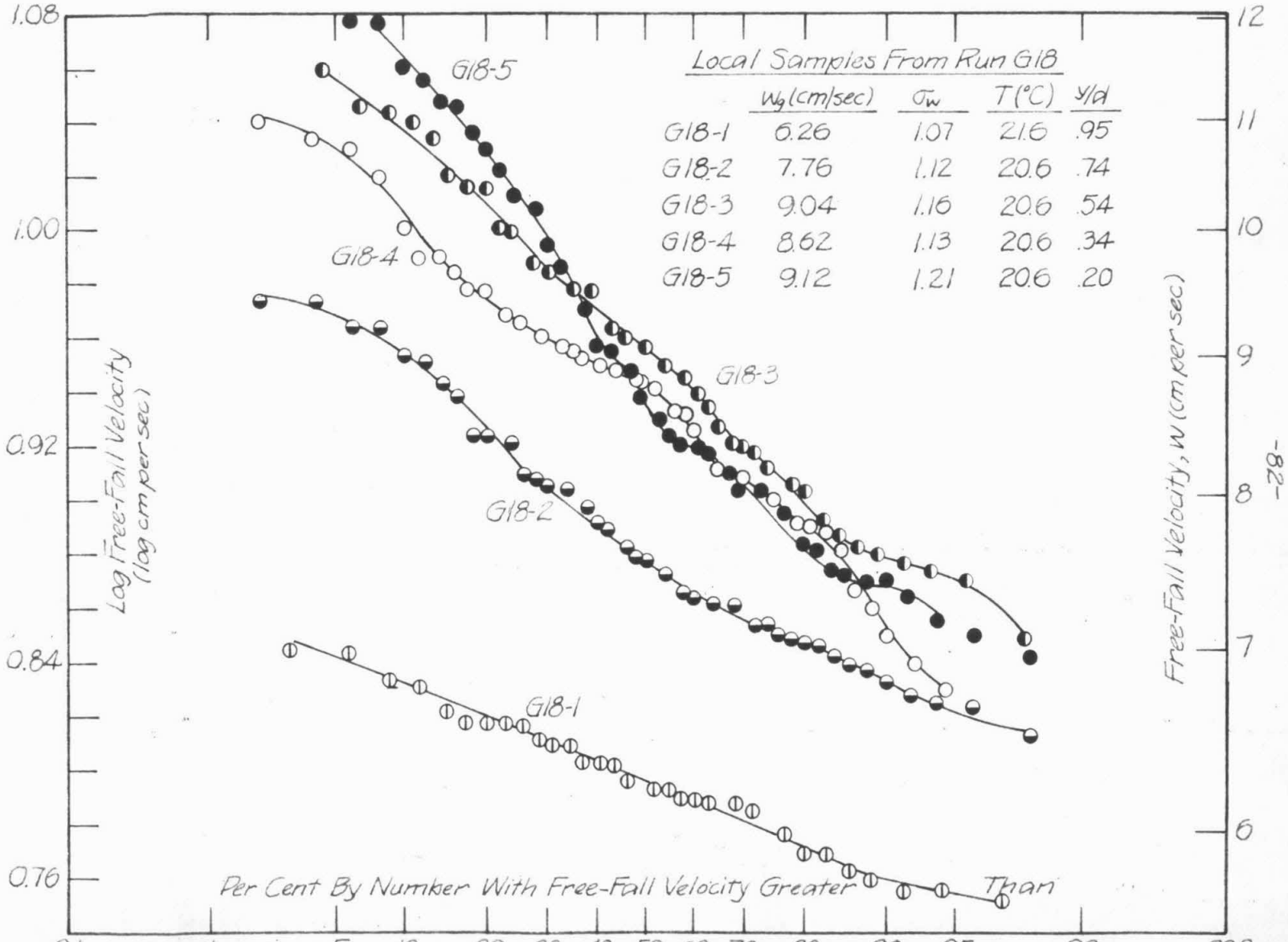

Fig. 4-17 Fall Velocity Distributions of Local Samples from Run G18

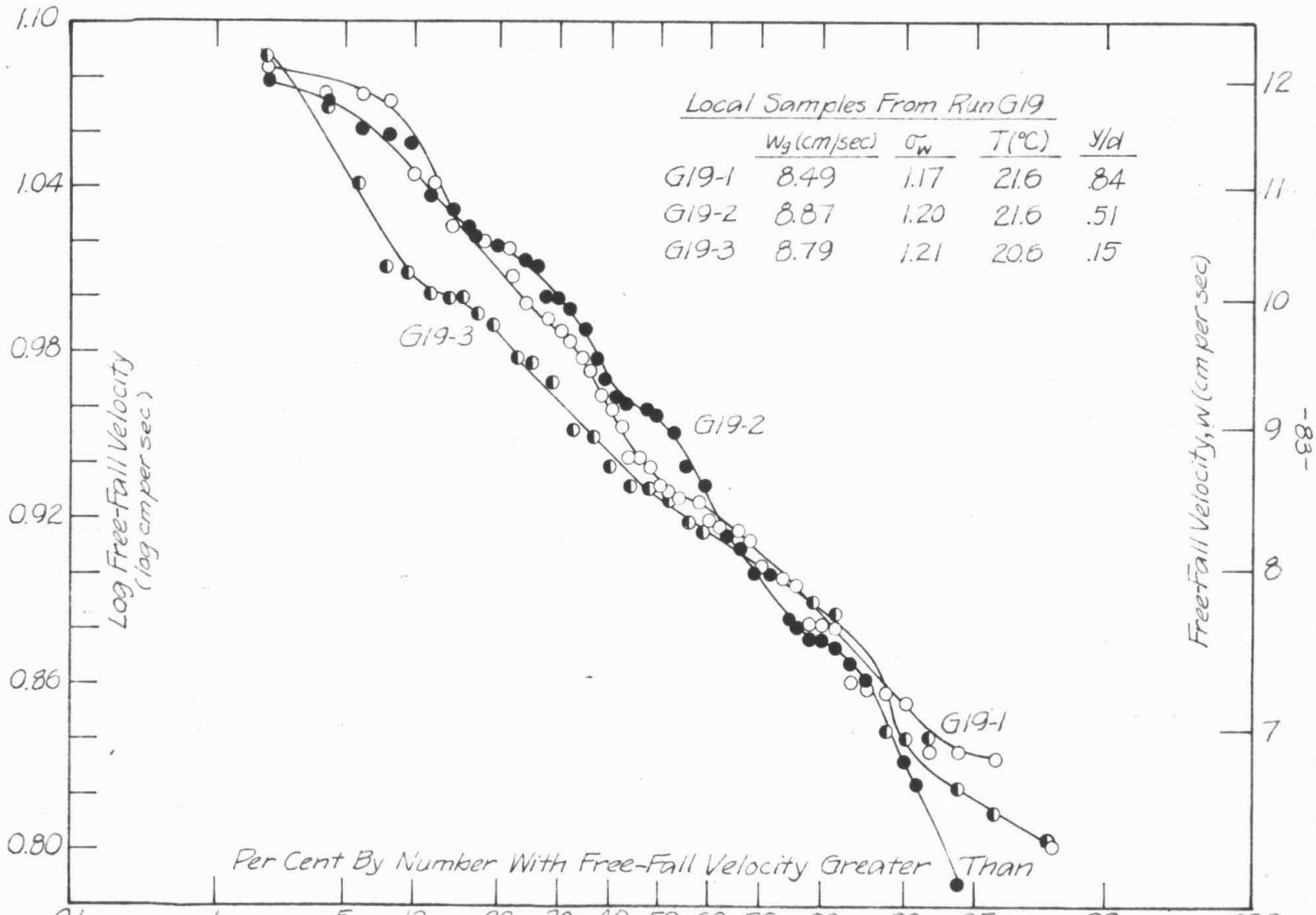

Fig. 4-18 Fall Velocity Distributions of Local Samples from Run G19

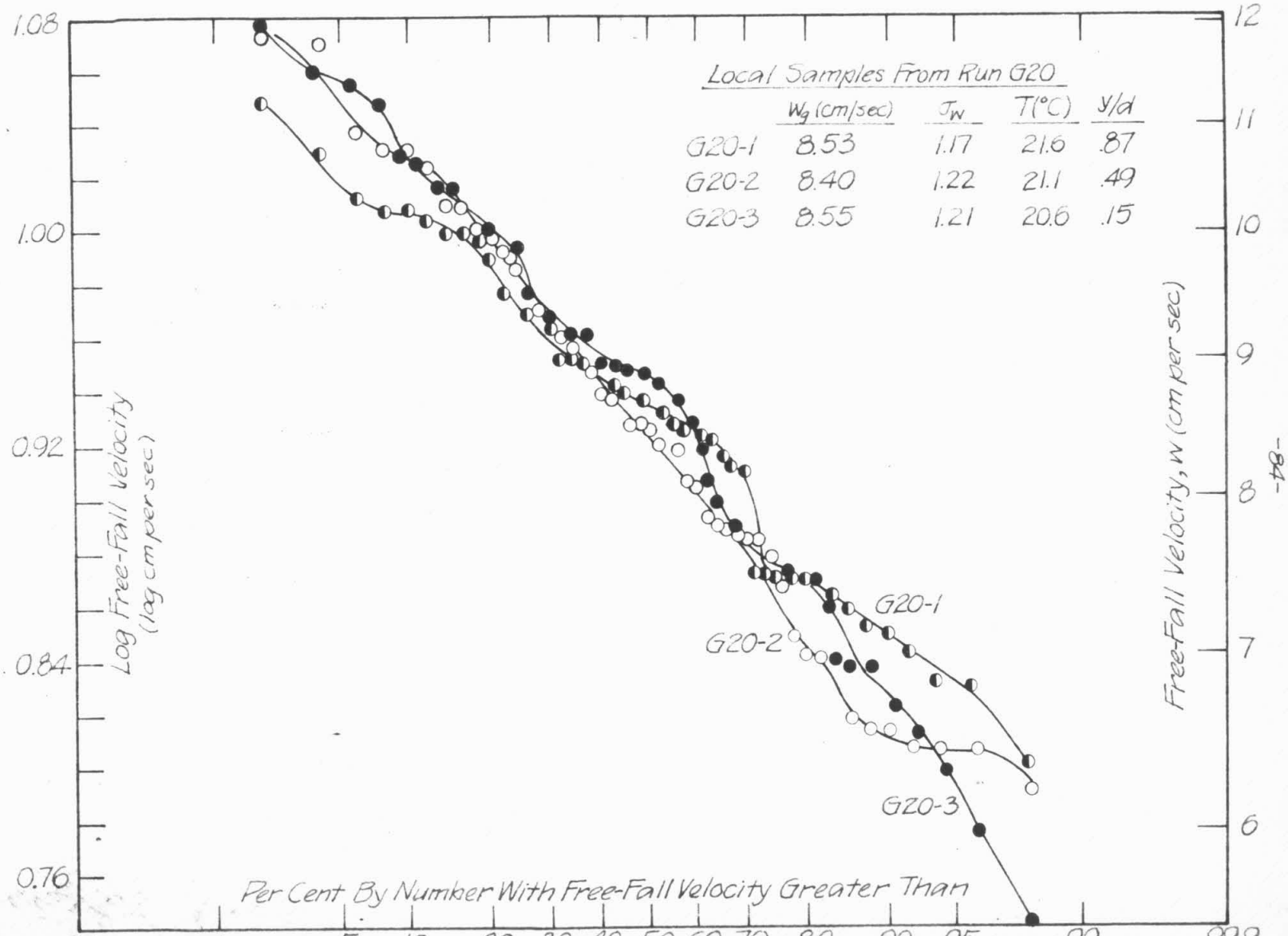

Fig. 4-19 Fall Velocity Distributions of Local Samples from Run G20

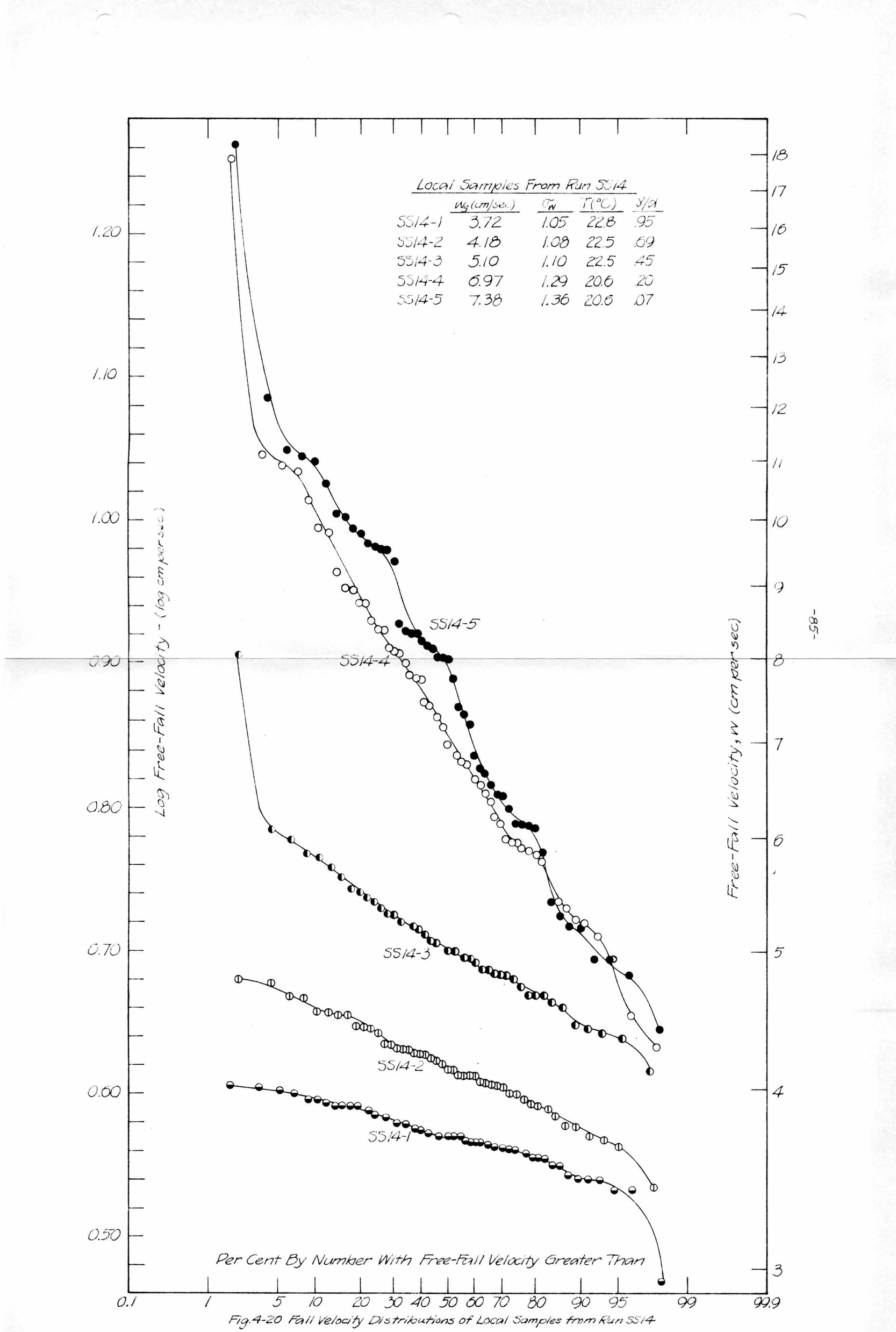

Fig. 4-20 Fall Velocity Distributions of Local Samples from Run SS14

the local samples. The distributions appear to be nearly log-normal and are described in Table 4-2 by a mean free-fall velocity and geometric standard deviation of free-fall velocities.

The local free-fall velocity distributions show some particular trends. In general, the mean velocity for those samples taken near the top of a suspension, that is, where the local concentration is smallest, is less than the mean fall velocity for those samples taken near the bottom of a suspension where the local concentration is the highest (see figure 4-8). In addition to this stratification of the suspension, a very striking characteristic of the distributions of particle free-fall velocity is the decrease in the geometric standard deviation of the free-fall velocities, σ_w, from bottom to top of the suspensions (see figure 4-9). This change is manifested in the change in slope of the various free-fall velocity distributions. One notes that σ_w decreases with decreasing concentration, C. This trend is clearly shown in figure 4-3 which is a graph of σ_w vs. local concentration, C, for all the experimental runs.

Figures 4-12 and 4-13 show the reproducibility of the results for the fall velocity distributions of the local samples. Two samples were split from each of the local samples taken at elevations $y/d = .44$ and $y/d = .26$ for experimental run A3. These samples are designated as A3-2 and A3-2S and A3-3 and A3-3S. Table 4-2 contains the tabulated results of the fall velocity distributions plotted in figures 4-12 and 4-13 which show that the local sample mean free-fall velocity and geometric standard deviation are reproducible to within one per cent.

4-5 Microphotographs of Local Samples from the Suspensions

Each of the local samples taken from a suspension was processed through a Jones sample splitter until a representative sample of about 50 particles was obtained. The microphotographs, figures 4-21 to 4-30, each show a total representative sample split from the local sample taken from the suspension.

Material A, the glass beads, shown in figures 4-21 to 4-23, appears to be very uniform in shape and can readily be described as glass spheres. However, in most of the photographs, one notices an occasional oddly shaped particle. This type of particle dramatically illustrates that the mechanism of sorting within the suspension is by free-fall velocity and not by particle size or particle shape alone. Although such a particle may be oddly shaped, undoubtedly it has a free-fall velocity that is nearly equal to that of the other particles in the sample. In general, there appears to be no outstanding visual differences in the particles from the experimental run series A, but with a close inspection one observes a tendency for the average particle size to be smaller for the samples taken from upper levels of the suspension.

The visual uniformity of the glass beads (see figures 4-21 to 4-23) might cause one to predict that such a material would fluidize in a uniform manner, however, as one notices in figure 4-4, the local concentration near the bottom of suspension A1 is about twice the local concentration near the top of the suspension. Also, although distribution of free-fall velocities is quite narrow (see figure 3-3), it can by no means be classified as one of those imaginary "uniform"

materials referred to by so many theoreticians. Material A is, however, the most uniform material used in this study and for practical purposes, it is certainly a more uniform material than one normally encounters. Emphasis on even its lack of uniformity is merely made to establish the need for the more detailed description of granular materials. Investigators who study fluidization phenomena have been content to report only the mean particle size of a granular material as determined by a sieve analysis. This information, in itself, is inadequate.

Materials Z and G are quartz sands. The individual particles appear to be sub-angular. Figure 4-24, samples from run Z20, visually shows a definite change in size for the five local samples. The particles, sample Z20-1, are smaller and more uniform in size than the particles in sample Z20-5 which comes from a lower level of the suspension. The difference in size in the local samples from runs Z21 and Z22, figures 4-25 - 4-26, is not so striking but still it is quite easily discernible.

The samples from run G18, figure 4-27, again show the definite change in size for the five local samples. Figures 4-28 and 4-29 are also samples of material G but for a higher mean concentration than run G18. The size difference for the samples, runs G19 and G20, appears to be even less discernible than the photographs of the glass beads, material A.

Figure 4-30 is for material S, a sand, which is the most non-uniform or widely distributed granular material studied. The change

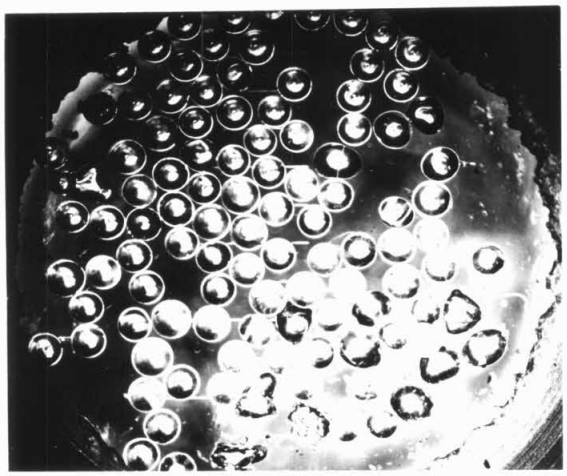

Sample A1-1 $w_g = 6.21$ cm/sec $\sigma_w = 1.03$
$y/d = 0.98$

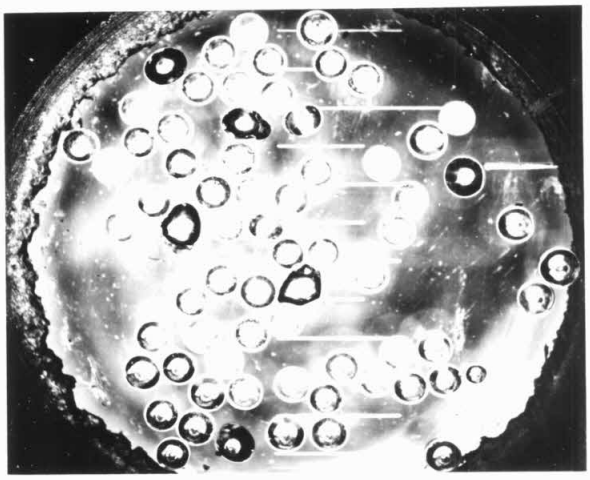

Sample A1-2 $w_g = 6.69$ cm/sec $\sigma_w = 1.04$
$y/d = 0.49$

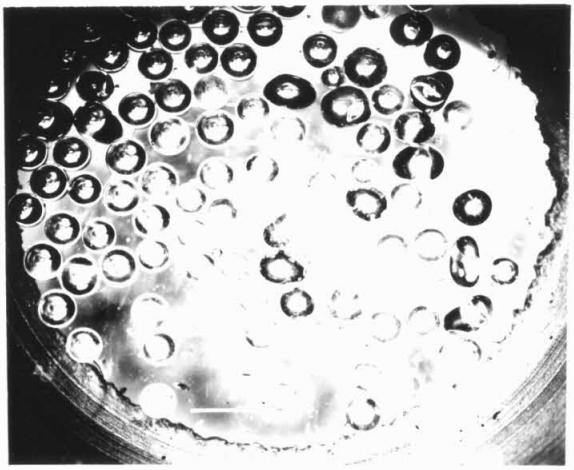

Sample A1-3 $w_g = 6.90$ cm/sec $\sigma_w = 1.07$
$y/d = 0.30$

Note that two scale divisions equal 1mm.

Fig. 4-21 Microphotographs of Samples of Glass Beads from Run A1

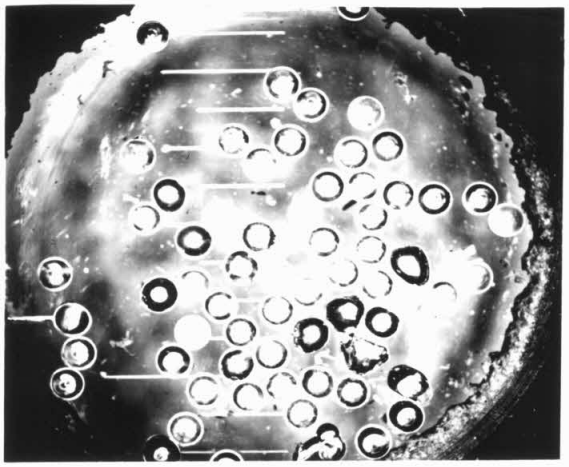

Sample A2-1 $w_g = 6.18$ cm/sec $\sigma_w = 1.04$
$y/d = 0.95$

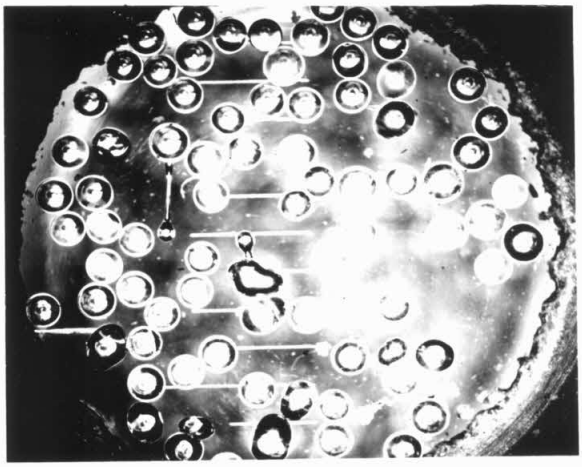

Sample A2-2 $w_g = 6.76$ cm/sec $\sigma_w = 1.05$
$y/d = 0.49$

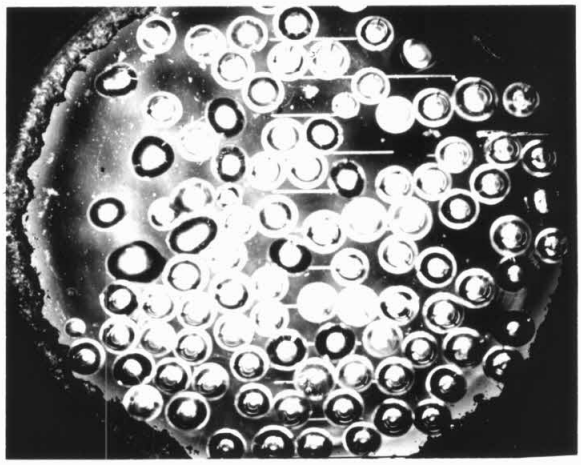

Sample A2-3 $w_g = 7.02$ cm/sec $\sigma_w = 1.09$
$y/d = 0.28$

Note that two scale divisions equal 1 mm.

Fig. 4-22 Microphotographs of Samples of Glass Beads from Run A2

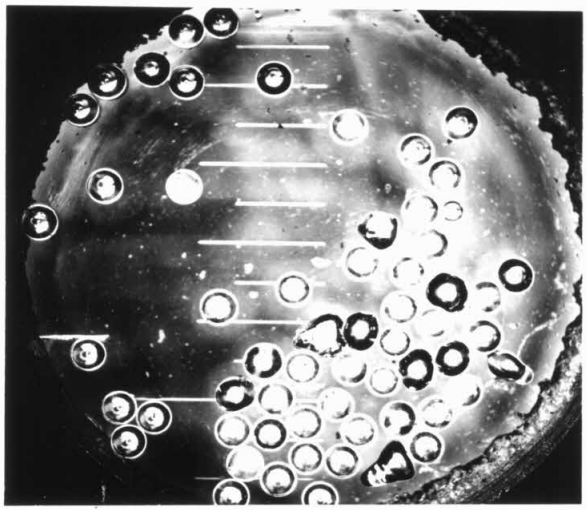

Sample A3-1 $w_g = 6.15$ cm/sec $\sigma_w = 1.04$
$y/d = 0.98$

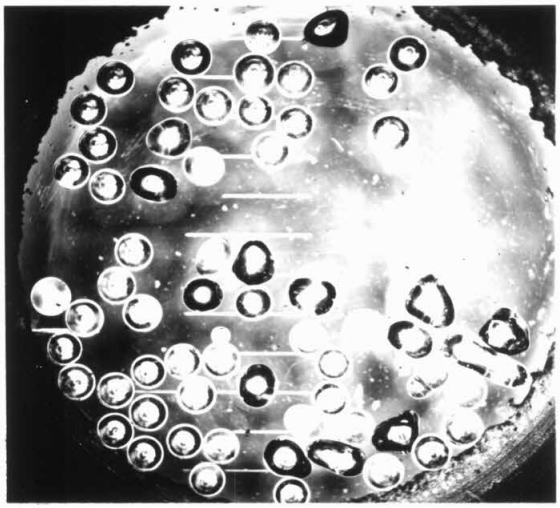

Sample A3-2 $w_g = 6.71$ cm/sec $\sigma_w = 1.08$
$y/d = 0.44$

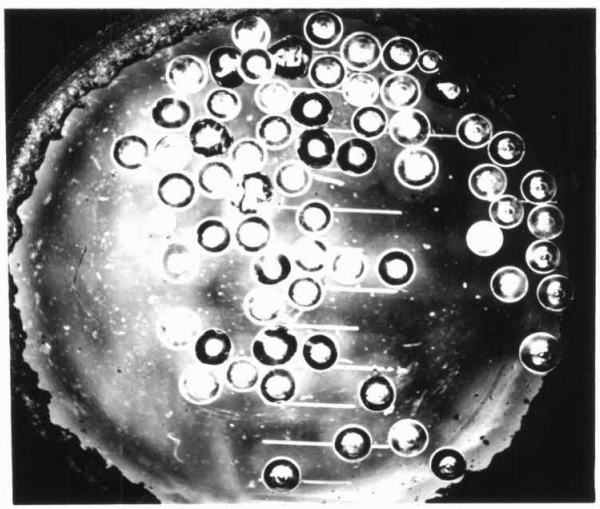

Sample A3-3 $w_g = 6.59$ cm/sec $\sigma_w = 1.06$
$y/d = 0.26$

Note that two scale divisions equal 1 mm.

Fig. 4-23 Microphotographs of Samples of Glass Beads from Run A3

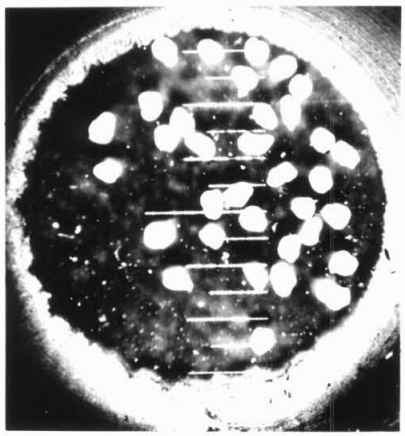

Sample Z20-1 w_g=5.32 cm/sec σ_w=1.03
y/d = 0.95

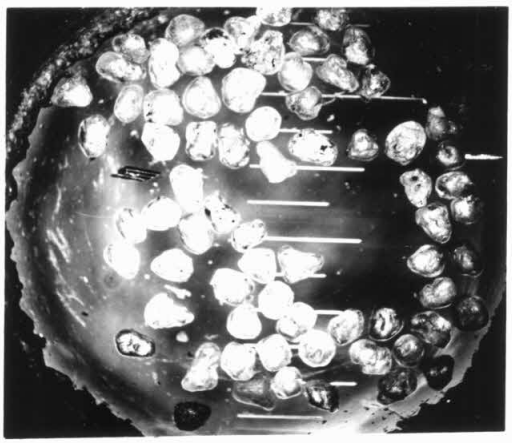

Sample Z20-2 w_g=5.60 cm/sec σ_w=1.06
y/d = 0.80

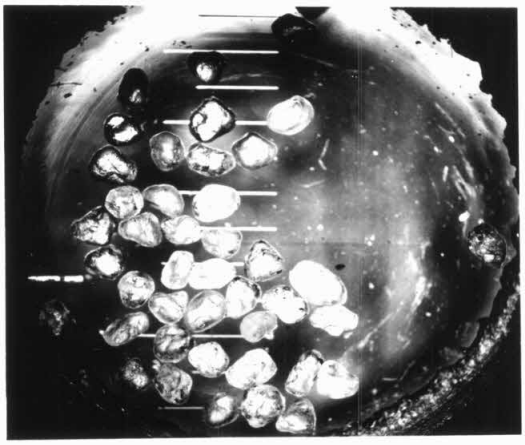

Sample Z20-3 w_g = 6.05 cm/sec σ_w=1.05
y/d = 0.60

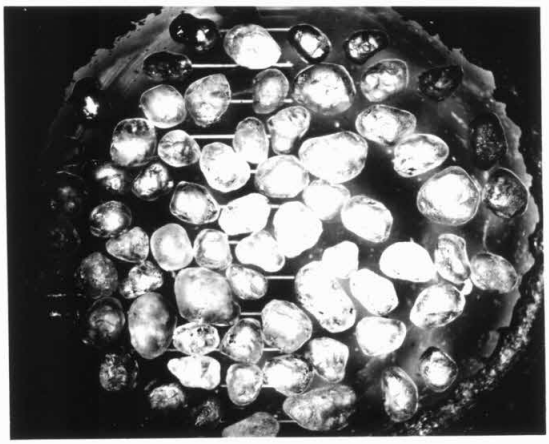

Sample Z20-4 w_g = 7.49 cm/sec σ_w= 1.17
y/d = 0.44

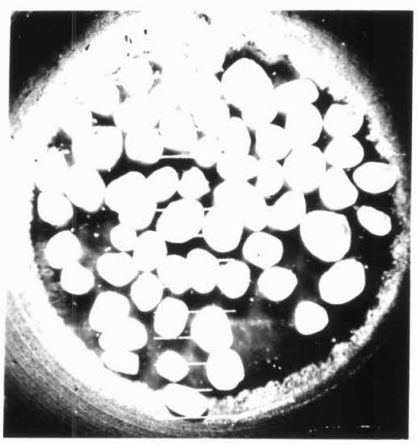

Sample Z20-5 w_g=9.14 cm/sec σ_w=1.15
y/d = 0.29

Note that two scale divisions equal 1 mm.

Fig. 4-24 Microphotographs of Samples of Sand Grains from Run Z20

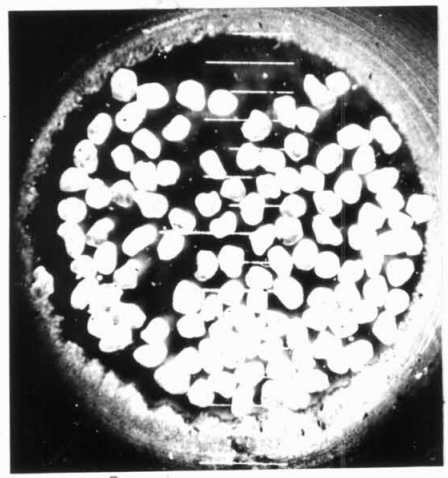

Sample Z21-1 $w_g = 5.35$ cm/sec $\sigma_w = 1.03$
$y/d = 1.0$

Sample Z21-2 $w_g = 6.11$ cm/sec $\sigma_w = 1.08$
$y/d = 0.74$

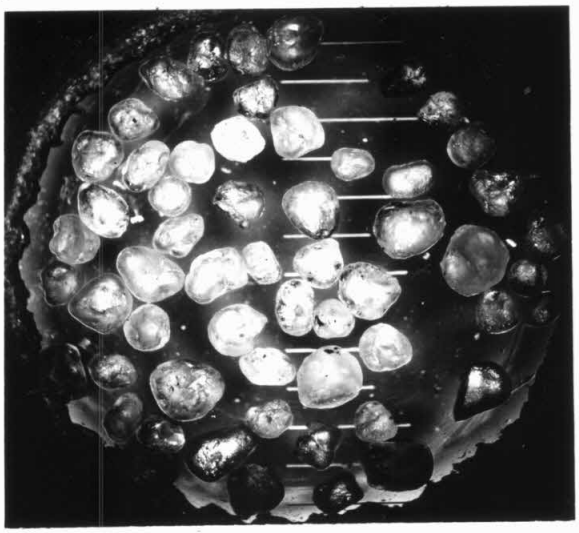

Sample Z21-3 $w_g = 7.76$ cm/sec $\sigma_w = 1.17$
$y/d = 0.51$

Note that two scale divisions equal 1 mm.

Fig. 4-25 Microphotographs of Samples of Sand Grains from Run Z21

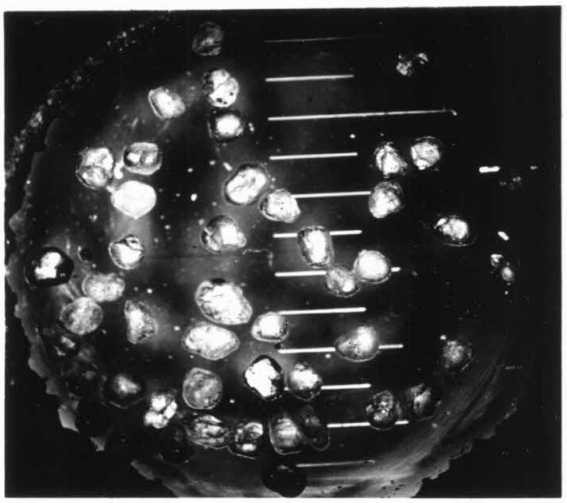

Sample Z22-1 w_g = 5.67 cm/sec σ_w = 1.07
y/d = 0.99

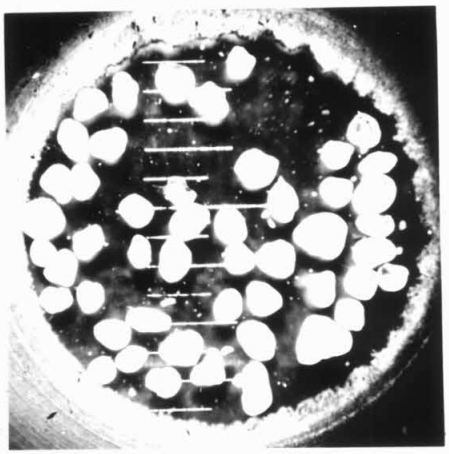

Sample Z22-2 w_g = 6.92 cm/sec σ_w = 1.21
y/d = 0.69

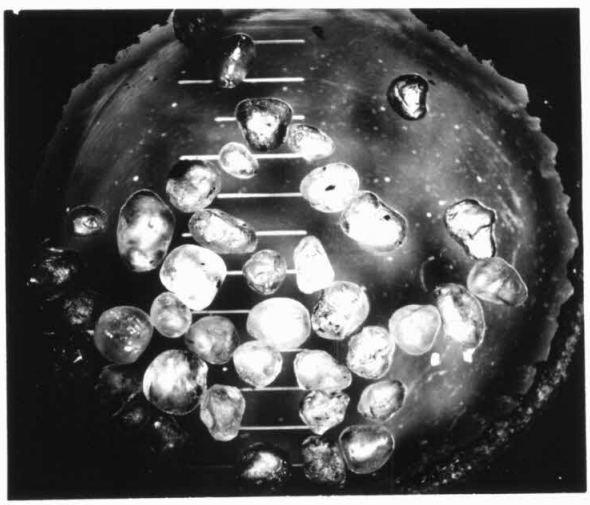

Sample Z22-3 w_g = 7.67 cm/sec σ_w = 1.19
y/d = 0.32

Note that two scale divisions equal 1 mm.

Fig. 4-26 Microphotographs of Samples of Sand Grains from Run Z22.

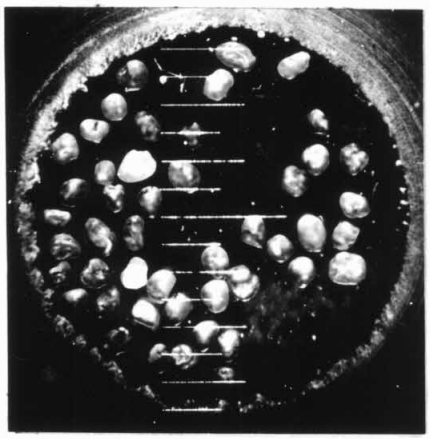

Sample G18-1 $w_g = 6.26$ cm/sec $\sigma_w = 1.07$
$y/d = 0.95$

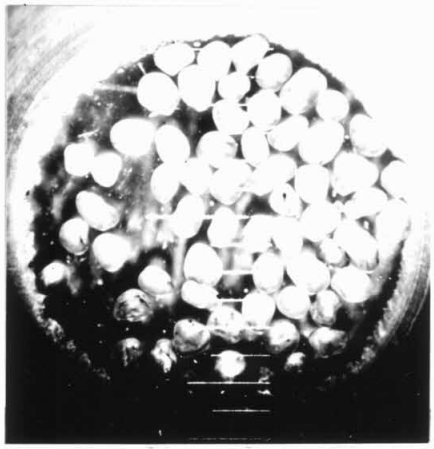

Sample G18-2 $w_g = 7.76$ cm/sec $\sigma_w = 1.12$
$y/d = 0.74$

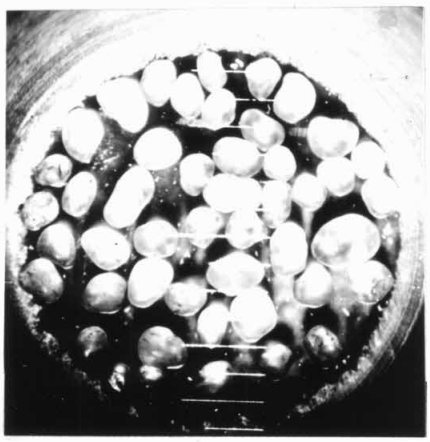

Sample G18-3 $w_g = 9.04$ cm/sec $\sigma_w = 1.16$
$y/d = 0.54$

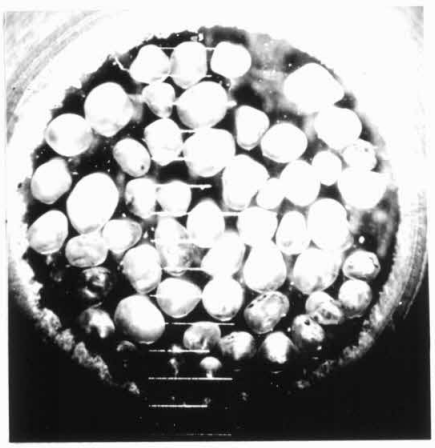

Sample G18-4 $w_g = 8.62$ cm/sec $\sigma_w = 1.13$
$y/d = 0.34$

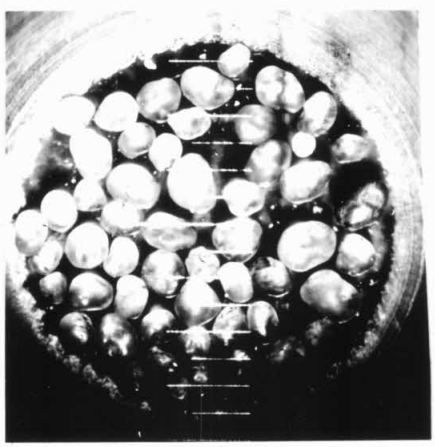

Sample G18-5 $w_g = 9.12$ cm/sec $\sigma_w = 1.21$
$y/d = 0.20$

Note that two scale divisions equal 1 mm.

Fig. 4-27 Microphotographs of Samples of Sand Grains from Run G18

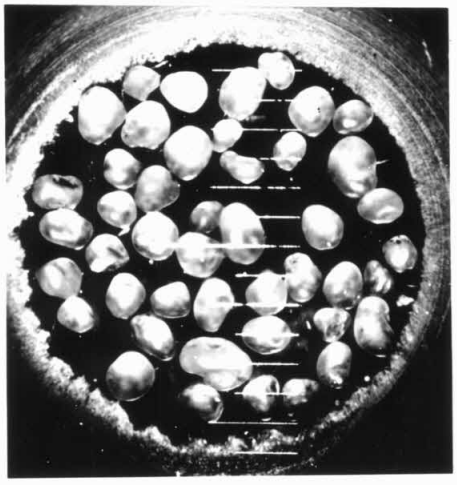

Sample G19-1 $w_g = 8.49$ cm/sec $\sigma_w = 1.17$
$y/d = 0.84$

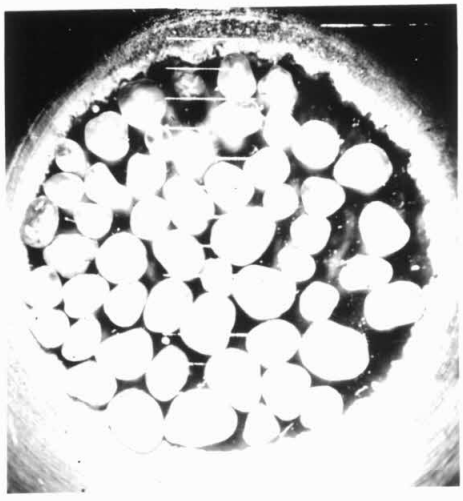

Sample G19-2 $w_g = 8.87$ cm/sec $\sigma_w = 1.20$
$y/d = 0.51$

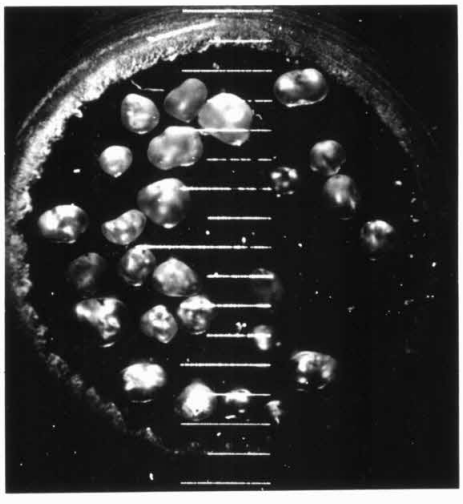

Sample G19-3 $w_g = 8.79$ cm/sec $\sigma_w = 1.21$
$y/d = 0.15$

Note that two scale divisions equal 1 mm.

Fig. 4-28 Microphotographs of Samples of Sand Grains from Run G19

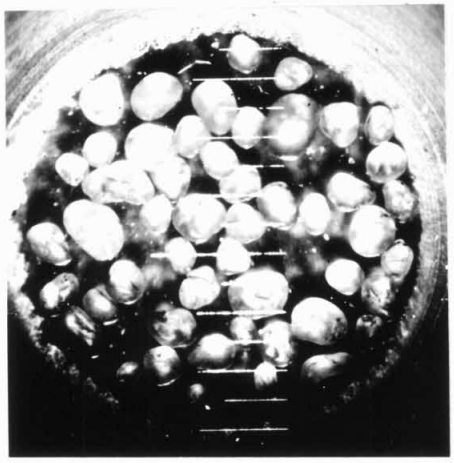

Sample G20-1 w_g = 8.53 cm/sec σ_w = 1.17
y/d = 0.87

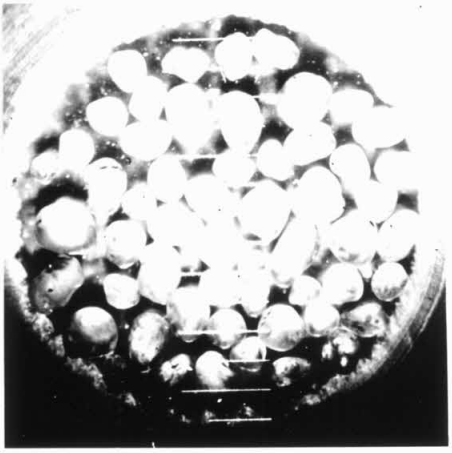

Sample G20-2 w_g = 8.40 cm/sec σ_w = 1.22
y/d = 0.49

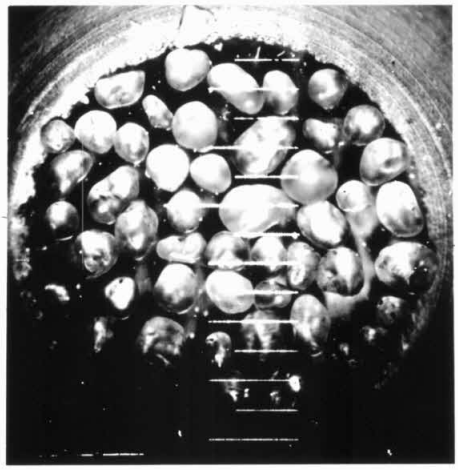

Sample G20-3 w_g = 8.55 cm/sec σ_w = 1.21
y/d = 0.15

Note that two scale divisions equal 1 mm.

Fig. 4-29 Microphotographs of Samples of Sand Grains from Run G20

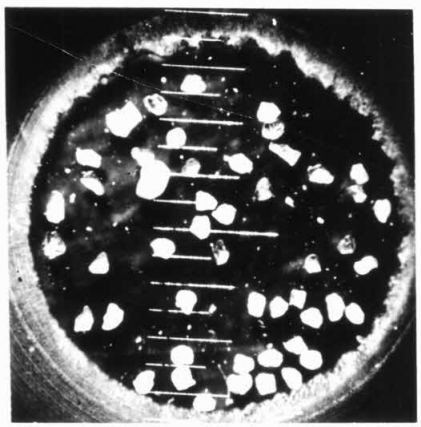

Sample SS14-1 $w_g = 3.72$ cm/sec $\sigma_w = 1.05$
$y/d = 0.95$

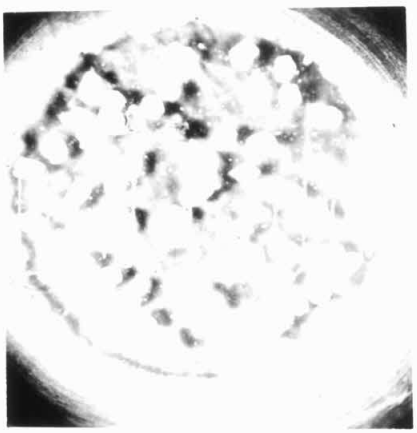

Sample SS14-2 $w_g = 4.18$ cm/sec $\sigma_w = 1.08$
$y/d = 0.69$

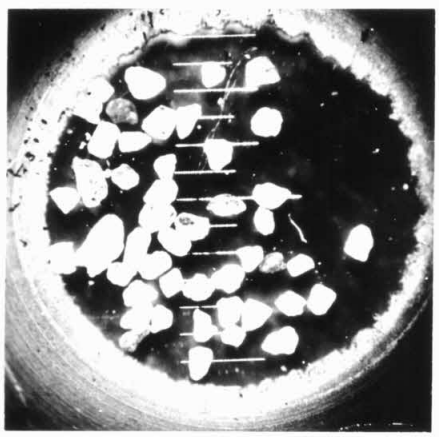

Sample SS14-3 $w_g = 5.10$ cm/sec $\sigma_w = 1.10$
$y/d = 0.45$

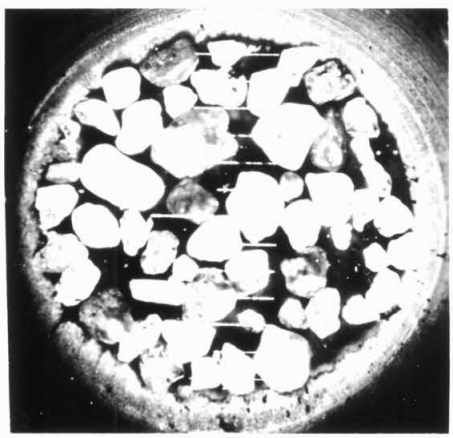

Sample SS14-4 $w_g = 6.97$ cm/sec $\sigma_w = 1.29$
$y/d = 0.20$

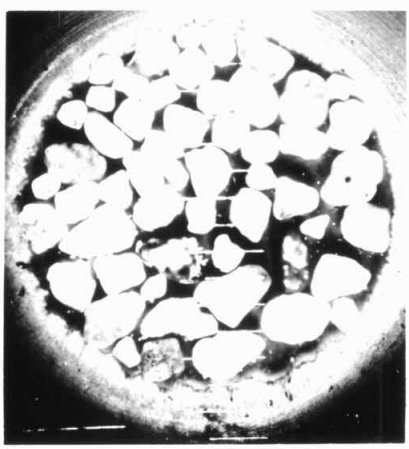

Sample SS14-5 $w_g = 7.38$ cm/sec $\sigma_w = 1.36$
$y/d = 0.07$

Note that two scale divisions equal 1mm.

Fig.4-30 Microphotographs of Samples of Sand Grains from Run SS14

in the average particle size is readily apparent from the photographs. Relative to the other materials studied, material S is the most angular.

4-6 Hindered Settling Velocity

Measurements of the hindered settling velocity of several suspensions were made using the photographic method described in chapter 2. The results of these measurements are presented in Table 4-3 where V_{H1} is the hindered settling velocity by the photograph method and V_{H2} is the hindered settling velocity obtained from measurements with a hand-held stopwatch. Comparing the values of the superficial velocity, $\bar{u}$, necessary to make a given suspension and V_H, the hindered settling velocity of the suspension, one observes that the hindered settling velocity is generally a few per cent less than the superficial velocity. This per cent difference is so small that it would be ignored if it were not so consistently in one direction. Attempts to find errors of sufficient magnitude in the measurements which would bias the data were unsuccessful. The superficial velocity is obtained by dividing the discharge of water through the column by the column cross-sectional area. The discharge measurement is considered good to ±1 per cent. The cross-sectional area of the column was checked by adding a known weight of water to the column and measuring the change in elevation of the water surface in the column. These measurements indicated that the column cross-sectional area was constant to within ±1 per cent of the value 1.01 ft^2. The camera, while taking the hindered settling photographs, was not held at the level of the falling upper surface of the suspension, but remained fixed at about the elevation of

the settled bed. Because of refraction of light through the 1/2 in. thick lucite wall and the fact that the elevation scale is on the outside of the column wall, the camera would not see the true elevation of the suspension surface. This refraction would cause the observed hindered settling velocity to be less than the true value. A computation based on the index of refraction of lucite and the relative position of the camera and the falling suspension showed this error to be quite small. Some measurements were made simultaneously with a hand-held stopwatch and with the photographic method. These results are given for material F, a quartz sand, $D_g = 0.456$ and $\sigma_g = 1.14$ in Table 4-3. The stopwatch measurements show that V_H appears to be less than $\bar{u}$ by an amount which is greater than the photographic method. Although the observer using the stopwatch can directly look at the falling suspension surface without refraction effects, he finds some difficulty in observing the surface because it is wavy. Subsequently, it is believed that this type of measurement is subject to more error than the determination of the hindered settling velocity from a plot of surface elevation vs. time as obtained from the photographs. In conclusion, the hindered settling velocity of a suspension appears to be nearly identical to the superficial velocity necessary to produce the suspension. However, because of the consistency of the small difference in the two quantities, the hindered settling velocity may be, if not identical, slightly less than the superficial velocity.

Some other information was obtained from the photographs of

the settling suspensions. Observations of the rate of rise of the settled bed showed that this quantity was not a constant. The rate of rise was consistently faster initially and then slowed down. By continuity, if the rate of fall of the entire suspension is taken as constant, and this was observed to be true, the non-uniform rate of rise of the settled bed would indicate that the concentration-depth profile for the suspension is not uniform. This information on the non-uniformity of the concentration-depth profile is consistent with the other measurements reported herein. The initial fast rate of rise indicates that initially more material is settling out of suspension than at later times. A slowing down of the rate of rise with time indicates that the concentration at higher levels in the suspensions is less than near the bottom, as observed by other more direct means.

Table 4-3

Comparison of Hindered Settling Velocity

and Superficial Velocity Measurements

Material	Run No.	Mean Concentration $\bar{C}$	Superficial Velocity $\bar{u}(\frac{cm}{sec})$	Hindered Settling Velocity $V_{H1}(\frac{cm}{sec})$	$V_{H2}(\frac{cm}{sec})$
A	HSI-1	.092	4.63	4.60	
A	HSI-2	.114	4.39	4.28	
A	HSI-3	.138	4.06	3.84	
A	HSI-4	.149	3.93	3.70	
A	HSI-5	.076	4.82	4.65	
A	HS2-1	.088	4.67	4.63	
A	HS2-2	.106	4.45	4.38	
A	HS2-3	.120	4.30	4.20	
A	HS2-4	.120	4.30	4.20	
Z	Z20	.112	4.70	4.62	
Z	Z21	.150	4.30	4.25	
Z	Z22	.216	3.60	3.42	
G	G11	.283	3.66	3.44	
G	G12	.236	4.24	3.85	
G	G13	.197	4.88	4.57	
G	G14	.177	5.12	5.04	
G	G15	.169	5.37	5.05	
G	G16	.156	5.49	5.20	
G	G17	.136	5.73	5.70	
G	G18	.154	5.40	5.15	
G	G19	.243	4.18	4.15	
G	G20	.243	4.21	3.95	
S	SS10	.187	3.19	2.82	
S	SS11	.165	3.29	3.34	
S	SS12	.125	3.60	3.60	
S	SS14	.130	3.57	3.42	
F	F1		5.41	5.29	5.41
F	F2		5.32	5.26	5.37
F	F3		4.53	4.50	4.38
F	F4		4.43		4.18
F	F5		4.55	4.42	4.44
F	F6		4.41	4.38	4.18
F	F7		3.61	3.59	3.40

V_{H1} = hindered settling velocity from photographs

V_{H2} = hindered settling velocity from hand-held stopwatch measurements

CHAPTER 5

DISCUSSION OF RESULTS

5-1 General Description of the Suspensions

Granular solids such as sand and glass beads which have mass densities that are about two and one-half times the density of water fluidize in water in a manner known as particulate fluidization. The term "particulately fluidized" means that the particles visually appear to be uniformly dispersed within the suspension. The upper surface of such a suspension is sharply defined (see figure 5-1) and stable. The interface is called stable because a particle getting into the region of clear fluid above the suspension encounters a local upward fluid velocity in that region which is less than the particle settling velocity, and therefore it settles back to the suspension interface. On the other hand, the lower suspension interface must be unstable. A particle getting into clear fluid below a suspension may fall away from the suspension. For this reason, in order to maintain a suspension, it is necessary that the lower interface be supported in some way by a screen or porous plate, even though the submerged weight of the particles is balanced by the fluid shear on the particles.

The particles in a suspension are in a continuous turbulent state of movement. If one were to fix his attention at a horizontal plane which is stationary in space (i.e., fixed to the column walls), clusters of particles would be observed to rise and fall across this plane. Swirls of fluid and particles are observed to move rapidly up, down, and across within the suspension. At times, a whirling packet of the

suspension spins fast enough to become clear fluid – the particles having been centrifuged out. In addition, wavelike disturbances constantly move to and fro across the upper interface between the clear fluid and the suspension. Explosion-like bursts, which have dimensions of the order of 100 times a particle diameter, cover the upper interface creating a three-dimensional wave pattern. Sometimes the whole suspension oscillates back and forth as if in resonance with the fluidization column geometry.

At the onset of fluidization of a fixed bed of particles, an interesting local instability is observed. The fixed bed does not become fluidized everywhere at once, but is characterized by local jets of particles and fluid which may be observed at the sand-fluid interface as shown in figure 5-2. Because of their physical appearance, these disturbances on the interface have been called "boils." Herein the boil will be defined as the entire region of the bed which is locally disturbed. The boils are circular in plan view with a diameter which is generally of the same order of magnitude as the depth of the settled bed, and often three or four occur simultaneously on the sand surface in the 30 cm square fluidization column. The central axis of the boil is apparently a channel or region of reduced resistance to the upward fluid flow where the concentration of particles is less than in the fixed bed. Up through the core, there is a rush of fluid and suspended particles which move radially outward on the upper sand surface. It is common for the boils themselves to move horizontally across the sand surface. Often, a single boil will split into two boils which move

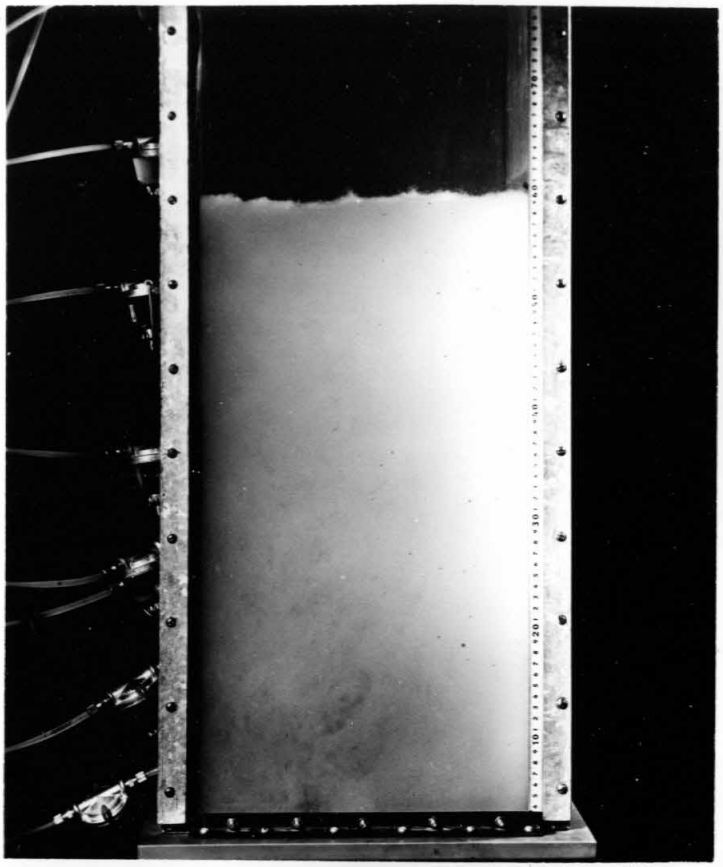

Fig. 5-1a Photograph of Suspension of Glass Beads - Run A2.
$\bar{u} = 4.48$ cm/sec $\bar{C} = 0.106$ $w_g = 0.67$ cm/sec $\sigma_w = 1.06$

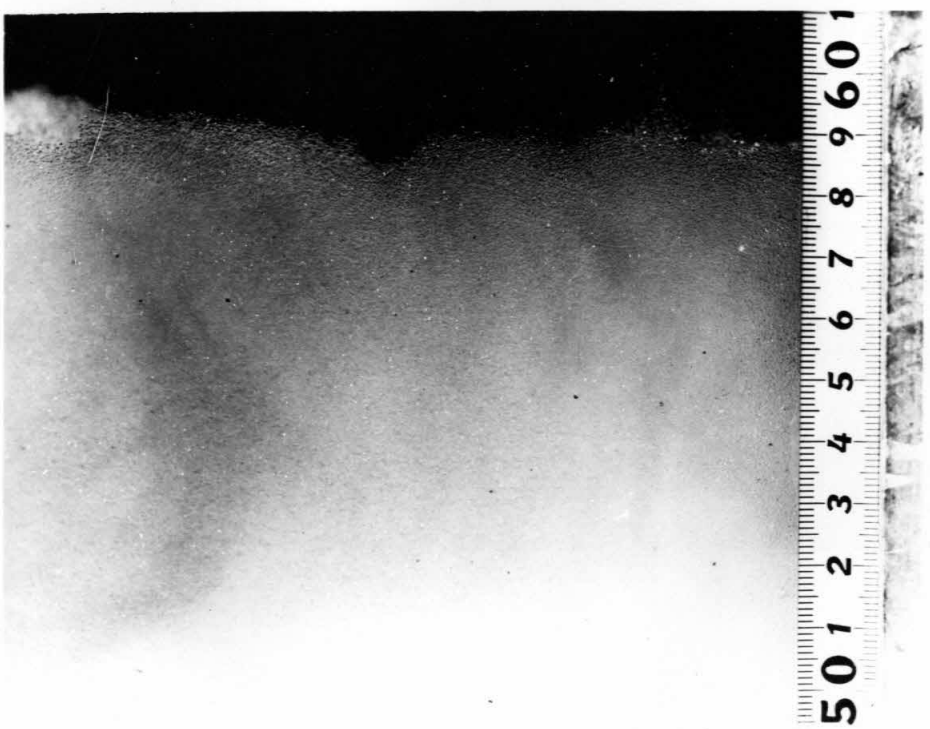

Fig. 5-1b Photograph of the Surface of Suspension of Glass Beads -Run A2. Note the waves on the surface.

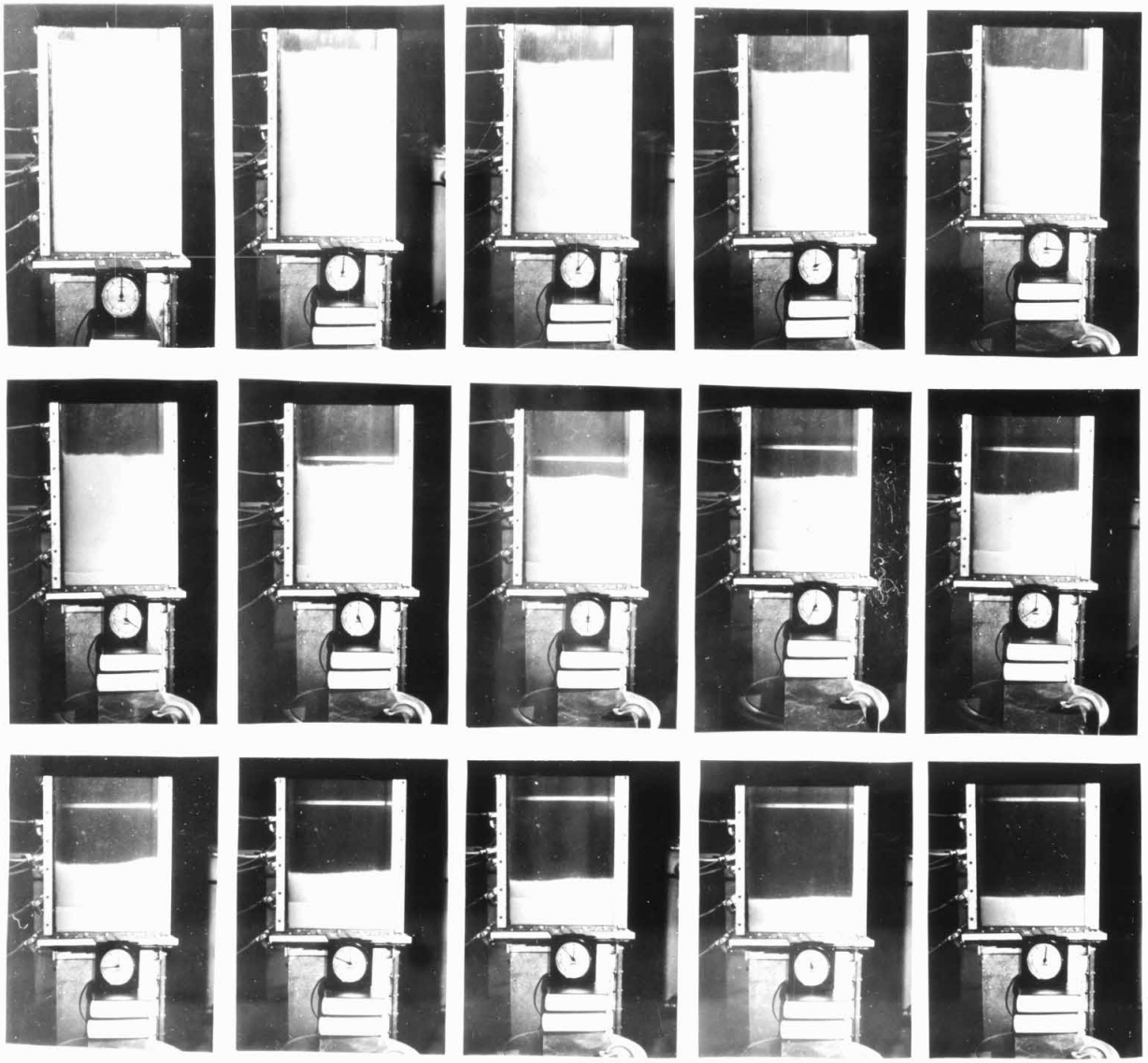

Fig. 5-c Hindered Settling of a Sand Suspension - Run Z 20. Time sequence goes from left to right, top to bottom. Clock has a ten second sweep.

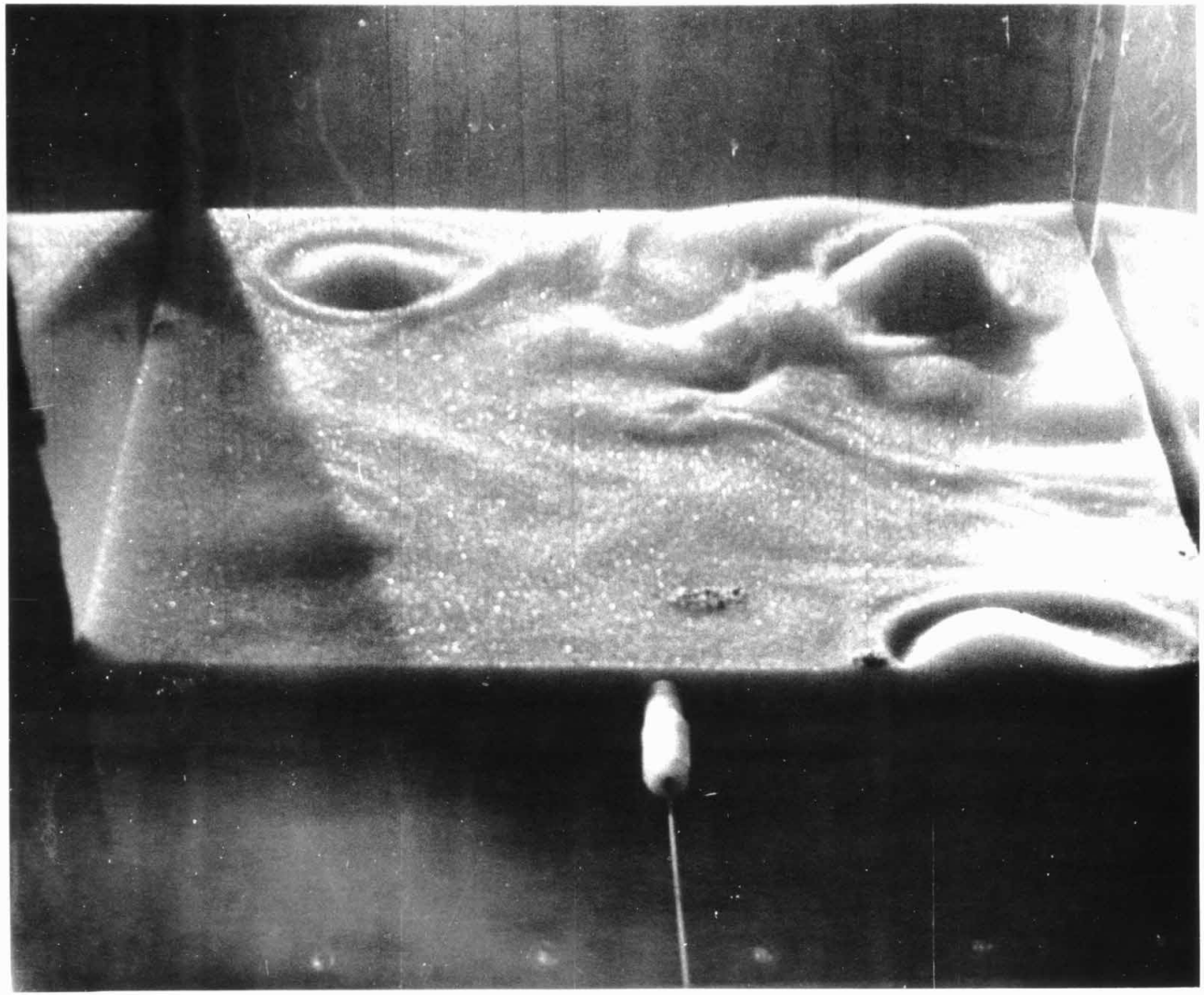

Fig. 5-2 Photograph of Sand Boils on the Surface of a Bed of Glass Beads.
Depth of settled bed ≈ 10cm. Width of bed ≈ 30cm X 30cm. $\bar{u} \approx 0.32$ cm/sec
$w_g = 6.67$ cm/sec $\sigma_w = 1.06$

away from each other. Generally, one of these "second-generation boils" will subside and cease to exist, and another portion of the fixed bed will become fluidized in the form of another boil.

The pattern of boils is quite stable with the exception that boils generated near the wall of the fluidization column tend to move to the wall and remain there rather than move about like the boils generated near the center of the column cross-section. There is also a noticeably frequent occurrence of boils in the corners of the column.

No quantitative study was made of this phenomenon, but the boils brought a great deal of amusement by their peculiar behavior. A qualitative experiment was performed using a two layer sand bed. The lower layer was a quartz sand dyed blue, $D_g = 0.535$ mm and $\sigma_g = 1.11$, and the upper layer was a quartz sand, light tan in its natural color, $D_g = 0.240$ mm and $\sigma_g = 1.08$. The relative settled depths of the two sands was 4 cm for the blue sand and 3 cm for the tan. At the onset of fluidization, local boils, about three or four in number with a plan view diameter of about 4 cm, appeared on the upper interface (i.e., the sand-water interface). These sand boils had the characteristic symmetric profile and behaved quite normally by moving about horizontally. However, the sand rushing up through the core of the boil and spreading itself out radially was always from the tan upper layer of smaller particles, thus indicating that the boil itself was confined to the upper sand layer. While it is possible that the triggering disturbance may have been in the lower (blue) sand bed, this experiment shows that the boils are not strictly limited to the peculiar entrance

conditions produced by flow through a porous plate or screen. In the laboratory, sand boils were produced in sand beds with several different entrance conditions -- a porous ceramic plate, a perforated metal plate, and a coarse gravel bed on top of the ceramic plate. The boils always were similar. Further discussion of sand boils may be found in the papers of Baylis (31) who comments on their occurrence during the backwashing of rapid sand filters in water treatment plants.

Another interesting reference to the subject of sand boils is a paper by Housner (8) where a transient boiling of some unconsolidated sand beds was observed after an earthquake in India. Housner describes the mechanism responsible for this transient sand boiling in terms of the well-known equations for flow through a saturated soil. If an overpressure is created at some depth in the soil due to the readjustment of the packing of the particles following a disturbance like a seismic wave, the soil body will be compressed and a certain quantity of the water squeezed out. Making use of a linear stress-strain relationship, the continuity equation, Darcy's law, and a static force balance equation saying that the total pressure at a point is due to the total weight of soil plus water above that point, Housner is able to show that the soil-water system readjusts itself to the overpressure by a diffusion process. The overpressure diffuses upward through the soil and if the gradient of the overpressure at the upper surface equals the buoyant weight of the soil, a quicksand condition will occur. Due to local inhomogeneities in the soil permeability, local increases in pressure produce isolated disturbances. For assumed values of

permeability and modulus of elasticity that are typical of a sandy soil, Housner is able to show that the production of jets of sand and water does not require overpressures larger than are typical of seismic disturbances.

5-2 Mean Concentration and Superficial Velocity

In chapter 1 the method used by Richardson and Zaki (4) for data analysis was discussed. They found that their data could be reasonably approximated by a straight line if they plotted the logarithm of the superficial velocity, $\bar{u}$, vs. the logarithm of the suspension porosity, (1-C), indicating a power relationship between $\bar{u}$ and (1-C) of the form $\bar{u} \sim (1-C)^n$ where n is the slope of the fitted line. However, upon extrapolating their data for $C \to 0$, Richardson and Zaki found that the extrapolated value of the superficial velocity, $\bar{u}_i$, equalled the representative free-fall velocity for the particles for particle Reynolds numbers less than 0.2, but did not equal the particle free-fall velocity for particles with Reynolds numbers outside the Stokes' range. Physically, as the concentration, C, of the suspended particles approaches zero, the flow condition becomes that of an isolated particle in an upward flow. One would expect that the superficial velocity must equal the free-fall velocity of the isolated particle in order to keep such a particle suspended. Differences between $\bar{u}_i$ and the representative free-fall velocity for Reynolds numbers > 0.2, which were of the order of 1 to 25 per cent, were explained by the fact that the diameter of their fluidization column was not always very large compared to particle diameters. Also, Richardson and Zaki

Table 5-1

Comparison of Extrapolated Values of Superficial Velocity and Representative Free-Fall Velocity

Material	Value of $\overline{u}$ for $\overline{C} \rightarrow 0$ $\overline{u}_i$ (cm/sec)	Representative Mean Free-Fall Velocity $\overline{\mu}$ (cm/sec)	Geom. Std. Dev. of Free-Fall Vel. σ_w	Ratio of $\frac{\overline{u}_i}{\overline{\mu}}$
A - Glass Beads	5.86	6.69	1.06	.876
Z - Sand	6.00	7.80	1.21	.779
G - Sand	8.90	8.95	1.16	.994
S - Sand	4.90	7.59	1.32	.646

calculated the representative free-fall velocity for the particles of various shapes but did not measure it directly.

Table 5-1 was prepared from data reported herein. Values of $\overline{u}_i$ were calculated by plotting the superficial velocity, $\overline{u}$, and the mean concentration, $\overline{C}$, in a manner similar to that of Richardson and Zaki; that is, $\overline{u}_i$ was obtained by determining the value of $\overline{u}$ for which $\overline{C} \rightarrow 0$ by extrapolation of a logarithmic graph of $\overline{u}$ vs $(1-\overline{C})$. Four values of $\overline{u}_i$ were calculated by the extrapolation, one for each of the four granular materials. The values of $\overline{\mu}$, the representative free-fall velocity, were obtained by dropping a sample of the particles and measuring the fall velocity as is explained in chapter 3. With the exception of material G, the differences between $\overline{u}_i$ and $\overline{\mu}$ are significant. One can most easily explain this difference, not in terms of column and particle diameter*, but by considering the problem of extrapolating the superficial velocity data for $\overline{C} \rightarrow 0$. The fact that this extrapolation is uncertain is easily seen from figures 4-1 and 4-2, chapter 4. As the concentration of suspended particles changes by orders of magnitude, the character of the problem must also change. One might expect that a relationship that holds true for data of one order of magnitude, for example, $0.10 \leq C \leq 0.50$, does not describe the problem when the concentration, C, becomes several orders of magnitude smaller, i.e., $C \rightarrow 0$.

In figure 4-1, the graph of mean concentration, $\overline{C}$, vs the ratio of the superficial velocity, $\overline{u}$, to the particle mean free-fall velocity,

* The width of the fluidization column is several hundred times larger than the diameter of a single particle for this study.

$\overline{\mu}$, one observes that the data for each material can be fitted with a smooth curve. This type of data is similar to that of previous investigators discussed in chapter 1, and similarly is limited to the same range of mean concentrations, i.e., $0.05 \leq \overline{C} \leq 0.50$. Comparing the trend of the experimental data in figure 4-1, chapter 4, with the reported results in figure 1-2, chapter 1, one sees that the trend is quite similar. One would have some difficulty in choosing between the several experimentally derived relationships plotted in figure 1-2 to fit best the data in figure 4-1. However, the assignment of mathematical curves to the experimental data of figure 4-1 does little to aid in the understanding of the physics of the suspension.

In figure 4-1, the curves fitted to the experimental data show different trends toward the lower values of mean concentration. This difference in the trend is dependent on the range of particle sizes composing the suspended material. For example, material S, the most widely distributed material, was found to have a mean concentration of about 10 per cent by volume when suspended with a superficial velocity that was about 50 per cent of the representative mean free-fall velocity, $\overline{\mu}$, for that material. For the material Z having practically the same mean particle Reynolds number, but $\sigma_w = 1.21$ compared to $\sigma_w = 1.32$ for material S, a value $\frac{\overline{u}}{\overline{\mu}} = 0.5$ produced suspension with mean concentrations of about 20 per cent by volume. In other words, for the same weight of granular material and for $\frac{\overline{u}}{\overline{\mu}} = 0.5$, a suspension of particles of material S would be about twice as deep as a suspension of the material Z. This lower mean concentration for

material S is caused by the wide range of free-fall velocities for its particles. The superficial velocity which is 50 per cent of the mean free-fall velocity is about 65 per cent of the w_{84} free-fall velocity, and only 35 per cent of the w_{16} free-fall velocity for material S. This means that the coarse fractions of material S, that is, those particles with large free-fall velocities, tend to assume a higher local concentration while the particles with smaller free-fall velocities tend toward lower local concentrations. This sorting of particles according to fall velocity (larger particles near the bottom, and smaller near the top) creates a concentration gradient, and a lower overall average concentration.

5-3 The Experimental Approach to the Fluidization Law

There are two experimental approaches that may be attempted in order to discover the relationship between fluid discharge, particle size, and concentration of the suspended particles. The first approach is to measure the mean properties of suspensions of uniform particles, and the second, to measure the local properties of suspensions of non-uniform particles.

Richardson and Zaki (4), being taken as representative of a whole group of investigators, attempted to obtain the "fluidization law" by carrying out a large series of experiments using uniform particles. From their experiments resulted some empirical formulae (chapter 1, sec. 1-4) which describe the fluidization behavior of uniform materials. It was tacitly assumed in their investigation that uniform particles when suspended in an upward flow produce a suspension in which the

local concentration is everywhere the same as the mean. Their formulae resulted from measurements of the mean concentration and mean particle size.

Another common assumption made by fluidization researchers is that suspensions of non-uniform particles can be treated as a succession of layers of uniform particles. The particles in each layer are assumed to be uniform in size, and as has been shown by experience, it is assumed that the coarsest particles accumulate at the bottom of a suspension and that the finest particles accumulate at the top. Further, they assume that the concentration in each of these successive layers is uniform also. A common procedure to predict the fluidization behavior of a non-uniform material is to first use the formulae of Richardson and Zaki, or something similar, to predict the concentration for each particle size and then to "stack" the various layers of different concentration on top of each other to obtain the concentration distribution for the entire suspension.

Because of the great difficulty in obtaining uniform material, Rouse (7) and the author, as reported herein, attempted a different approach for studying suspensions. Instead of measuring the mean properties of suspensions of uniform particles, they measured the local properties of suspensions of non-uniform particles. If the assumption that a suspension of non-uniform particles is the sum of uniform layers of uniform particles is correct, the results of both types of experiments, namely those of Richardson and Zaki and those of Rouse and the author,

should be identical. However, this does not appear to be completely true as will be explained below.

Figure 5-2a shows the local concentration data reported herein compared to a plotted curve based on the semi-empirical formula of Rouse (chapter 1, sec. 1-7). The comparison between the author's data and Rouse's formula is fairly good. By changing one of Rouse's coefficients by 3 per cent, the formula can be made to fit the experimental data favorably over the entire range of the data. Rouse (7) himself reported that his formula would fit his data better if he allowed the coefficient, B, to vary with particle Reynolds number. However, because of lack of data and for convenience he let the coefficient be unity. The fact that this coefficient is not a constant indicates a weakness in the analysis used by Rouse to derive his formula. Nevertheless, the plotted curve shown by Rouse to fit his experimental data also fits the experimental data of the author. It should be remembered that Rouse and the author performed experiments that were identical in nature. Rouse's experiments were restricted to a single granular material and his experimental methods were somewhat less refined than those of the author but the idea of both experiments was the same.

Figure 5-2b shows the comparison between the local concentration data reported herein and the plotted curves based on the empirical formulae of Richardson and Zaki (chapter 1, sec. 1-4). While the data fall within the range of the plotted curves of figure 5-2b, the comparison is not as favorable as the previous one with the work of Rouse. It should be remembered that the experimental data shown in figure 5-2b are

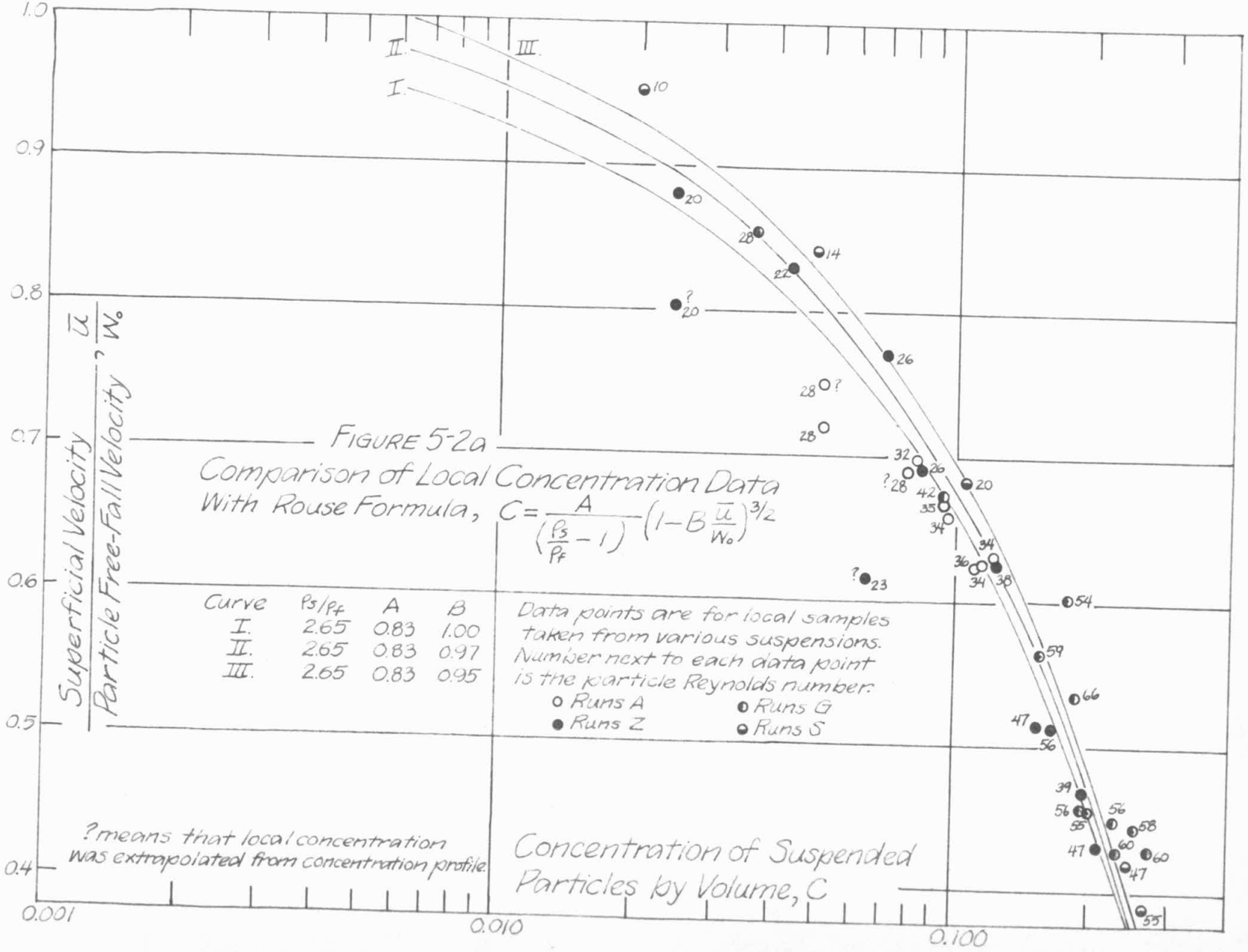

FIGURE 5-2a

Comparison of Local Concentration Data With Rouse Formula, $C = \frac{A}{\left(\frac{\rho_s}{\rho_f} - 1\right)}\left(1 - B\frac{\bar{u}}{W_o}\right)^{3/2}$

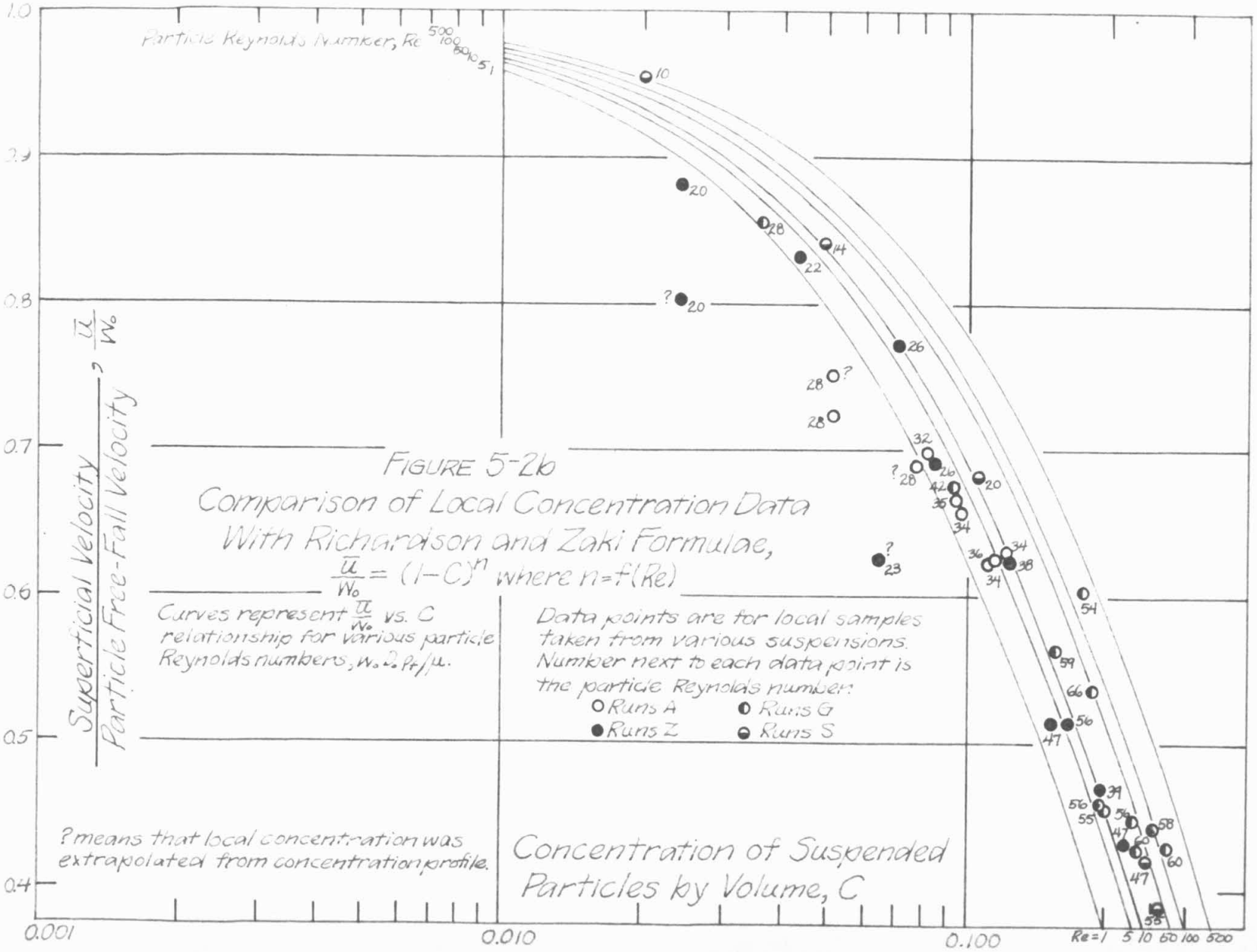

FIGURE 5-2b

Comparison of Local Concentration Data With Richardson and Zaki Formulae, $\frac{\bar{u}}{W_0} = (1-C)^n$ where $n = f(Re)$

from local measurements within suspensions, while the plotted curves are based on measurements of the mean properties of suspensions.

Since the experimental data obtained from measurements of mean properties of suspensions do not exactly coincide with the data obtained from local measurements, one must examine carefully the premises on which the experiments were based. It was already pointed out that there is great difficulty in preparing uniform materials. Measurements reported in chapter 4, figure 4-1, show that a separate relationship between mean concentration, particle size, and superficial velocity was obtained for each material studied. While the relationship between the variables for each material is unique, the relationships are shown to be strongly dependent on the standard deviation of particle sizes for the parent material. One might conclude, therefore, that the formulae of Richardson and Zaki are based on the mean properties of well sorted, but nevertheless non-uniform, materials and cannot be expected a priori to describe accurately the local properties of a suspension. However, due to the extensive nature of the study by Richardson and Zaki, it may be safe to assume that the granular materials used by them can be considered uniform for all practical purposes, even though the only information given about their granular materials was limited to the mean size.

From this comparison between the author's experimental data and the formulae of Richardson and Zaki (figure 5-2b), it is reasonable to conclude that as a first approximation for the local properties of a suspension of non-uniform particles one may use the formulae of

Richardson and Zaki. However, while these formulae allow one to make certain predictions about the nature of a suspension of non-uniform particles, it is clearly recognized from the differences in the local and mean data (figures 5-2a and 5-2b) that a suspension of non-uniform particles is not merely the sum of sorted layers of uniform particles. Further, it will be shown in the following sections that each level of a suspension is not independent of the rest of the suspension but is subject to the diffusion of particles and turbulent energy from above and below.

The lack of precise sorting in suspensions is illustrated in figures 5-3 to 5-5 which show the depth-concentration distribution for particles with free-fall velocities lying within chosen intervals. These figures were prepared from the weighted free-fall velocity distributions for the local samples and the local concentration of suspended particles from the level at which the samples were taken. Each of the figures is for a suspension that was sampled at five elevations, namely, runs G18, Z20, and SS14. The data are presented with the local sampling elevation, y, normalized by dividing by d, the total depth of the suspension. The limits of the chosen velocity intervals were arbitrarily chosen to differ by the fourth root of two. The curves fitted to the data clearly show some sorting. The upper limit of particle position is well defined for each interval, that is, there is a maximum elevation above which a particle does not go. For the particles with the smallest free-fall velocities, this maximum elevation is the upper surface of the suspension. The lower limit of particle position is not well defined. Thus, figures 5-3 to 5-5 indicate that the suspensions are not composed

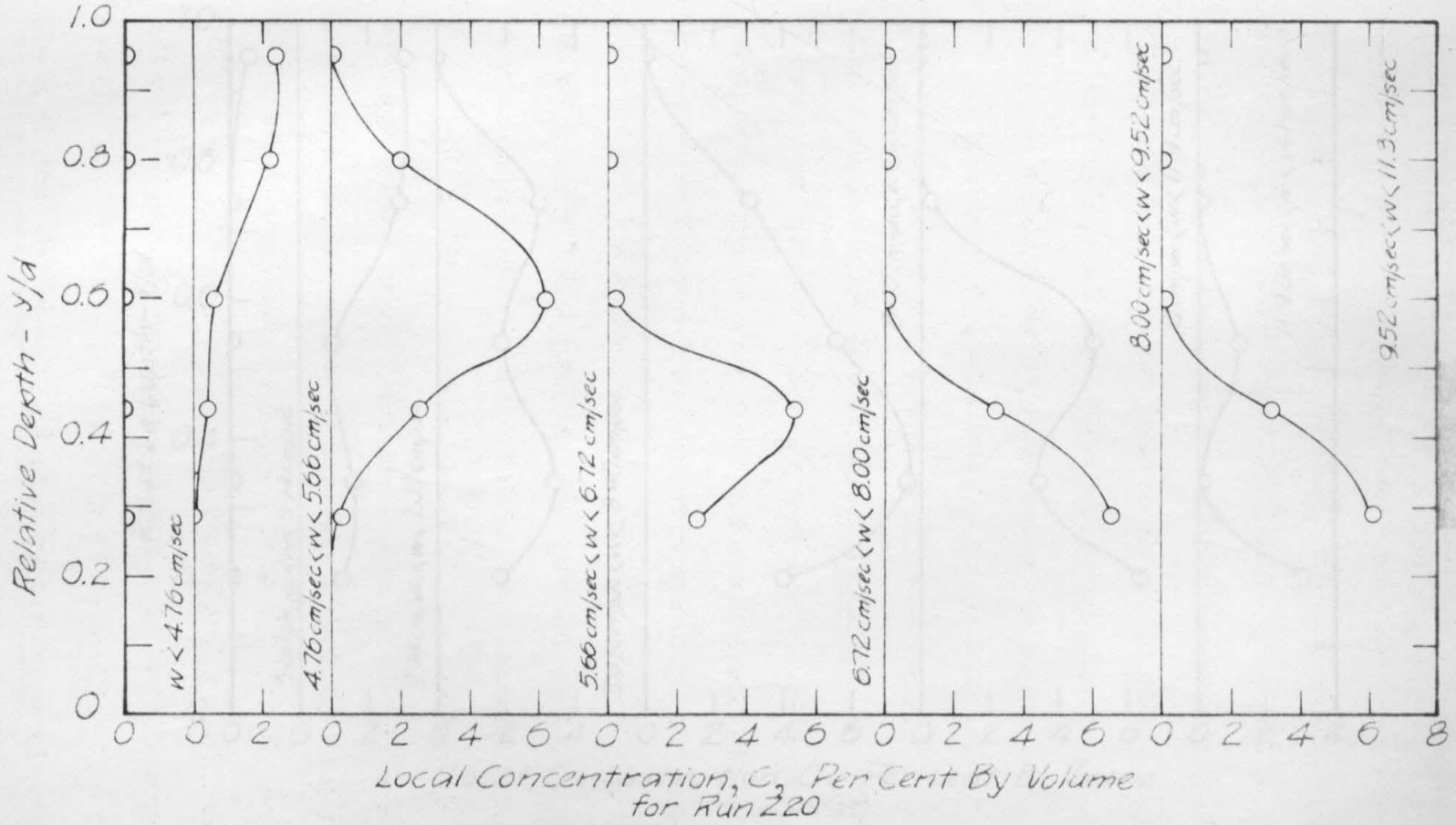

Fig. 5-3 Concentration-Depth Profile for Particles Having Fall Velocities in Intervals As Specified for Run 220

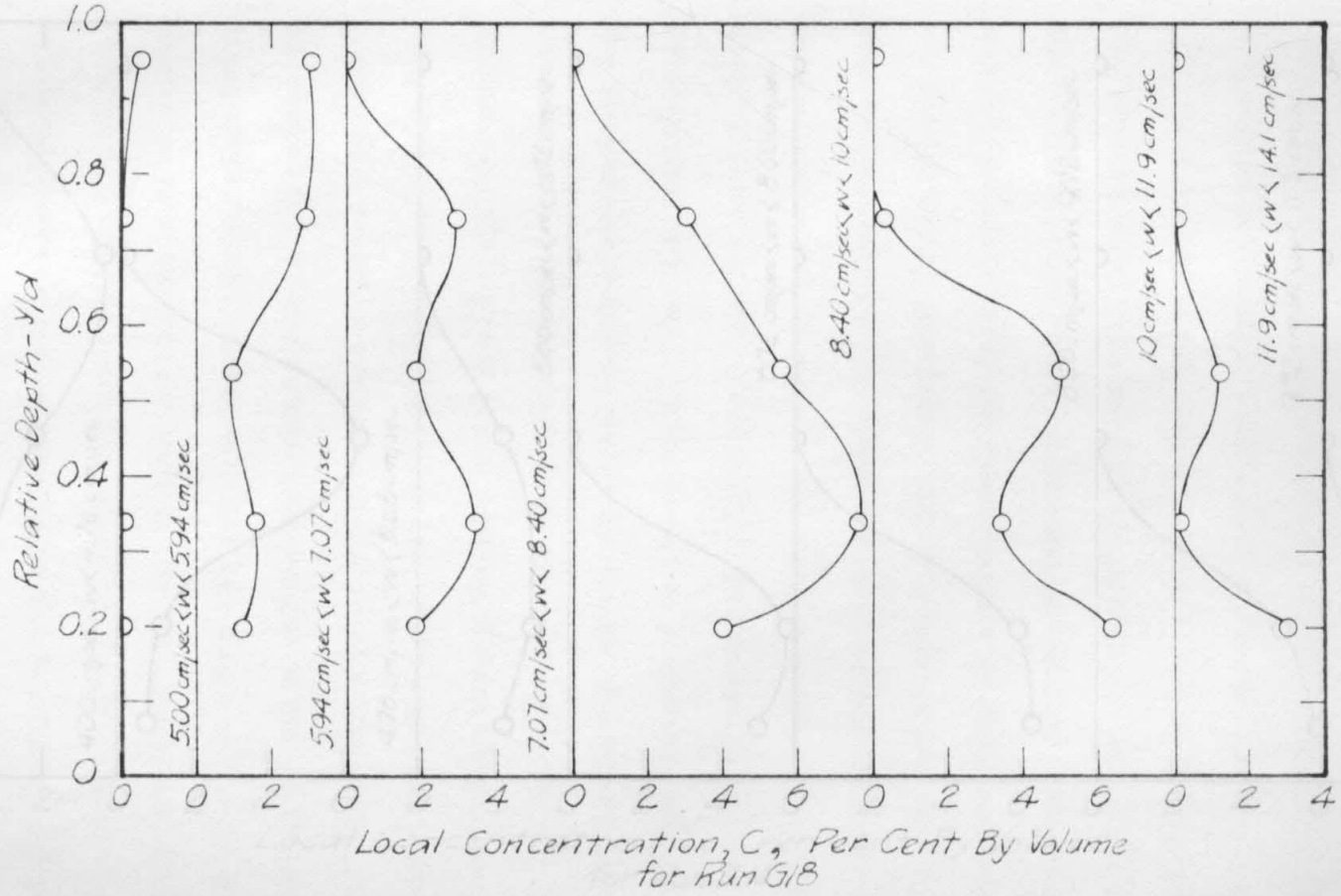

Fig. 5-4 Concentration-Depth Profile for Particles Having Fall Velocities in Intervals As Specified for Run 618

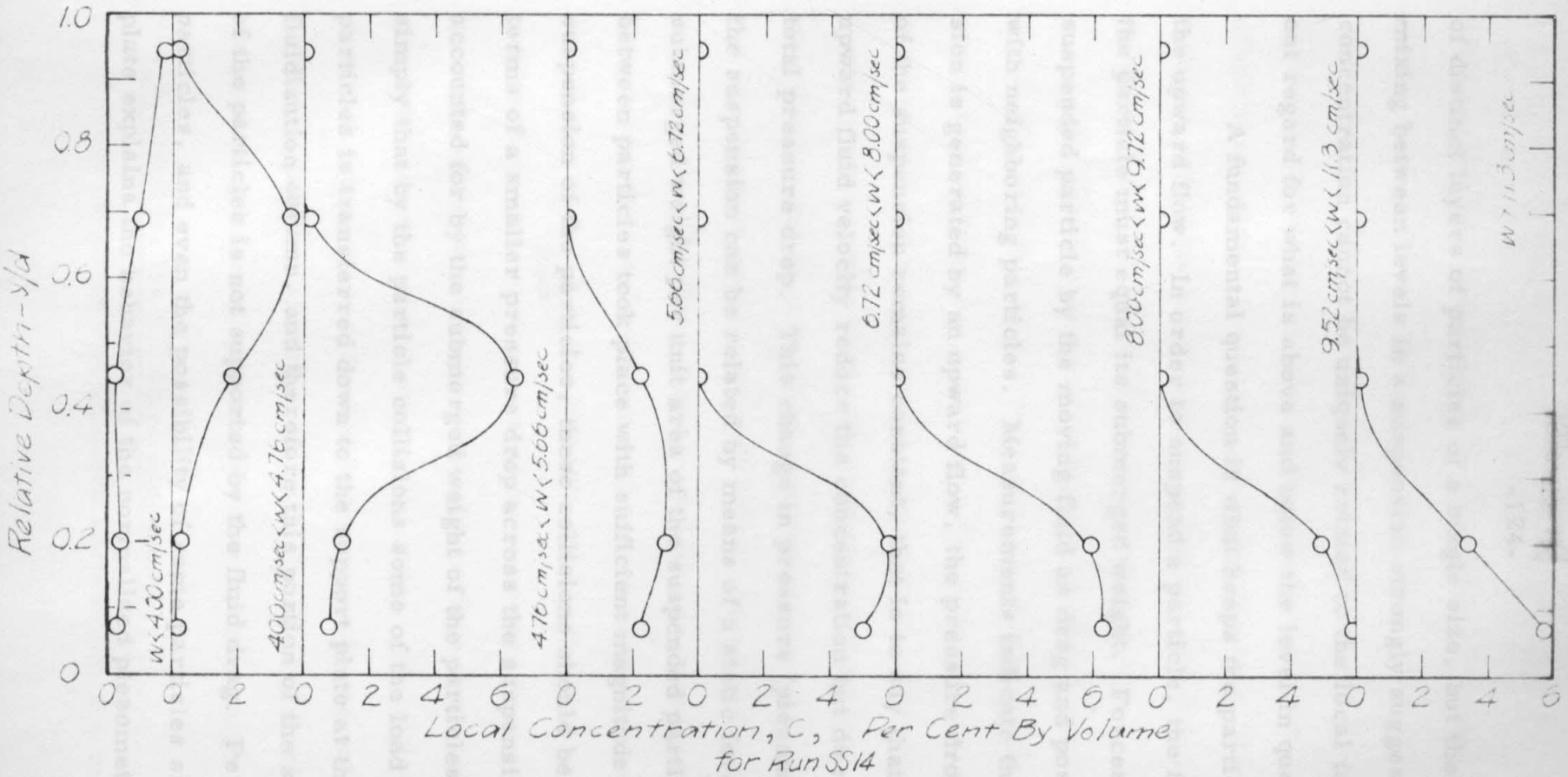

Fig. 5-5 Concentration-Depth Profiles for Particles Having Fall Velocities in Intervals As Specified for Run SS14

of distinct layers of particles of a single size, but there is mixing. This mixing between levels in a suspension strongly suggests that the local concentration cannot be uniquely related to the local fall velocity without regard for what is above and below the level in question.

A fundamental question is what keeps the particles suspended in the upward flow. In order to suspend a particle, the forces acting on the particle must equal its submerged weight. Forces are exerted on a suspended particle by the moving fluid as drag and possibly by collisions with neighboring particles. Measurements indicate that once a suspension is generated by an upward flow, the pressure drop across the height of the suspension remains constant, that is to say that increases in the upward fluid velocity reduce the concentration but do not change the total pressure drop. This change in pressure (piezometric head) across the suspension can be related by means of a static force balance to the submerged weight per unit area of the suspended particles. If collisions between particles took place with sufficient magnitude to aid in the suspension of the particles, these collisions should be manifested in terms of a smaller pressure drop across the suspension than can be accounted for by the submerged weight of the particles. This means simply that by the particle collisions some of the load of the suspended particles is transferred down to the support plate at the bottom of the fluidization column, and therefore this portion of the submerged weight of the particles is not supported by the fluid drag. Perhaps colliding particles, and even the possibility of some particles sitting on the support plate explains the behavior of the normalized piezometric head curves,

h/h_*, shown in figures 4-4 to 4-7, chapter 4. These curves, which should show a value of $h/h_* = 1$ at $y = 0$ if all the particles are supported by fluid drag, cannot be extrapolated to $y = 0$ and $h/h_* = 1$ without assuming unreasonably large concentrations of particles near the bottom of the suspension. However, generally speaking, it is believed that particle collisions are at most a secondary effect in keeping particles suspended in a liquid-solid fluidized suspension.

An unresolved question about a fluidized suspension is whether or not a suspension of perfectly uniform particles would have the same concentration from top to bottom. The premise that uniform particles produce uniform suspensions has been assumed by investigators performing experiments of the Richardson and Zaki type, although this premise has not been verified experimentally. As reported in chapter 4, the experiments using very well sorted glass beads indicate that such material when fluidized shows a variation in concentration from top to bottom of a suspension which is observed to be as much as five-fold (see figure 4-4). It is the author's opinion that due to the turbulent nature of a suspension generated by an upward flow even perfectly uniform particles when fluidized will produce suspensions in which the concentration will vary from top to bottom. The following section will deal with a model for a fluidized suspension based on the mixing and turbulent diffusion of suspended particles which introduces a mechanism for producing non-uniform suspensions of uniform particles.

5-4 A Model for the Fluidized Suspension

It is observed that fluidized suspensions are turbulent systems, and

measurements show clearly that in suspensions of non-uniform materials there is a tendency toward the sorting of sizes into various layers with mixing between the layers. Let us consider a model for a fluidized suspension based on the concept of turbulent diffusion of the suspended particles. The use of the diffusion equation implies a transport relationship for the particles similar to Fick's law for molecular diffusion, and similarly the equation is restricted to very dilute suspensions of particles. One cannot expect the diffusion model to hold true when the concentration of the particles approaches the value of concentration for a fixed (or settled) bed of particles.

The general one-dimensional diffusion equation for the suspended particles may be written

$$\frac{\partial C}{\partial t} = \frac{\partial}{\partial y}\left(\epsilon_m \frac{\partial C}{\partial y}\right) + \frac{\partial}{\partial y}\left(w_c C\right) - \frac{\partial}{\partial y}\left(uC\right) \qquad (5\text{-}1)$$

where C is the concentration of the suspended particles, ϵ_m is the local turbulent diffusion coefficient, u is a velocity which expresses the tendency of the flow to lift the particles upward, w_c is a velocity which expresses the tendency of the particles to settle under the action of gravity, and y is the vertical position coordinate defined as being positive upwards. These quantities will be subsequently defined in more detail. However, for convenience, u will be called the local upward transport velocity, and w_c will be called the group settling velocity. For the steady state, and zero net flux equation 5-1 reduces to

$$\epsilon_m \frac{dC}{dy} + (w_c - u)\, C = 0 \ . \qquad (5\text{-}2)$$

For purposes of discussion the velocity, w_c, is now defined as the group settling velocity (in a still fluid under the action of gravity) for a suspension of uniform particles held firmly in an imaginary matrix in which there is no concentration gradient. In this system there can be no relative movement of the particles within the matrix and no turbulent instabilities larger than the individual particle wakes. Under these conditions, it is evident that w_c must also be equal to the upward transport velocity necessary to generate this "fixed" matrix.

In a real, or free, suspension, the particles are not fixed but move about with a turbulent motion. With this turbulence and with a concentration gradient, whatever the causes, there must be vertical turbulent transport in a free suspension. Therefore, in a free suspension w_c must be slightly greater than u, in order that the net downward transport by advection

$$w_c C - uC$$

be balanced by the net upward turbulent transport

$$-\epsilon_m \frac{dC}{dy} .$$

While the general nature of the velocities w_c and u is evident, the exact identity of each is somewhat hazy. The effect of concentration of particles on the free-fall velocity of a single particle is not known. Experience based on the settling of an individual particle in a cylinder of still fluid, or near a wall, only indicates that concentration must reduce the particle fall velocity. Experiments (5) show that the decrease in fall

velocity is strongly dependent on the concentration and particle Reynolds number.

The velocity, u, which represents the tendency of the upward flow to transport the particles is also unknown. Let us consider the behavior of particles which have a unit weight identical to that of the fluid. If such particles are placed in an upward flow, it is apparent that they will move upward with the fluid flow. Thus, in this case, the local upward transport velocity is simply equal to the superficial velocity for very dilute suspensions but must be greater than the superficial velocity for suspensions which are not dilute. Particles which have a unit weight greater than that of the fluid will not simply be carried along with the flow but through the action of gravity will resist being transported by the fluid. For this case the local upward transport velocity is not clearly defined. It is the author's opinion, however, that the local upward transport velocity may be represented by a local fluid velocity within the suspension. One can estimate the local fluid velocity within a suspension on the basis that the particles reduce the cross-sectional area open to the flow, and therefore the local velocity through the particles is greater than the mean or superficial velocity. Thus, the local fluid velocity is strongly dependent on the local packing of the particles, but it is undoubtedly further influenced by the nature of the wakes associated with individual particles and clusters of particles. From this it is concluded that the local fluid velocity is also an unknown function of the local concentration and the local particle Reynolds number.

The preceding discussions indicate that the nature of w_c and u is

unknown even on a theoretical basis. Since the difference between these quantities is expected to be small, the estimation of it is subject to large errors. So far it may be concluded only that w_c is less than w_o, the free-fall velocity of an isolated particle, and it also appears that u is greater than $\bar{u}$, the superficial velocity.

It is quite evident that the turbulent diffusion coefficient ϵ_m is also an unknown. Experience in many different flow systems indicates a dependence of ϵ_m on Reynolds number. It has also been demonstrated that ϵ_m varies with the scale of a turbulent system such that ϵ_m increases as the size of the turbulent system increases. From the experimental observations reported herein it may be concluded that ϵ_m increases with increased concentration and increased particle size because the turbulence was observed visually to be the biggest at the bottom of the suspensions where the concentration is the largest and the particles are the coarsest.

While one is unable to solve analytically equation 5-2, because of the difficulty in stating the functional dependence of w_c, u, and ϵ_m on the local concentration, some information on the validity of the proposed model may be obtained from the experimental data evaluated in light of the diffusion equation. First, let us rewrite equation 5-2 in the form

$$\frac{d(\ln C)}{dy} = - \frac{(w_c - u)}{\epsilon_m} \qquad (5-3)$$

which shows that locally the ratio of the unknown parameters may be evaluated from the local slope of a semi-logarithmic graph of the

suspension concentration-depth profile. Two possibilities are then open to the investigator. If the magnitude of the difference between the quantities, w_c and u, somehow can be estimated, one may use the local slope value to evaluate the turbulent diffusion coefficient, ϵ_m. Or if measurements of ϵ_m or its value can be obtained by an independent means, then the measured slope may be used to evaluate the difference, $w_c - u$. From such concentration profile data, the validity of the assumptions about the general nature of the parameters, w_c, u, and ϵ_m can be further evaluated.

In the next section, the local concentration data reported herein will be evaluated in light of the diffusion equation 5-3.

5-5 Evaluation of the Local Concentration Profiles in Terms of the Diffusion Model

The data on local concentration vs. elevation in a suspension reported herein and plotted on arithmetic scales in figures 4-4 to 4-7, chapter 4, are presented again in figures 5-6 to 5-10 where the local concentration is plotted on a logarithmic scale and the elevation on an arithmetic scale.

Figures 5-6 and 5-7 show that the concentration decreases exponentially with increased elevation above the bottom of the suspension for runs A1, A2, A3, and A6. In each of these runs, the material fluidized was the glass beads, the most narrowly sorted material used in this study and one that may be considered as uniform for all practical purposes. The fact that the concentration-depth profiles are simple exponential functions of elevation means that the term on the right hand

side of equation 5-3 is constant for the full depth of each suspension. This is certainly not a result that could be expected a priori on the basis of the assumptions made in the previous section.

The concentration-depth profiles for the other materials studied herein are not described by a simple exponential relationship. However, as shown in figures 5-8 to 5-10, these concentration-depth profiles can be fitted by two straight lines on a semi-logarithmic graph. The two regions of exponential concentration-depth profile may indicate two types of turbulence production. The lower region near the bottom may be most strongly influenced by turbulence generated by jetting of fluid through the entrance plate, while the upper region is predominantly influenced by the turbulence generated by the suspended particles. The height of this lower region is not constant from suspension to suspension and so the entrance influence may not be a valid explanation. Another possible explanation for the abrupt change in concentration gradient may be the different behavior of various particle sizes in these non-uniform suspensions. As an aid in seeing the sorting of sizes relative to the concentration profiles, the particle Reynolds numbers (see Table 4-2, chapter 4) are noted on the profiles at the elevation of each local sample. Along each straight line portion the change in Reynolds number is gradual, but associated with the abrupt change in slope is a large change in particle Reynolds number.

The experimental runs G18, G19, and G20, all representing the fluidization of the same quartz sand, indicate the peculiar change in the

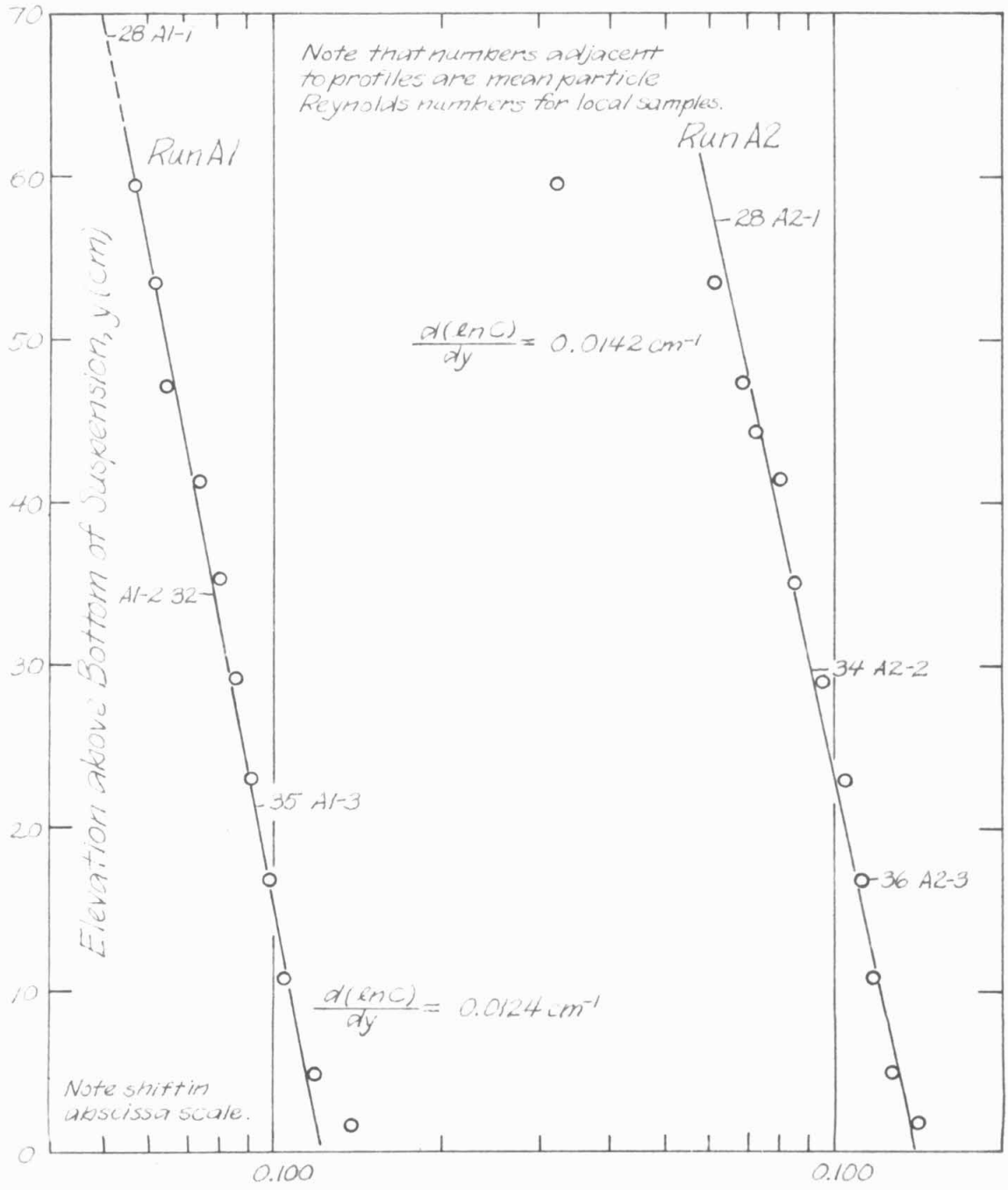

Fig. 5-6 Concentration-Depth Profiles for Runs A1 and A2

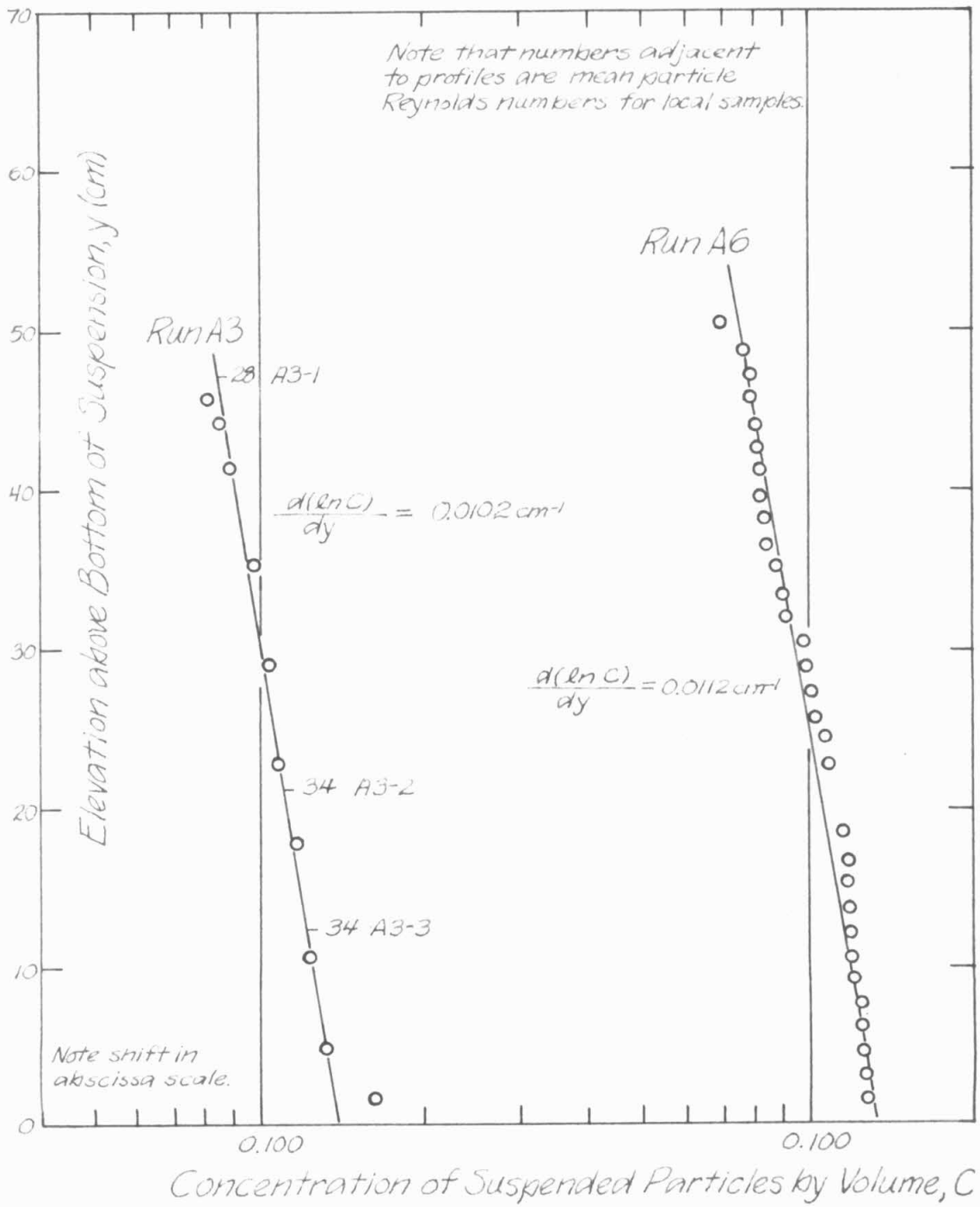

Fig. 5-1 Concentration-Depth Profiles for Runs A3 and A6

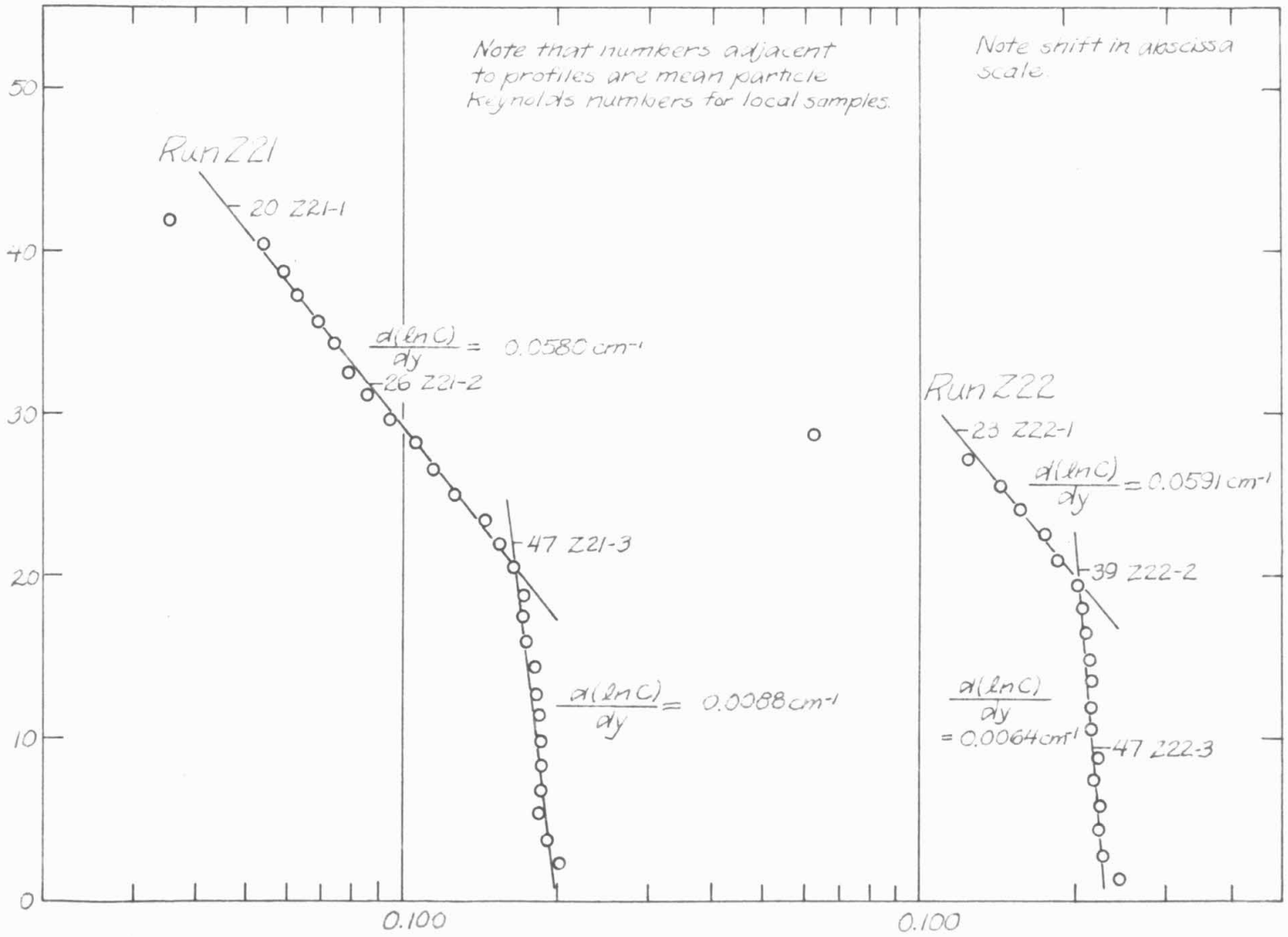

Fig. 5-8 Concentration-Depth Profiles for Runs Z21 and Z22.

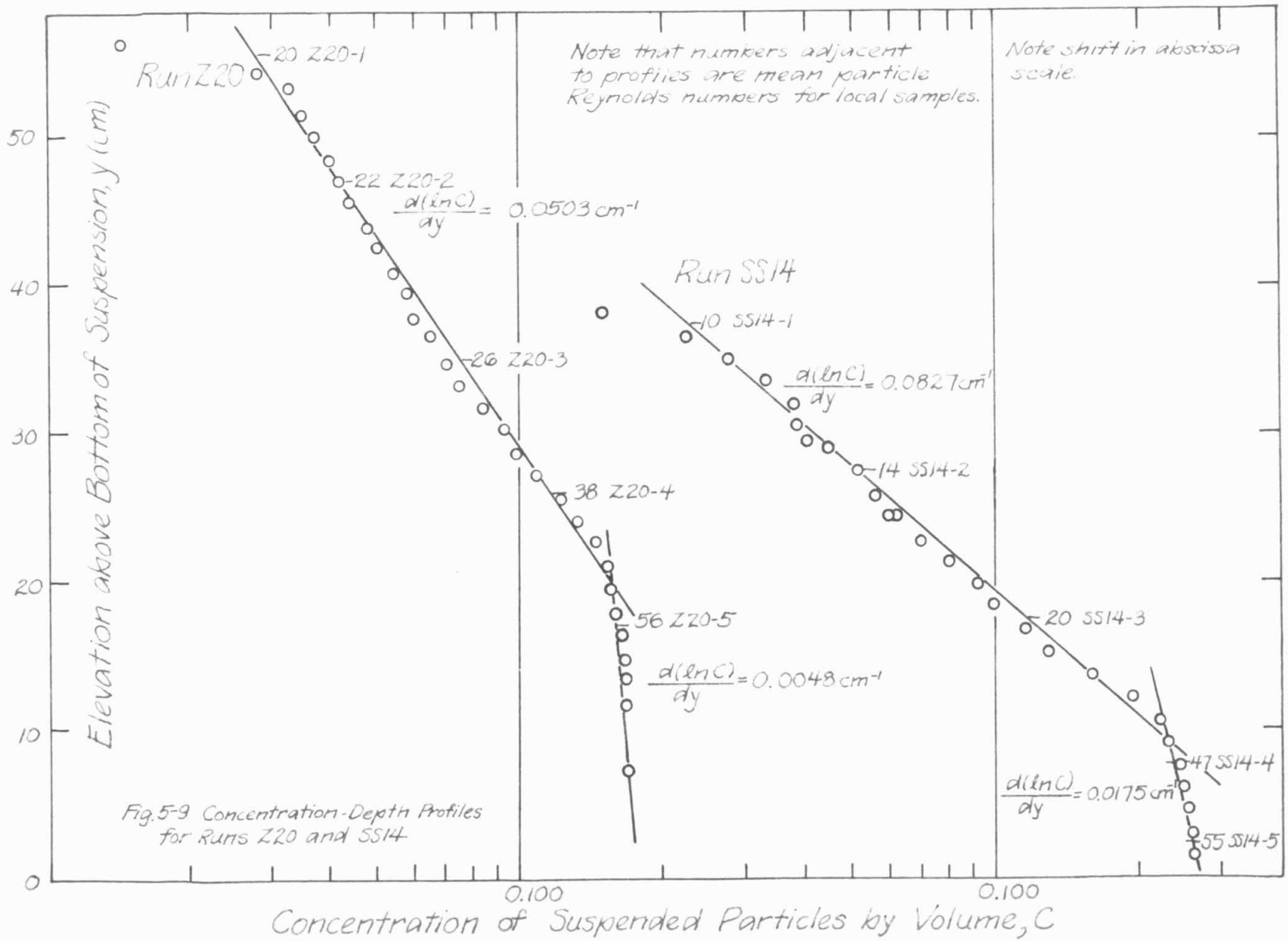

Fig. 5-3 Concentration-Depth Profiles for Runs Z20 and SS14

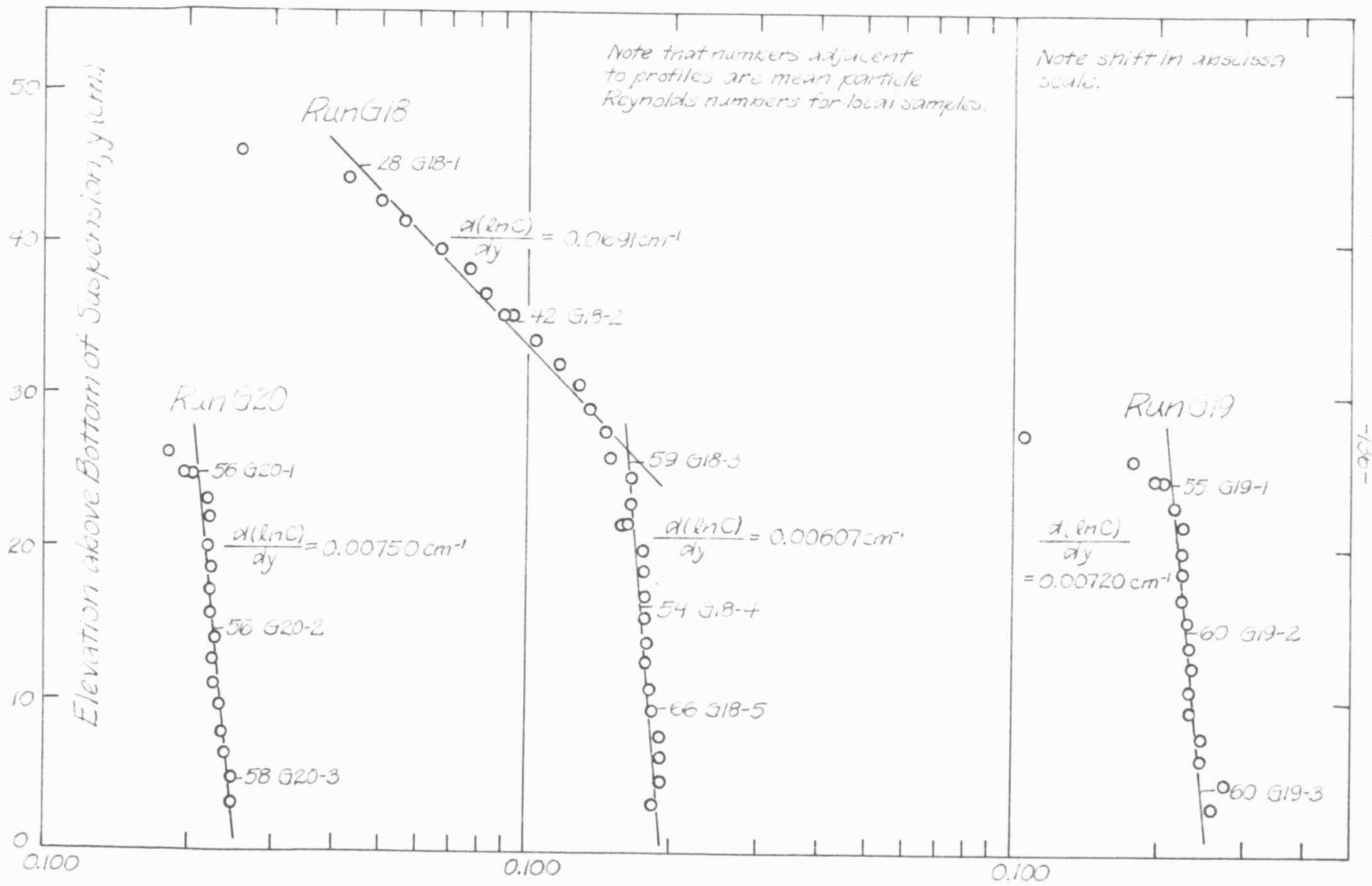

Fig. 5-10 Concentration-Depth Profiles for Runs G18, G19 and G20

nature of the concentration profiles. Runs G19 and G20 are for dense suspensions in which the expanded depth for each suspension is about 2.5 times the depth of the settled bed. The particles appear to be well mixed as indicated by the small change in the mean particle size over the depth (see also figures 4-18 and 4-19, chapter 4), and the concentration profile for each run is a simple exponential for the full suspension depth. Run G18 represents an expanded depth which is about 4.5 times the settled depth. Here again, the lower section appears well mixed, with a mean concentration slightly less than in runs G19 and G20, but the upper portion shows a steeper concentration gradient and more pronounced particle sorting. Similarly, the profiles for the other quartz sands, runs Z and SS14, also show the relative sorting and the abrupt profile change.

Looking again at the profiles for the uniform glass beads, let us examine on an order of magnitude basis the parameters of equation 5-3. For example, the slope of the concentration profile run A1, figure 5-6, indicates that the ratio $(w_c - u)/\epsilon_m$ is equal to 0.0124 cm^{-1}. A rough estimate of ϵ_m can be made on the basis of the Prandtl mixing length hypothesis which says that $\epsilon_m = \ell\sqrt{\overline{v'^2}}$ where ℓ is a characteristic mixing length and $\sqrt{\overline{v'^2}}$ is the root mean square of the local velocity fluctuations for the particles. It may be estimated that ℓ is of the order of 1 to 100 particle diameters, that is, $\ell \sim 0.05$ to 5 cm for particles with a mean size of 0.5 mm which is representative of the glass beads and the quartz sands used herein. Let us estimate that $\sqrt{\overline{v'^2}}$ is of the same order as the superficial velocity, namely 2 to 5 cm per sec for the

suspensions studied. For these values, ϵ_m is then calculated to be of the order of 0.1 to 25 cm^2 per sec. This range covers two orders of magnitude, but it is the author's opinion that a value of ϵ_m of the order of 10 cm^2 per sec is the best guess for the systems studied herein. Using these estimated values of ϵ_m, the difference $(w_c - u)$ for run A1 is calculated to be 0.0012 to 0.25 cm per sec, or about 0.025 to 5.4 per cent of the superficial velocity ($\bar{u}$ = 4.67 cm per sec) necessary to generate this suspension. Such a difference is very small, and as indicated in the previous section would be very difficult to predict. Similar calculations for the other suspensions also indicate such small differences for the quantities w_c and u for the non-uniform quartz sands.

For the suspensions studied, the alternative approach of estimating w_c and u was tried on the basis that w_c could be approximated by the representative local particle free-fall velocity, w_o, and u could be taken equal to the reduced cross-section fluid velocity. If u is calculated on the assumption that the particles are arranged in a simple cubic matrix of side length s, u has the value given by

$$\bar{u}\, s^2 = u\left(s^2 - \frac{\pi D^2}{4}\right) \quad \text{and} \quad C = \frac{\pi D^3}{6s^3}$$

or,

$$u = \bar{u}\, \frac{1}{1 - \frac{\pi}{4}\left(\frac{6C}{\pi}\right)^{2/3}} \quad .$$

Such a calculation for run A1 is summarized in the table below.

Sample	Local Conc., C	w_o ($\frac{cm}{sec}$)	u ($\frac{cm}{sec}$)	u ($\frac{cm}{sec}$)	w_o-u ($\frac{cm}{sec}$)	ϵ_m ($\frac{cm^2}{sec}$)
A1-1	0.051	6.22	4.67	5.60	0.62	50.0
A1-2	0.082	6.70	4.67	6.05	0.65	52.4
A1-3	0.094	6.99	4.67	6.20	0.79	68.6

The above values of ϵ_m based on the crude estimate of w_c and u are larger than the maximum estimate of ϵ_m based on the mixing length hypothesis. Nevertheless, the agreement is fairly good considering the speculative nature of both approaches to the problem. Similar calculations based on estimating w_c and u for the other suspension profiles shown in figures 5-6 to 5-10 indicate a variation in ϵ_m from 1 to 100 cm^2 per sec with the smallest values of ϵ_m occurring at the top of the suspensions and the larger values near the bottom. Attempts to correlate these estimates of ϵ_m with the other measured parameters, such as local concentration and relative depth were not successful.

It is believed that the introduction of the diffusion model for the fluidized suspension may indicate a new direction for the understanding of the seemingly elementary but complicated problem of suspensions generated by an upward flow. Previous investigators have empirically considered the problem of the fluidized suspension as flow through expanded porous media. However, as a consequence of the importance of the turbulence associated with the free movement of the particles, a better understanding of the physics of the problem can be developed by considering the phenomenon as a suspension of particles moving

relative to a fluid medium rather than a fluid moving relative to a fixed porous medium.

CHAPTER 6

SUMMARY AND CONCLUSIONS

The following conclusions are based on the results of an experimental investigation of the properties of suspensions of granular particles in an upward flow of water. Four materials covering a range of sizes having particle Reynolds numbers between 10 and 70 were studied by making detailed measurements locally within ten suspensions. Measurements of the mean properties of over one hundred suspensions are also reported herein. Concentrations in the suspensions generated by an upward flow were generally greater than those of typical hindered settling experiments but less than those of typical fluidization experiments by chemical engineers.

Granular particles with mass densities approximately two and one-half times the density of water and having particle Reynolds numbers in the range from 10 to 70 produce highly turbulent systems when fluidized with water. It was observed that there is the local generation of turbulence throughout the suspension with the highest intensity of turbulence being in the region where the local concentration is the largest.

6-1. Experimental Observations of Fluidized Suspensions

1. A comparison of the experimental measurements of the mean properties of suspensions of uniform particles and the local properties of suspensions of non-uniform particles show slightly different results relating particle size, superficial velocity, and concentration. These

differences indicate that a suspension of non-uniform particles is not a simple "stacking" of sorted layers of uniform particles but that each level in the suspension is influenced by the rest of the suspension and is subject to the diffusion of particles and turbulent energy from above and below. However, as a first approximation to the local relationship between particle size, concentration, and superficial velocity in non-uniform suspensions one may use the experimentally derived formulae of Richardson and Zaki (sec. 1-4, chapter 1) based on the mean values of particle size and concentration for suspensions of uniform particles.

2. Measurements of the mean concentration for an entire suspension and the ratio of the superficial velocity to the mean particle free-fall velocity yielded a separate relationship for each of the non-uniform materials studied (see figure 4-1). These relationships depend on the particle Reynolds number and the standard deviation of particle sizes for the parent materials and, therefore, are not given by the Richardson and Zaki formulae.

3. The local concentration in suspensions of uniform glass beads decreased exponentially with increased elevation above the bottom. For suspensions of non-uniform particles, the concentration gradient was even steeper, but the concentration-depth relationship was not a simple exponential function.

4. In a free suspension, turbulence and a vertical concentration gradient, whatever the causes, will produce an upward turbulent transport of particles which aids the upward fluid flow in balancing the tendency of the particles to settle under the action of gravity. This

turbulent diffusion can lead to noticeable non-uniformities in the concentration-depth profile for suspensions of even the most uniform particles.

5. Suspensions of non-uniform particles invariably show sorting with the particles with the smallest free-fall velocities near the top and the particles with the largest free-fall velocities at the bottom of a suspension (figures 5-3 to 5-5). The distributions of free-fall velocities obtained from point samples of these suspensions were nearly log-normally distributed (figures 4-10 to 4-20). The geometric standard deviations of the distributions of local particle free-fall velocity increased from top to bottom of a suspension (figure 4-9). This is another indication that the mixing, or turbulence, in a suspension is the largest where the concentration is also the largest.

6. Measurements of the hindered settling of suspensions and the fluidization of suspensions indicate that the hindered settling velocity is identical, for all practical purposes, to the superficial velocity necessary to maintain such a suspension. The data in Table 4-3, chapter 4, show that the superficial velocity was a few per cent greater than the hindered settling velocity. It was observed, however, that the intensity of the turbulence was less for the settling suspension than for the fluidized suspension. Locally, the generation of turbulence is largest where the concentration is largest. In a settling suspension, this region of highest concentration is the first to settle down and become quiescent. While there is still the local generation of turbulence, there is no longer the observed transport and decay of disturbances from bottom to top of the

suspension. Because the magnitude and nature of the turbulence is different in the settling suspension from the fluidized suspension, the two systems are not completely identical.

6-2. Properties of Granular Materials

The following conclusions apply to the properties of the granular materials used in this study.

1. If the distribution of sieve diameters for a granular material is log-normal, the distributions of sedimentation diameters and particle free-fall velocities are also log-normal.

2. The geometric standard deviation of the sedimentation diameters is less than the geometric standard deviation of the sieve diameters by an amount which increases as the geometric standard deviation increases. (see Table 3-3, chapter 3.)

3. Formulae have been derived relating the means of log-normal distributions by number and by weight for particle free-fall velocities and particle diameters. (see Appendices II-1 and II-2.)

APPENDIX I-1

Relationship between a Log-Normal Distribution of Free-Fall Velocities by Number and by Weight

Let us assume that a granular material is composed of particles which have free-fall velocities that are logarithmically normally distributed by weight. For such a material what is the distribution of free-fall velocities by number?

Let $\phi(\log w_o)d(\log w)$ represent the fractional amount by weight relative to the whole population of the granular material with free-fall velocities lying in the interval $w_o - \frac{\Delta w}{2} < w < w_o + \frac{\Delta w}{2}$ where $\Delta w = w_o d(\log w)$ and

$$\phi(\log w) = \frac{1}{\sigma\sqrt{2\pi}} \exp\left\{-\frac{1}{2}\left[\frac{\log w - \log \mu}{\sigma}\right]^2\right\} \qquad \text{(I-1)}$$

The function $\phi(\log w)$, given by equation I-1, is normally distributed about the mean value, $\log \mu$, with standard deviation, σ. It is convenient to introduce also the geometric standard deviation, σ_w, which is related to the standard deviation, σ, by $\sigma = \log \sigma_w$.

To change from a distribution by weight to a distribution by number, divide the distribution by weight, $\phi(\log w_o)d(\log w)$, by the weight of a particle having the free-fall velocity, w_o. At this point, let's restrict ourselves to particles which are spheres or which can be closely approximated as spheres. Then, the distribution by number, $f(\log w_o)d(\log w)$, may be written, except for a normalizing factor,

$$f(\log w_o)d(\log w) = \frac{\phi(\log w_o)d(\log w)}{\frac{\pi D^3}{6} \cdot \gamma_s} \qquad \text{(I-2)}$$

where $\frac{\pi D^3}{6} \cdot \gamma_s$ is the weight of a sphere with free-fall velocity, w_o.

In order to evaluate equation I-2, one needs a relationship between w and D. This relationship may be obtained from the drag coefficient, C_D, vs. Reynolds number, $\frac{wD}{\nu}$, curve (see Kennedy and Koh (25)) where

$$\frac{dw}{w} = \frac{1+m}{2-m} \cdot \frac{dD}{D} \tag{I-3}$$

and

$$m = -\frac{d(\log C_D)}{d(\log Re)}, \quad Re = \frac{wD}{\nu}$$

Equation I-3 requires that ν, the kinematic viscosity of the fluid, and γ_s and γ_f, the specific weights of the solid particles and the fluid respectively, be constant. If the ratio $\frac{1+m}{2-m}$ can be taken as a constant, equation I-3 may be integrated as follows:

$$w = \alpha_1 D^{\frac{1+m}{2-m}} \quad \text{or} \quad D = \alpha_2 w^{\frac{2-m}{1+m}} \tag{I-4}$$

where α_1 and α_2 are dimensional integration constants. Substituting the relationship between w and D from equation I-4 in equation I-2 and changing variables leads to:

$$f(x)dx = \frac{\phi(x)dx}{\frac{\pi D^3}{6} \cdot \gamma_s} = \frac{\phi(x)dx}{Bw^{3/\beta}} \tag{I-5}$$

where $x = \log w$, $\beta = \frac{1+m}{2-m}$, and B = a dimensional constant. Introducing the relationship between natural and common logarithms:

$$w^{3/\beta} = 10^{3x/\beta} = e^{3bx/\beta} \tag{I-6}$$

where b = 2.303.

Equation I-5 may now be written:

$$f(x)dx = \frac{1}{B} \cdot \frac{1}{\sigma\sqrt{2\pi}} \cdot \exp\left\{ -\frac{1}{2}\left[\frac{x-\bar{x}}{\sigma}\right]^2 \right\} \exp.\left\{ -\frac{3bx}{\beta} \right\} dx \qquad (I\text{-}7)$$

Completing the square of the exponent of equation I-7,

$$-\frac{1}{2}\left[\frac{x-\bar{x}}{\sigma}\right]^2 - \frac{3xb}{\beta} = \frac{1}{2\sigma^2}\left[x-\left(\bar{x} - \frac{3b\sigma^2}{\beta}\right)\right]^2 + \frac{9}{2} \cdot \frac{b^2\sigma^2}{\beta^2} - \frac{3b\bar{x}}{\beta}$$

Substituting the completed square into equation I-7,

$$f(x)dx = \frac{1}{\sigma\sqrt{2\pi}} \cdot \frac{1}{B} \cdot \exp.\left\{ -\frac{1}{2\sigma^2} \cdot \left[x-\left(\bar{x} - \frac{3b\sigma^2}{\beta}\right)\right]^2 + \frac{9}{2}\frac{b^2\sigma^2}{\beta^2} - \frac{3b\bar{x}}{\beta} \right\} dx \qquad (I\text{-}8)$$

Equation I-8 represents the distribution of free-fall velocities by number for a granular material which has its free-fall velocities log-normally distributed by weight.

To find the normalizing factor for equation I-8, one must integrate equation I-8 over all possible values of x. The normalized distribution of free-fall velocities by number, $F(x)dx$, is defined by:

$$\int_a^b F(x)dx = \frac{\int_a^b f(x)dx}{\int_{-\infty}^{+\infty} f(x)dx}$$

where $\int_{-\infty}^{+\infty} F(x)dx \equiv 1.$

As a result of this normalization, one obtains for the normalized distribution of free-fall velocities by number, $F(x)dx$:

$$\int_a^b F(\log w)d(\log w) = \int_a^b \frac{1}{\sigma\sqrt{2\pi}} \exp.\left\{ -\frac{1}{2\sigma^2}\left[\log w - \left(\log \mu - \frac{3b\sigma^2}{\beta}\right)\right] \right\} d(\log w) \qquad (I\text{-}9)$$

Equation I-9 shows that F(log w) is log-normally distributed with the same geometric standard deviation as the distribution of free-fall velocities by weight, ϕ(log w). The mean of the distribution F(log w), designated $\log w_g$, is related to $\log \mu$, the mean of the distribution ϕ(log w) by the following equation:

$$\log \mu = \log w_g + \frac{3b}{\beta} (\log \sigma_w)^2 \qquad \text{(I-10)}$$

where σ_w = geometric standard deviation of both distributions

and $\sigma = \log \sigma_w$.

Equation I-10 is the relationship employed to calculate the mean free-fall velocity by weight, μ, from the measured distributions of free-fall velocity by number presented in chapters 3 and 4.

In order to use equation I-10, one is restricted to the assumption that β is a constant. Table I-1, which was taken from Kennedy and Koh (25), shows the magnitude of the parameter β.

Table I-1

Relationship between β, m, and Reynolds Number, $\frac{wD}{\nu}$

Reynolds No., Re	$m = -\frac{d(\log C_D)}{d(\log Re)}$	$\beta = \frac{1+m}{2-m}$
0.4 and less	1.000	2.000
1	0.890	1.703
2	0.835	1.575
4	0.770	1.439
10	0.685	1.281
20	0.635	1.197
40	0.570	1.098
100	0.475	0.967
200	0.417	0.895
400	0.365	0.835
800	0.300	0.765
1000	0.275	0.739
2000	0.145	0.617
5000	0	0.500

From Table I-1 one sees that β is not a constant but changes with Reynolds number. However, if the range of Reynolds numbers for any particle population is small, like $20 \leq Re \leq 30$ or $40 \leq Re \leq 60$, the assumption that β is a constant is good within about 5 per cent. Fortunately, the granular materials studied, with one exception that is discussed in chapter 3, were sufficiently narrowly distributed to allow the application of equation I-10.

Appendix I-2

Relationship between a Log-Normal Distribution of Particle Diameters by Number and by Weight

Let us assume that a granular material is composed of particles which have diameters which are log-normally distributed by weight. For such a material what is the distribution of particle diameters by number? The previous section has been concerned with the same problem for free-fall velocities. Again let us restrict ourselves to particles which are spheres or can be closely approximated as spheres.

Let $\psi(\log D_o)d(\log D)$ represent the fractional amount by weight relative to the whole population of the granular material with particle diameters lying in the interval $D_o - \frac{\Delta D}{2} < D < D_o + \frac{\Delta D}{2}$ where $\Delta D = D_o d(\log D)$ and

$$\psi(\log D) = \frac{1}{\sigma\sqrt{2\pi}} \cdot \exp.\left\{ -\frac{1}{2}\left[\frac{\log D - \log D_g}{\sigma}\right]^2 \right\} \qquad \text{(I-11)}$$

The function $\psi(\log D)$ is normally distributed about the mean value, $\log D_g$, with standard deviation, σ. It is also convenient to introduce the geometric standard deviation, σ_g, which is related to the standard deviation, σ, by $\sigma = \log \sigma_g$.

To change from a distribution by weight to a distribution by number, divide the distribution by weight, $\psi(\log D_o)d(\log D)$, by the weight of a particle having the particle diameter, D_o. The distribution by number, $g(\log D_o)d(\log D)$, may be written, except for a normalizing factor:

$$g(\log D_o)d(\log D) = \frac{\psi(\log D_o)d(\log D)}{\frac{\pi D_o^3}{6} \cdot \gamma_s} \qquad \text{(I-12)}$$

where $\frac{\pi D_o^3}{6} \cdot \gamma_s$ is the weight of a sphere having diameter, D_o. Let us change the variable in equation I-12 and rewrite it in the following form:

$$g(x)dx = \frac{\psi(x)dx}{\frac{\pi\gamma_s}{6} \cdot 10^{3x}} \qquad \text{(I-13)}$$

where $x = \log D$.

Using the relationship between natural and common logarithms,

$$D^3 = 10^{3x} = e^{3bx} \qquad \text{(I-14)}$$

where $b = 2.303$.

Equation I-13 may now be written:

$$g(x)dx = \frac{1}{\frac{\pi\gamma_s}{6}} \cdot \frac{1}{\sigma\sqrt{2\pi}} \cdot \exp.\left\{-\frac{1}{2}\left(\frac{x-\bar{x}}{\sigma}\right)^2\right\} \exp.\left\{-3bx\right\} dx \qquad \text{(I-15)}$$

Equation I-15 represents the distribution of particle diameters by number for a granular material which has its particle diameters log-normally distributed by weight. Let us complete the square of the exponent of equation I-15:

$$-\frac{1}{2}\left[\frac{x-\bar{x}}{\sigma}\right]^2 - 3bx = -\frac{1}{2}\left[\frac{x-(\bar{x}-3b\sigma^2)}{\sigma}\right]^2 - 3\bar{x}b + \frac{9}{2}b^2\sigma^2$$

Substituting the completed square into equation I-15:

$$g(x)dx = \frac{1}{\sigma\sqrt{2\pi}} \cdot \frac{6}{\pi\gamma_s} \cdot \exp.\left\{-\frac{1}{2\sigma^2}\left[x-(\bar{x}-3b\sigma^2)\right]^2 - 3\bar{x}b + \frac{9}{2}b^2\sigma^2\right\} dx \qquad \text{(I-16)}$$

Equation I-16 may be normalized by integrating over all possible values of D and defining the normalized distribution of particle diameters by number, G(x)dx, by:

$$\int_a^b G(x)dx = \frac{\int_a^b g(x)dx}{\int_{-\infty}^{+\infty} g(x)dx}$$

where $\int_{-\infty}^{+\infty} G(x)dx \equiv 1.$

As a result of this normalization, one obtains for the normalized distribution of free-fall velocities by number, G(x)dx:

$$\int_a^b G(\log D)d(\log D) = \int_a^b \frac{1}{\sigma\sqrt{2\pi}} \cdot \exp.\left\{ -\frac{1}{2\sigma^2}[\log D - (\log D_g - 3b\sigma^2)]^2 \right\} d(\log D) \qquad \text{(I-17)}$$

Equation I-17 shows that G(log D) is log-normally distributed with the same geometric standard deviation as the distribution of particle diameters by number, ψ(log D). The mean of the distribution, G(log D), designated $\log D_M$, is related to the mean of the distribution ψ(log D) by the following equation:

$$\log D_M = \log D_g - 3b(\log \sigma_g)^2 \qquad \text{(I-18)}$$

where σ_g = geometric standard deviation of both distributions

$\sigma = \log \sigma_g$

and $b = 2.303$

The derivation of equation I-18 is not as restricted as the relationship for the mean free-fall velocities derived in the previous section.

Equation I-18 requires only that the particles be spheres or closely approximated as spheres, but there is no limit on the standard deviation of the distributions. It is quite convenient to analyze a granular material in terms of its weight fraction for various particle sizes. Fortunately, most natural sands appear to have their sizes (sieve diameters) log-normally distributed by weight. If one is interested in the total surface area of a population of particles, for example in the design of a fixed bed filter, one may conveniently use equation I-18 to convert the results of the sieve analysis (i.e., the weight distribution) to the particle distribution by number. The number of particles rather than their weight determines their total surface area.

APPENDIX II

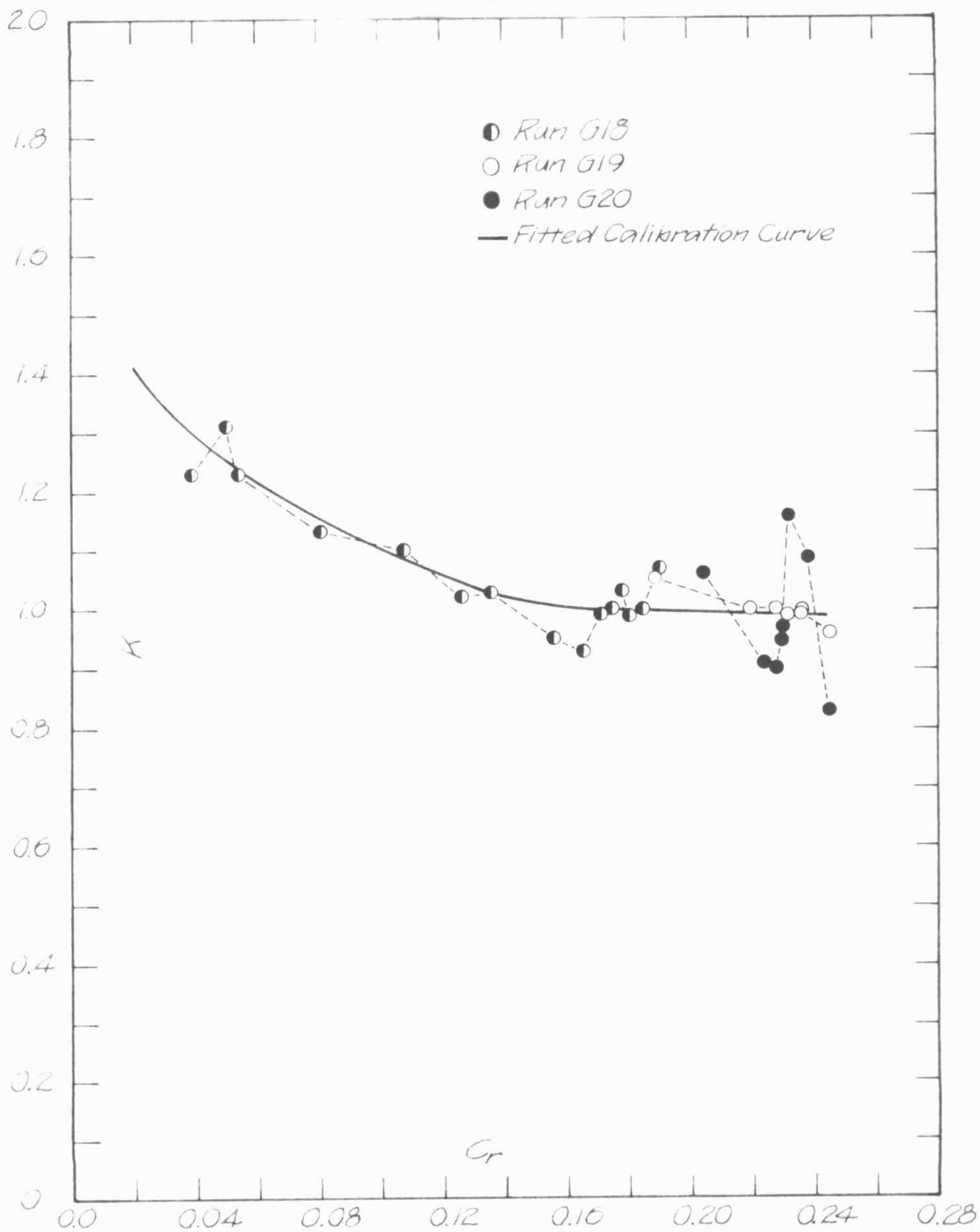

Fig II-1 Electrical Resistance Probe Calibration Curve for Material G

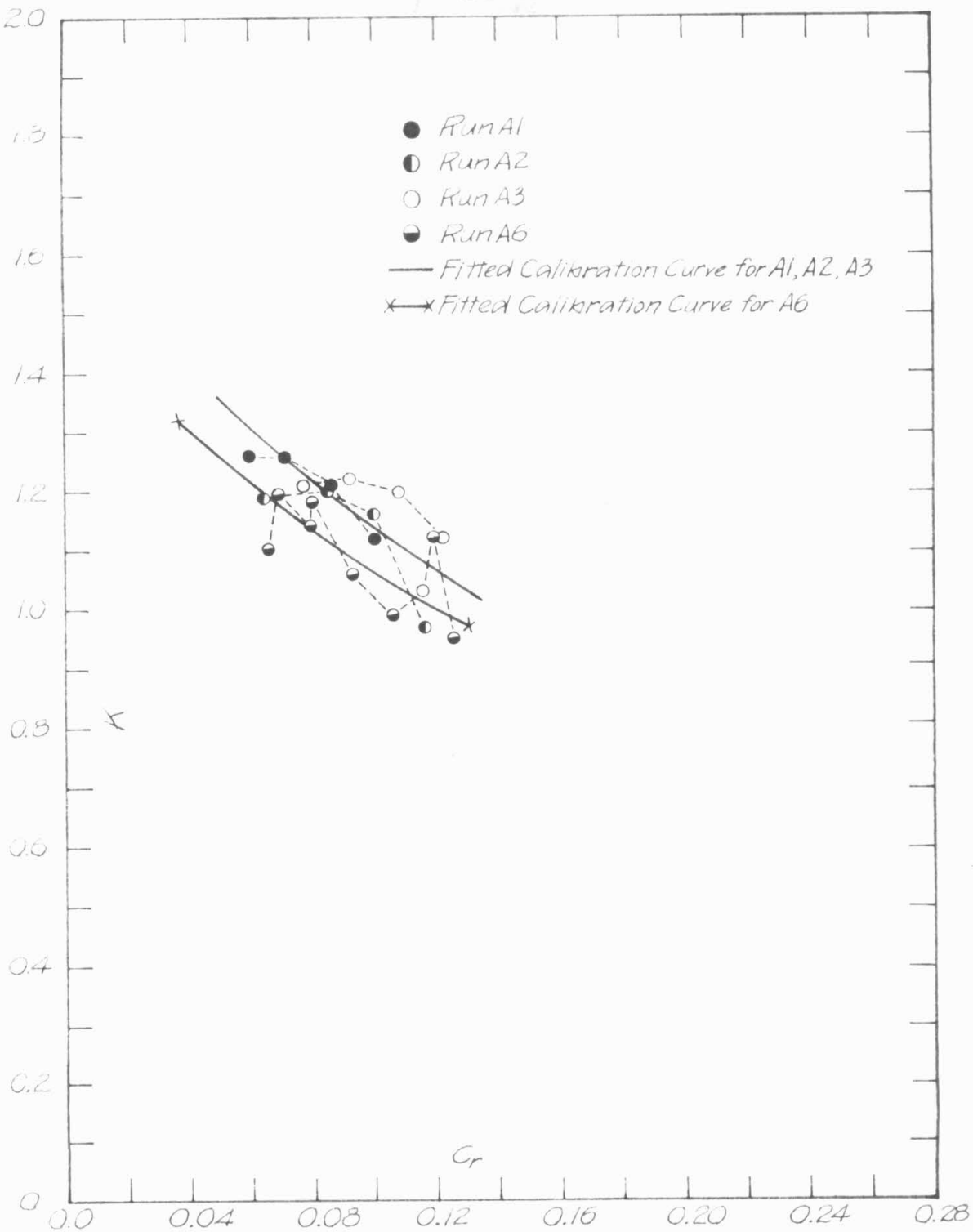

Fig. II-2 Electrical Resistance Probe Calibration Curve for Material A

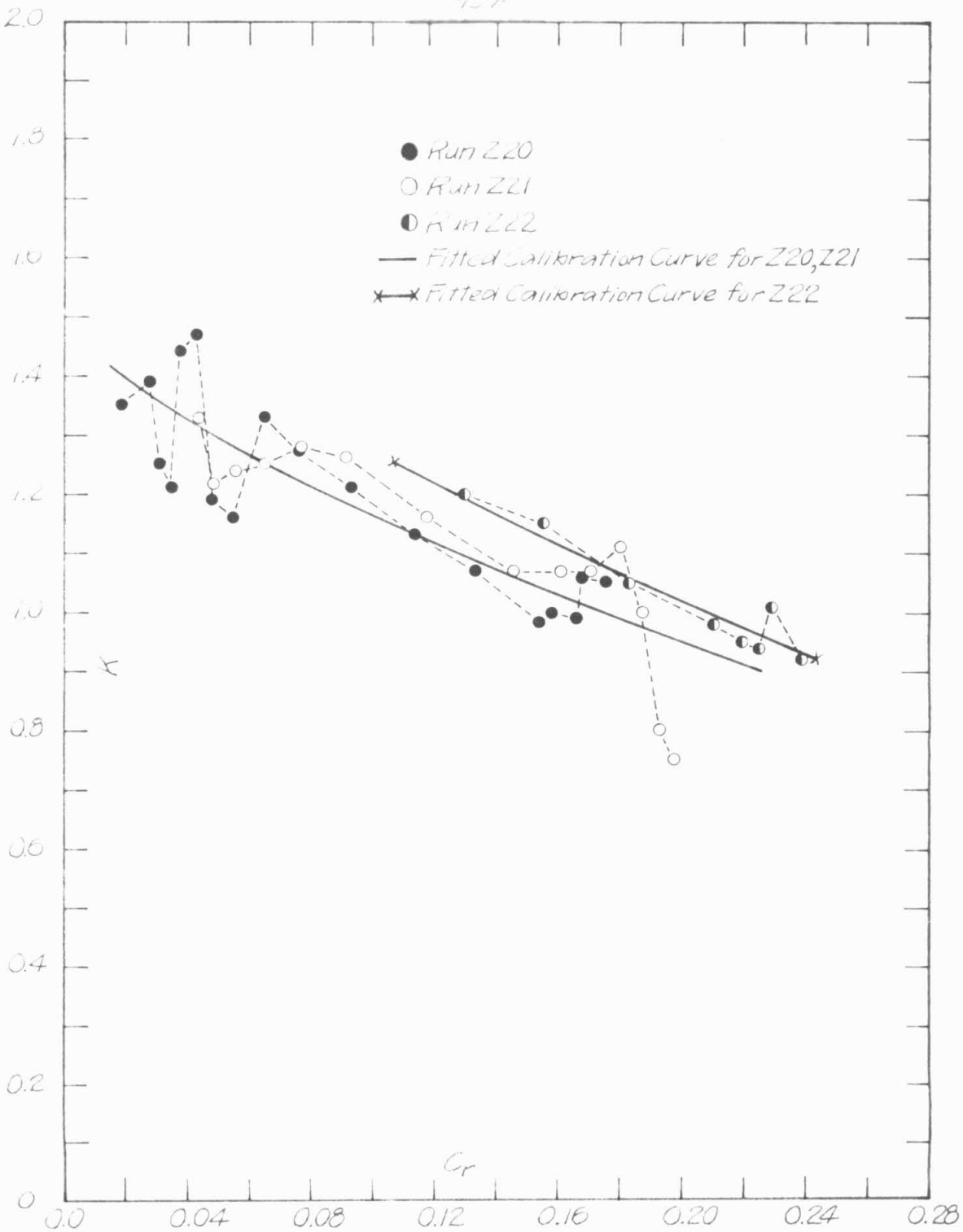

Fig. II-3 Electrical Resistance Probe Calibration Curve for Material Z

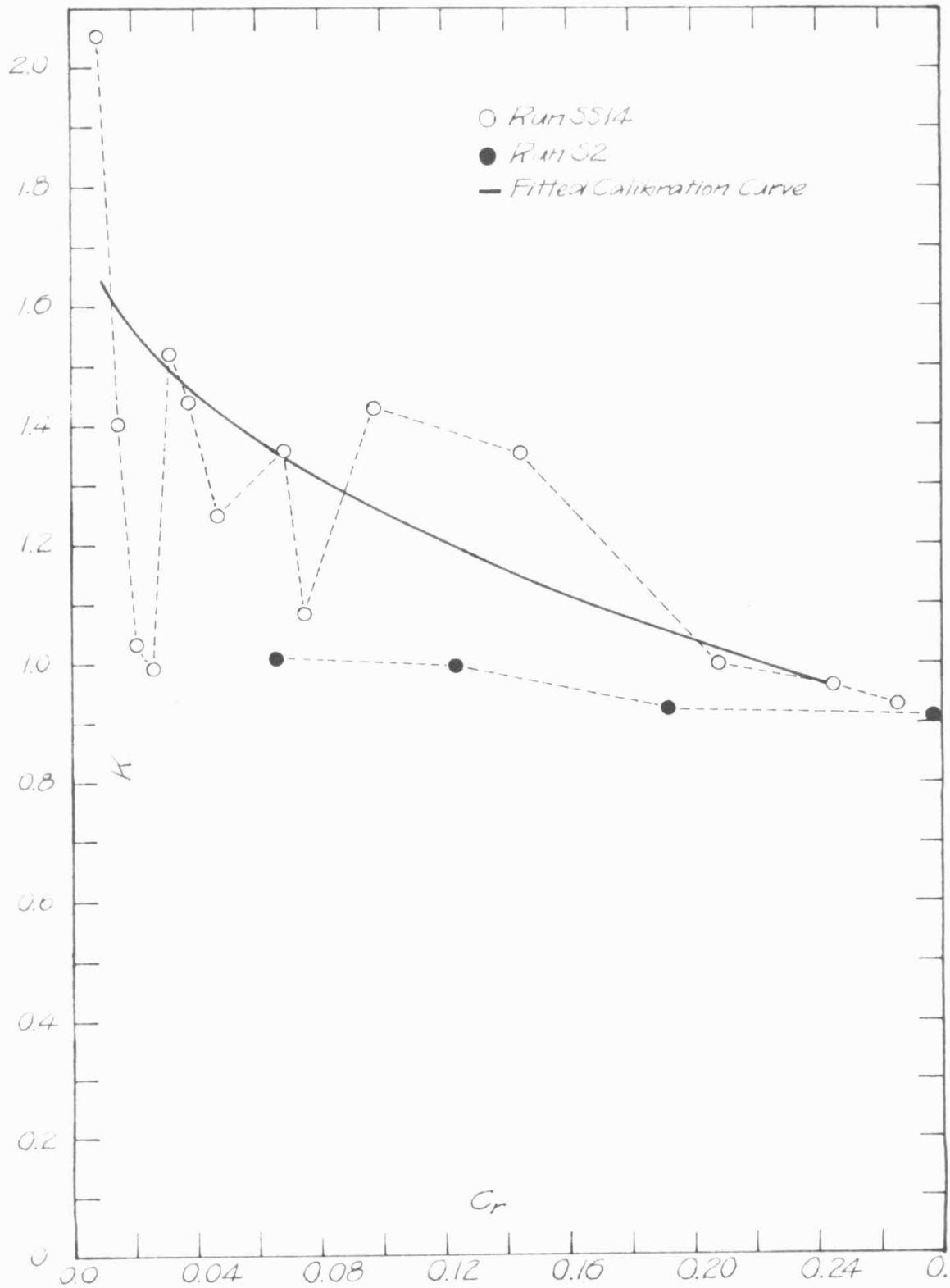

Fig. II-4 Electrical Resistance Probe Calibration Curve for Material S

Appendix II-2

Summary of Fluidization Data

The data for the fluidization of the four granular materials studied is presented in Table II-2. Each of the runs corresponding to a particular granular material may be identified with the letter identifying that material, for example, runs A and AA are for material A, the glass beads.

Column 1. $\overline{W}$ is the total dry weight of granular material in the fluidization column for the particular run. The number of significant figures given for each value of $\overline{W}$ varies because two different scales were used in the course of the experiments.

Column 2. d is the depth of the suspension measured with a fixed scale attached to one wall of the fluidization column.

Column 3. $\overline{u}$ is the superficial velocity or the discharge per unit cross-sectional area of the fluidization column. The cross-sectional area of the column is 1.01 ft^2(940 cm^2).

Column 4. T is the temperature of the water in the fluidization column during the run.

Column 5. $\overline{u}/\overline{\mu}$ is the ratio of the superficial velocity, $\overline{u}$, in the column to the particle mean free-fall velocity by weight, $\overline{\mu}$.

Column 6. $\overline{C}$ is the mean concentration by volume.

For certain runs (Z20, Z21, Z22, G18, G19, G20, SS14) several values of d, $\bar{u}$, T, and $\overline{C}$ are given. This is the range of values over which the quantities varied during the course of the run.

Table II-2

Summary of Fluidization Data

	1	2	3	4	5	6
Run No.	$\bar{W}$ (lb.)	d(cm)	$\bar{u}$ ($\frac{cm}{sec}$)	T(^{o}C)	$\bar{u}/\bar{\mu}$	$\bar{C} = \frac{\bar{W}}{\gamma_s A d}$
A1	30.00	70 ± ½	4.67	21.6	.697	.084
A2	29.96	60 ± ½	4.48	22.1	.669	.096
A3	29.90	48 ± 1	4.27	22.5	.637	.119
A4	29.83	54 ± ½	4.39	22.0	.655	.106
A5	29.83	54	4.39	22.6	.655	.106
A6	29.83	53	4.39	22.7	.655	.112
A7a	29.83	52 ± 1	4.30	21.8	.642	.112
$A7b_1$	29.83	71 ± ½	4.72	22.4	.704	.083
$A7b_2$	29.83	46	4.25	23.2	.634	.127
AA1	30.0	40	4.00	23.5	.597	.146
AA2	30.0	38	3.90	23.6	.582	.153
AA3	30.0	38	3.94	23.6	.588	.153
AA4	30.0	49	4.34	22.6	.648	.120
AA5	30.0	82	4.88	22.8	.728	.0712
AA6	30.0	80	4.75	22.8	.709	.0730
AA7	30.0	49.5	4.34	22.7	.648	.120
AA8	30.0	92	5.10	22.4	.761	.0636
AA9	30.0	58	4.52	21.5	.675	.101
AA10	12.15	23	4.64	21.2	.693	.0806
AA11	30.0	49.5	4.15	21.7	.619	.121
AA12	30.0	48.5	4.18	21.3	.624	.123
Z1	35.1	17.0	1.46	23	.190	.376
Z2	35.1	28	3.27	22	.425	.229
Z3	35.1	39	4.00	22	.520	.164
Z4	35.1	47	4.35	22	.565	.136
Z5	35.1	60.5	4.72	22	.613	.106

	1	2	3	4	5	6
Z6	35.1	61.5	4.73	22	.614	.104
Z7	35.1	71.5	4.92	22	.639	.089
Z8	35.1	83	5.08	22	.660	.077
Z9	35.1	11.0	0.329	22	.043	.582
Z10	35.1	11.5	0.680	22	.088	.557
Z11	35.1	12.2	0.982	22	.128	.525
Z12	35.1	14.5	1.31	22	.170	. 41
Z13	35.1	16.0	1.62	22	.210	.400
Z14	35.1	18.0	1.93	22	.251	.355
Z15	35.1	18.0	1.93	22	.251	.355
Z16	35.1	19.5	2.25	22	.292	.328
Z17	35.1	21.0	2.40	22	.312	.305
Z18	35.1	23.5	2.88	22	.374	.254
Z19	35.1	26.0	3.19	22	.414	.246
Z20	35.1	60.0	4.73	22.5	.614	.107
	35.1	58.8	4.70		.611	.109
	35.1	57.0	4.70	23.2	.611	.112
Z21	35.1	44.5	4.30	22.8	.559	.144
	35.1	43.0	4.30	23.0	.559	.149
	35.1	42.5	4.30	23.2	.559	.151
Z22	35.0	30.0	3.60	23.2	.468	.214
	35.0	29.5	3.60	23.3	.468	.216
G1	38.9	Not Fluidized	0.329	21.5	—	—
G2	38.9	"	0.680	21.5	—	—
G3	38.9	"	0.982	21.5	—	—
G4	38.9	15	1.31	21.5	.146	.472
G5	38.9	16	1.62	21.5	.181	.442
G6	38.9	17	1.93	21.5	.216	.417
G7	38.9	18.8	2.25	21.5	.251	.377
G8	38.9	19.5	2.40	21.5	.268	.363
G9	38.9	21	2.88	21.5	.322	.336
G10	38.9	22.3	3.19	21.6	.356	.318

	1	2	3	4	5	6
G11	38.9	25	3.66	21.6	.409	.283
G12	38.9	30	4.24	21.6	.474	.236
G13	38.9	36	4.88	21.6	.545	.197
G14	38.9	40	5.12	21.6	.572	.177
G15	38.9	45	5.37	21.6	.600	.169
G16	38.9	49	5.49	21.6	.613	.156
G17	38.9	56	5.73	21.7	.640	.136
G18	38.9	49	5.52	21.8	.617	.144
	38.9	47	5.46	21.8	.610	.151
	38.9	46	5.43	21.8	.607	.154
	38.9	46	5.40	22.2	.603	.154
G19	38.8	29	4.21	22.2	.470	.243
	38.8	29	4.18	22.2	.467	.243
	38.8	29	4.18	22.3	.467	.243
	38.8	29	4.18	22.3	.467	.243
G20	38.7	29.5	4.21	22.4	.470	.239
	38.7	29	4.21	22.4	.470	.243
	38.7	29	4.21	22.5	.470	.243
	38.7	29	4.21	22.5	.470	.243
SS1	28.28	10.4	0.329	22.4	.043	.494
SS2	28.28	10.8	0.680	22.4	.090	.480
SS3	28.28	$11.5\pm\frac{1}{2}$	0.982	22.4	.129	.442
SS4	28.28	$13\pm\frac{1}{2}$	1.31	22.4	.173	.391
SS5	28.28	$14\pm\frac{1}{2}$	1.62	22.4	.213	.365
SS6	28.28	$15.5\pm\frac{1}{2}$	1.93	22.4	.254	.329
SS7	28.28	$17.5\pm\frac{1}{2}$	2.25	22.4	.296	.295
SS8	28.28	19.5±1	2.40	22.4	.316	.262
SS9	28.28	22.5±1	2.88	22.4	.379	.227
SS10	28.28	27.5±1	3.19	22.4	.420	.187
SS11	28.28	$31\pm\frac{1}{2}$	3.29	22.5	.433	.165
SS12	28.28	$41\pm\frac{1}{2}$	3.60	22.5	.474	.125
SS13	28.28	51	3.78	22.5	.498	.101

	1	2	3	4	5	6
SS14	28.28	40±1	3.60	22.4	.474	.128
	28.28	40±1	3.57	22.5	.470	.128
	28.28	39.5±1	3.57	22.5	.470	.129
	28.28	39±1	3.57	22.5	.470	.130
S1a	28.62	39	3.48	22.2	.458	.133
S1b	28.62	750	3.78	22.4	.498	.104
S1c	28.62	25	2.89	22.5	.381	.207
S2	28.62	30	3.17	22.5	.418	.173
S3a	28.62	29	3.17	22.6	.418	.179
S3b	28.62	39	3.54	22.6	.466	.133
S3c	28.62	41	3.60	22.6	.474	.127
S3d	28.62	25	2.95	22.6	.389	.207

Appendix II-3

Summary of Local Concentration and Piezometric Head Data

Tables II-3

Run A1 d=70 cm $\bar{C}$=.084 h_*=.2848 ft.H_2O	Elevation y (cm.)	Local Conc. C	$C/\bar{C}$	y/d	Elevation y (cm.)	h (ft.H_2O)	h/h_*	y/d
	59.5	.0573	.682	.850	4.4	.2455	.862	.0628
	53.4	.0617	.735	.763	7.9	.2260	.794	.113
	47.2	.0651	.775	.674	20.1	.1640	.576	.287
	41.2	.0736	.876	.589	31.4	.1140	.400	.448
	35.1	.0804	.957	.501	42.8	.0730	.256	.611
	29.0	.0864	1.03	.414	58.6	.0270	.0948	.751
	22.9	.0924	1.10	.327	73.0	.0010	.00351	1.04
	16.8	.0992	1.18	.240				
	10.7	.106	1.26	.153				
	4.9	.119	1.42	.070				
	1.5	.138	1.64	.0214				

Run A2 d=60 cm $\bar{C}$=.096 h_*=.2844 ft.H_2O	y (cm.)	C	$C/\bar{C}$	y/d	y (cm.)	h (ft.H_2O)	h/h_*	y/d
	59.5	.0336	.350	.992	4.4	.2390	.840	.073
	53.4	.0611	.636	.890	7.9	.2200	.774	.132
	47.2	.0676	.704	.787	20.1	.1510	.531	.336
	41.2	.0805	.838	.687	31.4	.0950	.334	.524
	35.1	.0850	.885	.585	42.8	.0525	.185	.715
	29.0	.0960	1.00	.483	58.6	.0060	.021	.979
	22.9	.105	1.09	.382	73.0	.0005	.002	1.219
	16.8	.111	1.16	.280				
	10.7	.117	1.22	.153				
	4.9	.127	1.32	.0817				
	1.5	.142	1.48	.0250				
	44.2	.0720	0.750	.737				

Run A3
d=48 cm
$h_* = .2839$ ft. H_2O
$\bar{C} = 119$

y (cm.)	C	C/$\bar{C}$	y/d	y (cm.)	h (ft. H_2O)	h/h_*	y/d
45.7	.0809	.680	.952	4.4	.2375	.836	.092
44.2	.0847	.711	.921	7.9	.2235	.787	.165
41.2	.0885	.743	.858	20.1	.1365	.481	.419
35.1	.0986	.828	.731	31.4	.0740	.261	.654
29.0	.104	.874	.604	42.8	.0230	.081	.892
22.9	.109	.916	.447	58.6	.000	0	1.221
16.8	.118	.991	.350				
10.7	.123	1.033	.223				
4.9	.132	1.109	.102				
1.5	.162	1.361	.031				

Run A6
d= 53cm
$\bar{C} = .112$
$h_* = .2832$ ft H_2O

y (cm.)	C	C/$\bar{C}$	y/d	y (cm.)	h (ft. H_2O)	h/h_*	y/d
50.3	.0685	.612	.949	4.8	.2365	.835	.091
48.8	.0762	.680	.921	9.8	.2075	.732	.185
47.2	.0775	.692	.891	14.8	.1750	.618	.279
45.8	.0781	.697	.864	19.8	.1460	.515	.374
44.2	.0800	.714	.834	24.8	.1200	.424	.468
42.7	.0814	.727	.806	29.8	.0955	.337	.562
41.2	.0815	.728	.777	34.8	.0720	.254	.657
39.6	.0817	.730	.747	39.8	.0520	.184	.751
38.2	.0826	.738	.721	44.8	.0315	.111	.845
36.6	.0844	.754	.691	49.8	.0140	.049	.940
35.1	(.0872 / .0857)	(.779 / .765)	.662				
33.6	(.0920 / .0884)	(.822 / .789)	.634				
32.0	.0911	.814	.604				
30.5	.0977	.872	.576				
29.0	.0994	.888	.547				
27.4	.101	.902	.517				
25.9	.104	.929	.489				
24.4	.108	.964	.460				
22.9	.109	.973	.432				

Run A6 Cont'd	y (cm.)	C	$C/\overline{C}$	y/d
	18.3	.116	1.036	.345
	16.8	.118	1.054	.317
	15.2	.117	1.045	.287
	13.7	.119	1.063	.259
	12.2	.119	1.063	.230
	10.7	.120	1.072	.202
	9.2	.121	1.081	.174
	7.6	.124	1.107	.143
	6.1	.125	1.116	.115
	4.6	.125	1.116	.087
	3.0	.126	1.125	.057
	1.5	.129	1.152	.028
	0.2	.119	1.063	.004

Run Z20
d=58.5 cm
$\overline{C}$=.109
h_*=.3467 ft.H_2O

y (cm.)	C	C/$\overline{C}$	y/d	y (cm.)	h (ft.H_2O)	h/h_*	y/d
56.1	.0144	.132	.959	4.8	.2840	.819	.082
54.6	.0280	.257	.934	7.3	.2590	.747	.125
53.1	.0327	.300	.908	9.8	.2355	.679	.168
51.5	.0352	.323	.881	12.3	.2130	.514	.210
50.0	.0374	.343	.855	14.8	.1910	.551	.253
48.5	.0396	.363	.829	17.3	.1700	.490	.296
47.0	.0416	.382	.804	19.8	.1485	.428	.339
45.4	.0440	.404	.776	22.3	.1275	.368	.381
43.9	.0480	.440	.751	24.8	.1100	.317	.424
42.4	.0500	.459	.725	27.3	.0925	.267	.467
40.9	.0536	.492	.699	29.8	.0795	.229	.510
39.3	.0584	.536	.672	32.3	.0660	.190	.552
37.8	.0602	.552	.646	34.8	.0560	.162	.595
36.3	.0655	.601	.621	37.3	.0480	.138	.638
34.8	.0701	.643	.595	39.8	.0405	.117	.681
33.2	.0754	.692	.568	42.3	.0301	.087	.723
31.7	.0844	.774	.542	44.8	.0255	.074	.766
30.2	.0930	.853	.516	47.3	.0195	.056	.809
28.7	.0978	.897	.491	49.8	.0150	.043	.852
27.1	.109	1.000	.463	52.3	.0090	.026	.894
25.6	.122	1.119	.438	54.8	.0060	.017	.937
24.1	.133	1.220	.412	57.3	.0025	.007	.980
22.6	.144	1.321	.386	59.8	.0005	.001	1.023
21.0	.152	1.394	.359				
19.5	.155	1.422	.333				
18.0	.160	1.468	.308				
16.5	.165	1.514	.282				
14.9	.168	1.541	.255				
13.4	.168	1.541	.229				
11.9	.169	1.550	.203				
7.3	.170	1.560	.125				

Run Z20 Cont'd.	y (cm.)	C	$C/\overline{C}$	y/d
	5.8	.173	1.587	.099
	4.3	.174	1.596	.074
	2.7	.186	1.706	.046
	1.2	.186	1.706	.021

Run Z21
d=43.0 cm
$\overline{C}$=.149
h_*=.3467 ft.H_2O

y (cm.)	C	C/$\overline{C}$	y/d	y (cm.)	h (ftH_2O)	h/h_*	y/d
41.8	.0356	.239	.972	4.8	.2685	.774	.112
40.3	.0535	.359	.937	7.3	.2485	.717	.170
38.7	.0589	.395	.900	9.8	.2280	.658	.228
37.2	.0633	.425	.865	12.3	.2065	.596	.286
35.7	.0693	.465	.830	14.8	.1775	.512	.344
34.2	.0744	.499	.795	17.3	.1520	.438	.402
32.6	.0786	.527	.758	19.8	.1280	.369	.461
31.1	.0855	.574	.723	22.3	.1065	.307	.519
29.6	.0950	.637	.688	24.8	.0865	.249	.577
28.1	.108	.725	.654	27.3	.0690	.199	.635
26.5	.115	.772	.616	29.8	.0540	.156	.693
25.0	.128	.859	.582	32.3	.0420	.121	.751
23.5	.144	.966	.547	34.8	.0315	.091	.809
22.0	.153	1.027	.512	37.3	.0230	.066	.868
20.4	.163	1.094	.475	39.8	.0150	.043	.926
18.9	.171	1.147	.440	42.3	.0085	.025	.984
17.4	.171	1.147	.405	44.8	.0020	.006	1.042
15.9	.176	1.181	.370				
14.3	.181	1.215	.333				
12.8	.182	1.221	.298				
11.3	.185	1.241	.263				
9.8	.186	1.248	.228				
8.2	.188	1.261	.191				
6.7	.187	1.254	.156				
5.2	.185	1.241	.121				
3.7	.193	1.295	.086				
2.1	.202	1.355	.049				

Run Z22 $\overline{d=29.5}$ cm $\overline{C}=.216$ $h_*=.3458$ ft.H_2O	y (cm.)	C	C/$\overline{C}$	y/d	y (cm.)	h (ft.H_2O)	h/h_*	y/d
	28.7	.0625	.289	.973	4.8	.2605	.753	.163
	27.1	.125	.579	.919	7.3	.2370	.685	.247
	25.6	.145	.671	.868	9.8	.2025	.585	.332
	24.1	.157	.727	.817	12.3	.1740	.503	.417
	22.6	.174	.806	.766	14.8	.1450	.419	.502
	21.0	.184	.852	.712	17.3	.1175	.340	.586
	19.5	.202	.935	.661	19.8	.0895	.259	.671
	18.0	.207	.958	.610	22.3	.0640	.185	.756
	16.5	.210	.972	.559	24.8	.0405	.117	.841
	14.9	.214	.991	.505	27.3	.0225	.065	.925
	13.4	.216	1.000	.454	29.8	.0050	.014	1.010
	11.9	.216	1.000	.403				
	10.4	.216	1.000	.353				
	8.8	.221	1.023	.298				
	7.3	.219	1.014	.247				
	5.8	.222	1,028	.197				
	4.3	.223	1.032	.146				
	2.7	.224	1.037	.092				
	1.2	.242	1.120	.041				

Run G18 d=47 cm $\overline{C}$=.151 h_*=.3848 ft.H_2O	y (cm.)	C	C/$\overline{C}$	y/d	y (cm.)	h (ft.H_2O)	h/h_*	y/d
	45.8	.0257	.170	.975	4.8	.3101	.783	.102
	44.2	.0428	.283	.941	7.3	.2730	.710	.155
	42.7	.0496	.328	.909	9.8	.2460	.640	.209
	41.2	.0562	.372	.877	12.3	.2230	.580	.262
	39.6	.0656	.434	.843	14.8	.1975	.514	.315
	38.1	.0760	.503	.811	17.3	.1730	.450	.368
	36.6	.0815	.540	.779	19.8	.1500	.390	.421
	35.1	.0940	.622	.747	22.3	.1270	.330	.475
	33.6	.103	.682	.715	24.8	.1085	.282	.528
	32.0	.118	.781	.681	27.3	.0875	.228	.581
	30.5	.129	.854	.649	39.8	.0700	.182	.634
	29.0	.134	.887	.617	32.3	.0530	.138	.687
	27.5	.144	.953	.535	34.8	.0385	.100	.741
	25.9	.149	.986	.551	37.3	.0280	.073	.794
	24.4	.166	1.099	.519	39.8	.0170	.044	.847
	22.9	.164	1.086	.487	42.3	.0100	.026	.900
	21.4	.162	1.072	.455	44.8	.0040	.010	.953
	19.8	.174	1.152	.421	47.3	.0020	.005	1.007
	18.3	.173	1.145	.389				
	16.8	.177	1.172	.358				
	15.2	.177	1.172	.323				
	13.7	.179	1.185	.292				
	12.2	.176	1.165	.260				
	10.7	.180	1.192	.228				
	9.2	.183	1.211	.196				
	7.6	.190	1.258	.162				
	6.1	.190	1.258	.130				
	4.6	.190	1.258	.098				
	3.0	.182	1.205	.064				
	35.1	.0904	.598	.747				
	21.4	.160	1.059	.455				

Run G19 $\overline{d=29\ cm}$ $\overline{C}=.243$ $h_*=.3842$ ft.H_2O	y (cm.)	C	$C/\overline{C}$	y/d	y (cm.)	h (ft.H_2O)	h/h_*	y/d
	27.5	.105	.432	.949	4.8	.2790	.726	.166
	25.9	.177	.728	.894	7.3	.2465	.642	.252
	24.4	.203	.835	.842	9.8	.2140	.557	.338
	22.9	.216	.889	.790	12.3	.1830	.476	.424
	21.4	.223	.918	.738	14.8	.1505	.392	.511
	19.8	.226	.930	.683	17.3	.1200	.312	.597
	18.3	.227	.934	.631	19.8	.0885	.230	.683
	16.8	.227	.934	.580	22.3	.0585	.152	.769
	15.2	.231	.951	.524	24.8	.0300	.078	.856
	13.7	.232	.955	.473	27.3	.0050	.013	.942
	12.2	.234	.963	.421				
	10.7	.231	.951	.369				
	9.2	.232	.955	.317				
	7.6	.248	1.021	.262				
	6.1	.248	1.021	.210				
	4.6	.276	1.136	.159				
	3.0	.260	1.070	.104				
	24.4	.196	.807	.842				

Run G20 d=29 cm $\bar{C}$=.243 h_*=.3832 ft.H_2O	y (cm.)	C	C/$\bar{C}$	y/d	y (cm.)	h (ft.H_2O)	h/h_*	y/d
	27.5	.107	.440	.948	4.8	.2945	.769	.166
	25.9	.186	.765	.895	7.3	.2670	.697	.252
	24.4	.201	.827	.841	9.8	.2395	.625	.338
	22.9	.221	.909	.790	12.3	.1965	.513	.424
	21.4	.225	.926	.738	14.8	.1665	.435	.510
	19.8	.226	.930	.683	17.3	.1360	.355	.597
	18.3	.228	.938	.631	19.8	.1075	.281	.683
	16.8	.227	.934	.579	22.3	.0805	.210	.769
	15.2	.227	.934	.524	24.8	.0530	.138	.855
	13.7	.231	.951	.472	27.3	.0235	.061	.941
	12.2	.230	.946	.421	29.8	.0040	.010	1.026
	10.7	.230	.946	.369	32.3	.0010	.003	1.114
	9.2	.238	.979	.317				
	7.6	.243	1.000	.262				
	6.1	.246	1.012	.210				
	4.6	.254	1.045	.159				
	3.0	.252	1.037	.103				
	24.4	.207	.852	.841				

Run SS14
d=39.5 cm
$\bar{C}$=.129
h_*=.2807 ft. H_2O

y (cm.)	C	C/$\bar{C}$	y/d	y (cm.)	h (ft. H_2O)	h/h_*	y/d
36.6	.0225	.174	.927	4.8	.1965	.700	.122
35.1	.0278	.215	.889	7.3	.1630	.581	.185
33.6	.0331	.257	.851	9.8	.1310	.467	.248
32.0	.0378	.293	.810	12.3	.1025	.365	.311
30.5	.0381	.295	.772	14.8	.0765	.273	.375
29.0	.0443	.343	.734	17.3	.0575	.205	.438
27.4	.0509	.394	.694	19.8	.0465	.166	.501
25.9	.0556	.431	.656	22.3	.0355	.126	.565
24.4	.0617	.478	.618	24.8	.0275	.098	.628
22.9	.0698	.541	.580	27.3	.0200	.071	.691
21.4	.0803	.622	.542	29.8	.0135	.048	.755
19.8	.0920	.713	.501	32.3	.0100	.036	.818
18.3	.0985	.763	.463	34.8	.0070	.025	.881
16.8	.117	.907	.425	37.3	.0040	.014	.944
15.2	.129	1.000	.387	39.8	.0015	.005	1.008
13.7	.160	1.240	.347				
12.2	.195	1.511	.309				
10.7	.222	1.721	.271				
9.2	.233	1.806	.233				
7.6	.246	1.907	.192				
6.1	.250	1.938	.154				
4.6	.253	1.968	.116				
3.0	.260	2.015	.076				
1.5	.260	2.015	.038				
24.4	.0603	.467	.618				
29.0	.0433	.336	.734				
38.1	.0158	.122	.965				

APPENDIX III

SUMMARY OF NOTATION

The page numbers listed refer to the page on which the symbol first appears.

			Page
A	=	cross-sectional area of fluidization column	43
C	=	local volume concentration of suspended particles	4
$\overline{C}$	=	mean volume concentration of suspended particles $= W/\gamma_s Ad$	43
C_r	=	theoretical concentration of suspended particles by Maxwell's formula $= R-R_f/R+\frac{1}{2}R_f$	34
d	=	total depth of a suspension	43
D	=	particle diameter	4
D_g	=	geometric mean sieve diameter	45
D_s	=	sedimentation diameter	56
g	=	acceleration due to gravity	5
h	=	piezometric head of fluid	3
h_*	=	theoretical piezometric head of fluid equivalent to the total weight of the granular material in the fluidization column $= \frac{W}{\gamma_s A}\left(\frac{\gamma_s}{\gamma_f} - 1\right)$	67
k	=	permeability coefficient	3
K	=	hydraulic conductivity or permeability $= k\gamma_f/\mu$	4
K	=	electrical resistance probe calibration coefficient	37
Re	=	Reynolds number $= wD/\nu$	7
R	=	resistivity	34
T	=	water temperature	
y	=	vertical coordinate	36
y	=	elevation above the bottom of a suspension	

		Page
$\bar{u}$	= superficial velocity = discharge per total cross-sectional area of fluidization column = Q/A	5
u_i	= intercept velocity determined from extrapolation of experimental data	8
W	= total dry weight of granular material in the fluidization column	43
w	= free-fall velocity of an isolated particle	6
w_g	= geometric mean free-fall velocity by number	50
μ	= dynamic viscosity of fluid	3
μ	= geometric mean free-fall velocity by weight for local samples	50
$\bar{\mu}$	= geometric mean free-fall velocity by weight for parent materials	60
γ_f	= unit weight of fluid = $\rho_f g$	3
γ_s	= unit weight of particles = $\rho_s g$	67
ρ_f	= mass density of fluid	5
ρ_s	= mass density of particles	5
ν	= kinematic viscosity of fluid = μ/ρ_f	61
σ	= standard deviation	145
σ_g	= geometric standard deviation of distribution of sieve diameters	45
σ_s	= geometric standard deviation of distribution of sedimentation diameters	57
σ_w	= geometric standard deviation of distribution of free-fall velocities	7
ϵ	= porosity $\equiv$ 1-C	4

BIBLIOGRAPHY AND REFERENCES

1. Kynch, G. Y., "The Slow Motion of Two or More Spheres through a Viscous Fluid," Journal of Fluid Mechanics, Vol. 5, Part 2, Feb. 1959, pp. 193-208.

2. Hashimoto, H., "On the Periodic Fundamental Solutions of the Stokes Equations and Their Application to Viscous Flow Past a Cubic Array of Spheres," Journal of Fluid Mechanics, Vol. 5, Part 2, Feb. 1959, pp. 317-328.

3. McNown, J. S., "Particules en Mouvement Lent," La Houille Blanche, Vol. 6, No. 5, 1951, pp. 711-722.

4. Richardson, J. F. and Zaki, W. N., "Sedimentation and Fluidization, Part I," Trans. Instn. Chem Engrs, Vol. 32, 1954, pp. 35-53.

5. McNown, J. S. and Lin, Pin-Nam, "Sediment Concentration and Fall Velocity," Proceedings of the Second Midwestern Conference on Fluid Mechanics, Ohio State University, 1952, pp. 401-412.

6. Rouse, Hunter, "Experiments on the Mechanics of Sediment Suspension," Proceedings of the Fifth International Congress for Applied Mechanics, 1938.

7. Rouse, Hunter, "Suspension of Sediment in Upward Flow," Investigations of the Iowa Institute of Hydraulic Research 1939-40, University of Iowa Studies in Engineering Bulletin 26, pp. 14-22.

8. Housner, G. W., "The Mechanism of Sandblows," Bulletin of the Seismological Society of America, Vol. 48, April 1958, pp. 155-161.

9. Randall, D. E. and Millwright, S.S., "Experimental Determination of the Pressure Drop through a Pebble Bed," Sandia Corporation Research Report SC-4354 (TR), Sept. 1959.

10. Ismail, H. M., "Turbulent Transfer Mechanism and Suspended Sediment in Closed Channels," Trans. Am. Soc. Civ. Engrs., Vol. 117, 1952, pp. 409-446.

11. Vanoni, V. A., "Transportation of Suspended Sediment by Water," Trans. Am. Soc. Civ. Engrs., Vol. 111, 1946, pp. 67-133.

12. Morse, R. D. and Ballou, C. O., "The Uniformity of Fluidization - Its Measurement and Use," Chem. Engr. Progress, Vol. 47, No. 4, April 1951, pp. 199-204.

13. Lamb, Owen P. and Millen, J. M., "An Electrical Method for Measuring Air Concentration in Flowing Air-Water Mixtures," Univ. of Minnesota, St. Anthony Falls Hydraulic Laboratory, Technical Paper No. 2, Series B, March 1950.

14. Velock, Sidney and Gorin, M., "The Electrical Conductance of Suspensions of Ellipsoids and Its Relation to the Study of Avian Erythrocytes," Journal of General Physiology, Vol. 23, 1940, pp. 753-771.

15. Hanratty, T. J., Latinen, G., and Wilhelm, R., "Turbulent Diffusion in Particulately Fluidized Beds of Particles," A.I.Ch.E. Journal, Sept. 1956, pp. 372-380.

16. Leva, Max, "Fluidization," McGraw-Hill, 1959.

17. Zenz, F. A. and Othmer, D. F., "Fluidization and Fluid Particle Systems," Reinhold Publishing Corp., 1960.

18. Happle, J., and Epstein, N., "Flow in Cubical Assemblages of Uniform Spheres," Ind. and Eng. Chem., Vol. 46, 1954, pp. 1187 ff.

19. Wilhelm, R. H. and Kwauk, M., "Fluidization of Solid Particles," Chem. Eng. Progress, Vol. 44, No. 3, 1948, p. 201 ff.

20. Stauffer, J. D., "Physical Characteristics of Supported Fluidized Beds," Ph.D. Thesis, Northwestern University, Dept. of Chemical Engineering, Evanston, Ill., 1955. University Microfilm No. 19046, Ann Arbor, Michigan.

21. Hazen, A., "Storage to be Provided in Impounding Reservoirs," Trans. Am. Soc. Civ. Engrs., Vol. 77, 1914, pp. 1539-1669.

22. Chanishvili, A. G., "Air Entrainment and Vertical Downward Motion of Aerated Flows," Proceedings of the 8th Congress of the International Association for Hydraulic Research, Montreal, Canada, 1959, Vol. 2, 8D, pp. 1-22.

23. Otto, George H., "A Modified Logarithmic Probability Graph for the Interpretation of Mechanical Analysis of Sediments," J. Sediment. Petrol., Vol. 9, No. 2, 1939, pp. 62-76.

24. Thomas, H. A., Jr., "Frequency of Minor Floods," J. Boston Soc. Civil Engrs. 35, 1948, pp. 425-442.

25. Kennedy, J. F., and R.C.Y.Koh, "The Relation between the Frequency Distributions of Sieve Diameters and Fall Velocities of Sediment Particles," Journal of Geophysical Research, Vol. 66, No. 12, 1961, pp. 4233-4246.

26. U.S. Inter-Agency Committee on Water Resources, Subcommittee on Sedimentation, 1957, "Some Fundaments of Particle Size Analysis," Rept. 12, U. S. Government Printing Office, 1957.

27. Wilson, B. W., "The Sedimentation of Dense Suspensions of Microscopic Spheres," Australian Journal of Applied Science, Vol. 4, No. 2, 1953, pp. 274-299.

28. Scheidegger, A. E., "The Physics of Flow through Porous Media," The Macmillan Company, New York, 1960, p. 313 ff.

29. Fair, G. F., and J. C. Geyer, "Water Supply and Waste-Water Disposal," John Wiley and Sons, Inc., New York, 1956, p. 951 ff.

30. Maxwell, J. C., "A Treatise on Electricity and Magnetism," Oxford-Clarendon Press, 1873.

31. Baylis, J., "Head Loss in Backwashing Filters," Pure Water, Vol. VII, No. 5, Dept. of Water and Sewers, Bureau of Water, Chicago, Illinois, May, 1955, pp. 61-77.